NUREG/CR-5094

Application of Stochastic Methods to the Simulation of Large-Scale Unsaturated Flow and Transport

Prepared by D.J. Polmann, E.G. Vomvoris, D. McLaughlin,
E.M. Hammick, L.W. Gelhar

Massachusetts Institute of Technology

Prepared for
U.S. Nuclear Regulatory
Commission

NUREG/CR-5094

Application of Stochastic Methods to the Simulation of Large-Scale Unsaturated Flow and Transport

Manuscript Completed: April 1988
Date Published: September 1988

Prepared by
D.J. Polmann, E.G. Vomvoris, D. McLaughlin,
E.M. Hammick, L.W. Gelhar

T.J. Nicholson, NRC Project Manager

Massachusetts Institute of Technology
Department of Civil Engineering
77 Massachusetts Avenue
Cambridge, MA 02139

Prepared for
Division of Engineering
Office of Nuclear Regulatory Research
U.S. Nuclear Regulatory Commission
Washington, DC 20555
NRC FIN B8956

ABSTRACT

Numerical simulations are used to demonstrate features of large-scale flow and transport in heterogeneous unsaturated soils using effective expressions derived from a stochastic theory developed at MIT. The case of stratified soil is examined for one- and two-dimensional (2D) flow and 2D transport. Finite-difference methods are used in the flow analysis and a random-walk algorithm is used for transport. Input parameters are derived from statistics of soil samples collected at the site of a large-scale tracer experiment conducted by New Mexico State University (NMSU). This study examines spatial variability of saturated and unsaturated hydraulic conductivity regarding effects on the bulk character of moisture flow and solute transport (directional rates of movement and spreading of the plume). The numerical simulations demonstrate tension-dependent anisotropy, hysteresis and macrodispersion derived in the stochastic theory based on this spatial variability. These features cannot be explained using conventional deterministic models. Preliminary results suggest that the stochastic theory is better able to simulate the bulk character of the NMSU flow experiments compared to a deterministic model. Sensitivity analyses identify major factors of soil variability which control moisture flow and spreading. Results of this study indicate the need for careful experimental design and soils data collection.

TABLE OF CONTENTS

Abstract iii

Table of Contents v

List of Figures vii

List of Tables xi

Acknowledgement xiii

Executive Summary 1

1. Introduction 1-1
- 1.1 Background and Motivation 1-1
- 1.2 Report Scope and Content 1-3

2. Review of Stochastic Unsaturated Flow and Transport Theory 2-1
- 2.1 Introduction 2-1
- 2.2 Stochastic Unsaturated Flow Theory 2-6
  - 2.2.1 Brief Review of Related Work 2-6
  - 2.2.2 Stochastic Description of Unsaturated Soil Hydraulic Properties 2-9
  - 2.2.3 Derivation of Large-Scale Models and Effective Parameters 2-10
  - 2.2.4 The Stratified Soil Case 2-16
  - 2.2.5 Operational Modifications to the Basic Theory 2-22
- 2.3 Stochastic Unsaturated Transport Theory 2-26
  - 2.3.1 Derivation of Large-Scale Models and Effective Parameters 2-26
  - 2.3.2 The Equations for the Mean Transport Model 2-33

3. The Experiments at Las Cruces 3-1
- 3.1 Introduction 3-1
- 3.2 Procedures for Collection and Analysis of Soils Data 3-1
  - 3.2.1 Lysimeter Soils 3-1
  - 3.2.2 Field Soils 3-3
- 3.3 Lysimeter Experiment 3-5
- 3.4 Large-scale Field Experiment 3-5

4. The Mean Flow Model 4-1
- 4.1 Introduction 4-1
- 4.2 Numerical Implementation 4-2
- 4.3 Verification of the Numerical Solution Technique 4-3
- 4.4 Availability of Data for Input 4-4
- 4.5 One-Dimensional Application 4-7
  - 4.5.1 Configuration and Auxiliary Conditions 4-7
  - 4.5.2 Model Input Parameters 4-12
  - 4.5.3 Hysteresis of Effective Conductivity 4-13

4.5.4 Model Results for the Stochastic Case 4-13
4.5.5 Model Results for a Deterministic Case 4-21
4.5.6 Comparison with Field Data 4-21
4.6 Two-Dimensional Application 4-24
4.6.1 Configuration and Auxiliary Conditions 4-24
4.6.2 Model Input Parameters 4-26
4.6.3 Hysteresis and Anisotropy of Effective Conductivity 4-26
4.6.4 Model Results for the Nominal Case 4-29
4.6.5 Model Results for a Deterministic Analysis 4-34
4.6.6 Model Results for Sensitivity Analyses 4-37
4.7 Summary and Future Research Needs 4-45

5. The Mean Transport Model 5-1
5.1 Introduction 5-1
5.2 Random Walk Model 5-1
5.3 Two-Dimensional Application 5-4
5.3.1 Methods and Procedures 5-4
5.3.2 Example Results 5-6
5.4 Summary and Future Research Needs 5-9

6. Summary and Conclusions 6-1

References R-1

Appendix A-1

LIST OF FIGURES

Figure		Page
1-1	Conceptualization of the various physical processes which affect contaminant transport at a near-surface low-level waste site	1-2
2-1	Unsaturated hydraulic conductivity versus capillary tension head for the Maddock sandy loam	2-3
2-2	Capillary tension head versus soil moisture content for the Panoche silty clay loam	2-4
2-3	Saturated hydraulic conductivity versus depth at the Las Cruces trench site	2-5
2-4	Variance of capillary tension head versus mean capillary tension head for the Panoche silty clay loam	2-19
2-5	Vertical and horizontal hydraulic conductivities versus mean capillary tension head for the Maddock sandy loam	2-20
2-6	Log hydraulic conductivity versus mean tension head	2-25
2-7	Coordinate system corresponding to the principal anisotropy axes	2-29
2-8	Longitudinal macrodispersivities versus mean capillary tension head	2-34
3-1	Top view of lysimeter facility	3-6
3-2	Schematic view of lysimeter filled with alternate layers of Berino loamy fine sand and Glendale clay loam	3-7
3-3	Top view of trench and irrigated area	3-8
3-4	Side view of trench with location of tensiometers and suction tubes	3-10
4-1	Comparison of solution technique to other methods for one-dimensional flow	4-5
4-2	Comparison of solution technique to other methods for two-dimensional flow	4-6
4-3	Physical structure and boundary conditions for the one-dimensional simulation	4-11

Figure		Page

Figure		Page
4-4	Effective hydraulic conductivity versus mean tension for selected values of $\partial H/\partial t$ during one-dimensional flow	4-14
4-5	Propagation of tension front during wetting/drying cycle in the one-dimensional simulation	4-15
4-6	Hysteresis of effective hydraulic conductivity during wetting/drying cycle at 1- and 2-meter depths	4-17
4-7	Propagation of moisture front during wetting/drying cycle in the one-dimensional simulation	4-18
4-8	Propagation of tension front in the one-dimensional simulation using larger spatial discretization	4-19
4-9	Variance of tension versus depth during wetting/drying cycle in the one dimensional simulation	4-20
4-10	Propagation of tension front during wetting/drying cycle in the deterministic, layered one-dimensional simulation	4-22
4-11	Field-measured moisture distribution during wetting/drying cycle in the layered lysimeter	4-23
4-12	Configuration of the field experiment and its representation in the numerical model simulations for the two-dimensional case	4-25
4-13	Effective hydraulic conductivity versus mean tension for selected values of $\partial H/\partial t$ during two-dimensional flow	4-28
4-14	Contributions of selected input parameters to the anisotropy of effective hydraulic conductivity	4-30
4-15	Tension distribution and the spreading of moisture during the wetting cycle; nominal simulation	4-32
4-16	Spatial gradients of tension and the redistribution of moisture; nominal simulation	4-33
4-17	Hysteresis and anisotropy of effective hydraulic conductivity during the wetting/drying cycle at 0.5 meter depth under the wetted strip	4-35

Figure		Page
4-18	Spatial views of mean pressure, tension variance and mean moisture content during the wetting/drying cycle; nominal simulation	4-36
4-19	Tension distribution and the spreading of moisture during the wetting cycle; deterministic analysis	4-38
4-20	Spatial gradients of tension and the redistribution of moisture; deterministic analysis	4-39
4-21	Tension distribution and the spreading of moisture during the wetting cycle; sensitivity to wetter initial conditions; stochastic analysis	4-41
4-22	Tension distribution and the spreading of moisture during the wetting cycle; sensitivity to decreased σ_a^2; stochastic analysis	4-42
4-23	Tension distribution and the spreading of moisture during the wetting cycle; sensitivity to decreased correlation length; stochastic analysis	4-43
5-1	Spatial location of 2000 particles during wetting/drying cycle after impulse injection; deterministic case	5-8
5-2	Spatial location of 20,000 particles during wetting/drying cycle after impulse injection; stochastic case	5-10
5-3	Longitudinal and lateral movement of selected particles; deterministic case	5-11
5-4	Longitudinal and lateral movement of selected particles; stochastic case	5-12
5-5	Perspective view of contoured data showing spatial variations of bulk concentration	5-13
5-6	Contours of equal bulk concentration showing spatial variations within the plume	5-14

LIST OF TABLES

Table		Page
4-1	Survey of spatial variability data applicable to the stochastic model	4-8
4-2	Summary of input data for selected 2D flow simulations	4-27
4-3	Resulting mean flow effects for changes in input parameters	4-44
5-1	Asymptotic macrodispersivities for the 2D simulation	5-7

ACKNOWLEDGEMENTS

The research described in this report is part of a continuining study of contaminant transport in heterogeneous unsaturated soils supported by the U.S. Nuclear Regulatory Commission (USNRC) through the research project entitled "Stochastic Analysis of Solute Transport in Unsaturated Soils" (FIN B8956).

Thomas Nicholson of the USNRC served as Project Manager for the project and contributed significantly to this work through his enthusiastic support of the the MIT research and the cooperative work with New Mexico State University (NMSU) and Pacific Northwest Labs (PNL). Tom raised many important questions and inspired considerable thought and discussion during our lively group meetings.

We also acknowledge several MIT researchers who have made significant contributions to this work. Andrew Tompson provided extensive assistance in the application of the stochastic unsaturated flow theory, and also developed the random walk transport model which served as a basis for the transport model used here. Michael Celia offered many useful comments and critical evaluations of theoretical and application issues, and contributed significantly during development of the numerical simulators. Rachid Ababou provided several helpful suggestions regarding numerical applications and testing of the flow model.

Peter J. Wierenga of NMSU was responsible for developing the field experiment designed to evaluate the stochastic theory; his suggestions and cooperation are gratefully acknowledged. Glendon Gee of PNL also provided useful insights on modeling and interpretation of experiments. His awareness of significant issues continues to make important contributions to our group discussions.

Computational support for the development of the numerical models described here and the many extensive simulations was provided by the Microvax computer facility at the Ralph M. Parsons Laboratory at MIT.

EXECUTIVE SUMMARY

This report describes the results of numerical simulations of moisture flow and solute transport conducted by MIT as part of a continuing project examining heterogeneous unsaturated soils. Previous work in this project used stochastic theory to derive "effective" expressions for large-scale processes in field soils. New features of tension-dependent anisotropy, hysteresis and macrodispersion caused by spatial variability of soil hydraulic properties were identified. The study described here used numerical simulation of the stochastic theory to demonstrate these features and to identify the soil parameters which have important effects on the bulk flow behavior. This work was closely integrated with ongoing field and laboratory experiments being conducted at New Mexico State University (NMSU). These studies combine theory, simulation and experiment and highlight areas which merit future investigation.

Natural soil heterogeneity (spatial variability) is represented in the MIT theory by a small number of parameters which are based on statistics of soil sample properties. The effects of this heterogeneity on large-scale processes are included in the analyses by using effective soil properties which are derived from the statistical parameters. The numerical models use these effective properties to predict bulk characteristics of moisture flow and solute transport. Uncertainty in these predictions is acknowledged and an estimate of the variance of mean tension is provided.

The field conditions simulated in this study may resemble low-level-waste disposal sites. The focus of the study is on one- and two-dimensional analyses of the NMSU experiments, illustrating some of the field-scale effects which will occur in the heterogeneous environments of actual waste sites. These simulations are not intended to "validate" the MIT model, but rather serve to demonstrate anisotropy, hysteresis and macrodispersion -- factors which control the rate and direction of contaminant transport at field scale. Conventional models do not explain these features; one- and two-dimensional simulations based on deterministic analyses of the same physical systems reveal qualitatively different behavior and results which compare less favorably to the field experiments.

Citing recent improvements, this report summarizes the MIT stochastic theory for the case of stratified soils. Emphasis is given to assumptions and approximations which were introduced to facilitate simulation of field conditions. The numerical method for flow simulation is outlined and test problems are compared with other numerical techniques. Results of one- and two-dimensional simulations are discussed and compared to the NMSU experiments and deterministic simulations. A study of the sensitivity of two-dimensional results to changes in input parameters is summarized, identifying the key soil properties which control bulk behavior. The theoretical basis and numerical method for solute transport are summarized and the two-dimensional analysis of a conservative solute is presented.

Review of preliminary data from the NMSU experiments suggests that the stochastic flow simulations are better able to predict the bulk rates of movement and spreading of the moisture plume compared to a deterministic simulation. Preliminary results of the transport modeling further the understanding of controlling factors of contaminant migration and identify the need for refinements of the theory for application to actual sites.

The parameters used in the present study represent the mean and variability of saturated conductivity, the mean and variability of the unsaturated conductivity versus tension relation, and the correlation structure of the saturated conductivity. Spatial variability of specific moisture capacity is neglected. The sensitivity analyses show that the correlation structure of the stratified system and the variability of the unsaturated conductivity relation are particularly important in predicting large-scale movement and spreading. These parameters are usually lacking in the research literature. Reliable and efficient methods for field and laboratory measurements are strongly encouraged in support of future studies to further understand field-scale phenomena. Improvements in the numerical solution of nonlinear systems are also called for regarding both computer processing time and storage space. This is required to facilitate the practical study of large time- and space-scale problems inherent in waste-sitings in expansive unsaturated soils. Further application of stochastic models and the study of actual field sites should incorporate spatial variability of specific moisture capacity, allow generalized functional forms of the hydraulic conductivity relations and include unsteady transport components.

CHAPTER 1

INTRODUCTION

1.1 Background and Motivation

The U.S. Nuclear Regulatory Commission (USNRC) has been directed by Congress in the Low Level Radioactive Waste Policy Amendments Act of 1985 to develop regulatory guidance and to assist the states in siting and assessing future low-level waste (LLW) disposal facilities. General performance objectives and technical requirements for such facilities are outlined in Subparts C and D of 10 CFR 61 [Office of the Federal Register (1987)] and discussed in more detail in NUREG-1200, the USNRC's Standard Review Plan [USNRC (1987)]. Both of these documents emphasize near-surface land disposal in the unsaturated zone. Subpart C of 10 CFR 61 limits the concentrations of radioactive materials "which may be released to the general environment in groundwater, surface water, air, soil, plants and animals" and Subpart D states that near-surface sites "shall be capable of being characterized, modeled, analyzed and monitored". These requirements form the basis for the extensive discussion of site meteorology, geology, and hydrology presented in NUREG-1200.

Subsurface hydrology is a particularly important aspect of site characterization because subsurface water and vapor transport are the primary natural pathways for the movement of contaminants from a disposal facility to the accessible environment. Such transport may move *in any direction* -- down to the water table, laterally into adjacent soils and root systems, or upward towards the atmosphere. This is illustrated in a schematic way in Figure 1-1, which shows some of the subsurface transport processes found at a typical low-level disposal site. A site analysis needs to consider all of these processes if it is to satisfy the broad requirements of 10 CFR 61, Part C.

Analysis of subsurface contaminant transport is complicated by a number of factors. These include the difficulty of observing subsurface processes, the long time scales required for experiments, and the need to account for soil-water interactions and spatial variability. The situation is particularly complex in the unsaturated zone, where soil properties change dramatically with moisture content. Since spatial variability and nonlinear behavior greatly complicate the equations which describe unsaturated flow and transport, performance assessments for unsaturated sites must rely heavily on numerical models. This is explicitly acknowledged in the groundwater characterization section of NUREG-1200.

This report describes recent applications of MIT's stochastic approach for modeling contaminant transport in heterogeneous unsaturated soils. These applications are part of a USNRC research project entitled "Stochastic Analysis of Solute Transport in Unsaturated Soils" (FIN B8956). Other aspects of this project include the development of basic theory [Mantoglou and Gelhar (1985, 1987a, b, c)], large-scale simulation studies [Tompson et al (1987, 1988); Ababou et al (1988)], and collaboration with other USNRC contractors responsible for field experiments being carried out near Las Cruces, New Mexico [Wierenga et al (1986a, b, 1988)]. The overall goal of MIT's research has been to develop and apply a

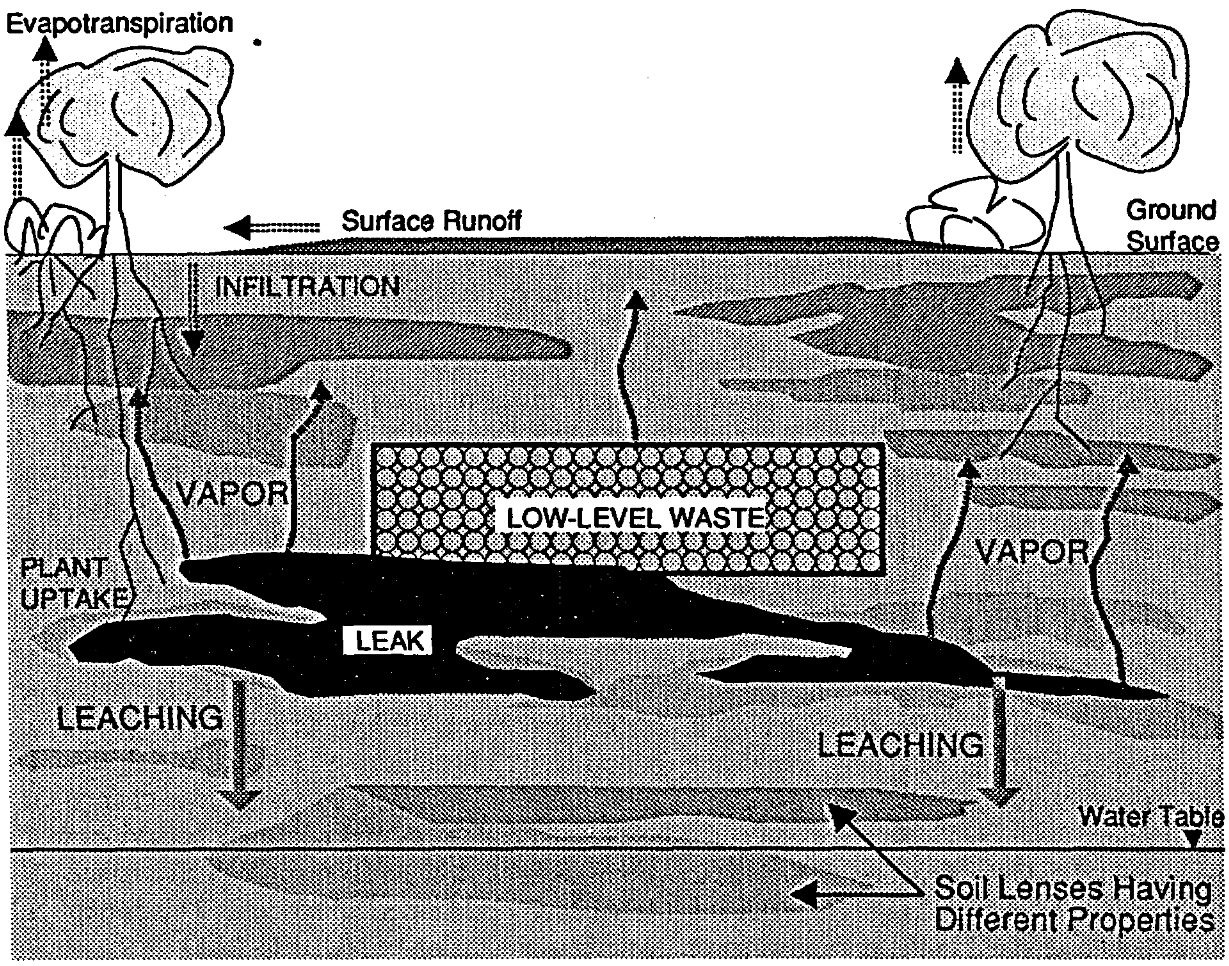

Figure 1-1. Conceptualization of the various physical processes which affect contaminant transport at a near-surface low-level waste site

promising new approach for analyzing field-scale contaminant transport in heterogeneous unsaturated soils.

The MIT stochastic approach to unsaturated flow and transport has a number of important advantages. It is able to represent natural variability with a relatively small number of parameters which can be estimated from field observations. It yields relatively simple expressions for the "effective" soil properties which influence the large-scale behavior of contaminant plumes. Numerical models based on such effective parameters can be used to analyze waste migration in situations where data limitations make conventional deterministic modeling impractical. Finally, the stochastic approach explicitly acknowledges the uncertainty associated with predictions of subsurface contaminant transport. This makes it particularly compatible with a broader analysis of exposure risk.

Although MIT's stochastic theory is relatively new, it already promises to change the way hydrologists and soil physicists think about unsaturated flow and transport at the field scale. Traditional deterministic models of the unsaturated zone cannot account for the highly variable soil conditions found in natural environments unless they are provided with enormous amounts of data. A detailed three-dimensional characterization of a site having dimensions on the order of 50 by 50 by 10 meters could easily require tens of thousands of soil samples [Ababou et al (1988)]. Since this is impractical, most deterministic models rely on highly aggregated descriptions which cannot account for the spreading and dispersion caused by small-scale heterogeneities.

It is important to note that small-scale fluctuations in soil properties are important because they have large-scale consequences (e.g., anisotropy amd macrodispersion). On the other hand, small-scale fluctuations in moisture content or concentration may not be particularly important, at least from a licensing point-of-view. Stochastic methods capitalize on this contrast by treating small-scale soil property fluctuations as if they were random and then focusing on mean (i.e., large-scale) moisture and solute behavior. In this way, the large-scale consequences of local variability are incorporated in the analysis without requiring a detailed characterization of individual soil layers and anomalies. This is why the stochastic approach can provide such an efficient characterization of heterogeneous real-world sites.

Since the MIT stochastic theory relies on many assumptions and approximations, it needs to be tested in the field. The best way to do this is to carry out field experiments with extensive monitoring such as the USNRC-sponsored Las Cruces experiments cited earlier. Theoretical predictions of moisture and solute movement can then be compared with field observations, both to test the theory and to identify areas where it may be improved. The work described in this report is part of a long-term validation process which is closely tied to field experimentation and related laboratory analysis. The results presented here help to show how models and field experiments can benefit one another. The model can be used to aid in design of the experiment and the experiment can be used to improve the model. We believe this is the most efficient way to develop the predictive capabilities the USNRC needs in order to satisfy its regulatory objectives.

1.2 Report Scope And Content

The theoretical basis for MIT's stochastic approach is conveniently summarized in the set of papers by Mantoglou and Gelhar (1987a, b, c). Our goal here is to describe how the theory can be applied to field conditions which resemble those which may be found at a typical arid low-level waste disposal site. We focus on one- and two-dimensional analyses of the Las Cruces field experiments mentioned above and described in more detail in Wierenga et al (1986a, b, 1988). These analyses are not intended to replicate actual experimental conditions or to "validate" a particular simulation model. Rather, they are intended to illustrate some of the field-scale effects which we believe will occur in the heterogeneous environments encountered at real low-level waste sites. These effects include lateral spreading of contaminants (tension-dependent anisotropy) and large-scale hysteresis which cannot be explained with conventional models. As the Las Cruces experiments progress we expect to observe, in the field, the large-scale behavior predicted by the stochastic theory. Further refinements to the theory and models, based on careful field observations, should enable us to develop practical tools which can be used to guide the site characterization and performance assessment studies mandated by 10 CFR 61 and NUREG-1200.

Chapter 2 provides a summary of MIT's stochastic theory which emphasizes the assumptions and approximations introduced to facilitate numerical simulation of large-scale field conditions. This chapter includes discussions of both unsaturated flow and solute transport. It also reviews relevant research conducted by other investigators. Chapter 3 describes the Las Cruces field experiment and related laboratory analyses. Of particular interest is the significant local heterogeneity and anisotropy observed at this site, which extends over only a few tens of meters.

Chapter 4 presents the results of one- and two-dimensional simulations of moisture flow in the Las Cruces lysimeter and trench experiments. These simulations provide predictions of the mean (or large-scale) tension and moisture content distributions anticipated at the site. They also yield estimates of the standard deviations of small-scale fluctuations about the mean tension. Most of the fluctuations observed in the field can be expected to lie within confidence intervals constructed from these standard deviations. Chapter 4 also includes a set of sensitivity results which indicate where future field investigations should be focused. Chapter 5 presents preliminary two-dimensional transport results for a generic conservative solute. Although these results are based on some simple approximations which should be refined before the transport model is applied to actual sites, they do offer further understanding of the factors which control contaminant migration in the unsaturated zone. Chapter 6 summarizes the major conclusions of the modeling studies, with an emphasis on some of the important qualitative insights provided by the stochastic theory. This chapter also considers some of the implications of our research results.

CHAPTER 2

REVIEW OF STOCHASTIC UNSATURATED FLOW AND TRANSPORT THEORY

2.1 Introduction

This section is a brief synopsis of the stochastic unsaturated flow and transport theory applied in Chapters 4 and 5. The detailed presentation of the theory can be found in Mantoglou and Gelhar (1985, 1987a, b, c). The emphasis here is on the assumptions underlying the theoretical developments and simplifications made in its implementation.

The term "stochastic theory" is used only as an abbreviation of the particular methodological approach outlined in Mantoglou and Gelhar (1985, 1987a, b, c) and summarized here. Numerous other methodologies which also adopt a stochastic viewpoint are described in the literature [e.g., Dagan (1984); Winter et al (1984); Jury et al (1982); Andersson and Shapiro (1983); Bresler and Dagan (1981, 1983)] but these will not be discussed in detail in this report.

Partially saturated soils include solid, liquid and gaseous phases. The hydraulic properties of soil systems which are generally of interest in the study of moisture flow under partially saturated conditions involve a dependency on the potential of the liquid phase. The total potential of soil water can be thought of as a sum of the separate contributions of various factors, including the gravitational potential, the pressure potential, and the osmotic potential, all expressed in equivalent units [see, for example, Hillel (1980)]. The work presented here assumes that the osmotic potential is negligible or has negligible effect on the flow system, so that interest is restricted to the gravitational and pressure terms.

Employing units of length, local conditions in the soil water can be represented as a total hydraulic head ϕ composed of pressure and gravitational heads by writing $\phi = -\psi - z$, where ψ is referred to as *suction head* or *tension head* since it corresponds to a negative pressure in the water and z is the vertical coordinate increasing downward. Note that an increase in ψ represents a decrease of pressure in the water.

The flow of water in porous media under unsaturated conditions has been described mathematically with equations which have been experimentally verified under laboratory conditions at a length scale up to a few tens of centimeters (the small or "local" scale). The local-scale soil hydraulic properties of interest in the developments that follow are:

1. the hydraulic conductivity, evaluated as a function of tension (the $K-\psi$ relationship)
2. the moisture content, evaluated as a function of tension (the $\theta-\psi$ relationship)

The conductivity represents the ability of the soil system to transmit water under a gradient in hydraulic head, and the moisture content represents a ratio of the volume of water present to the bulk soil–air–water volume. These properties can be determined experimentally for a given soil sample and are known to vary significantly among different samples of the same soil and among different soils. The heterogeneity of properties within a small region can be illustrated, for example, by recognizing that different $K-\psi$ and $\theta-\psi$ relations may be determined for a number of samples taken from a given type of soil. Figures 2-1 and 2-2 depict variations in these properties for the Maddock and Panoche soils. Note that both the magnitude of K and θ and the slopes of the $K-\psi$ and $\theta-\psi$ curves vary from sample to sample, and that the $K-\psi$ relation tends to be somewhat more variable than the $\theta-\psi$ relation for the given set of samples. The saturated conductivity, K_s, is also known to differ widely among samples taken in close proximity. Figure 2-3 illustrates a variability in K_s of over two orders of magnitude, based on samples taken along a vertical transect extending 6 meters.

This study is intended to further the understanding of the way spatial variability affects the flow of moisture and the transport of solutes at the large scales of interest in field applications. We are concerned with the bulk (or "mean") character of the large-scale system rather than with the details of small-scale flow and transport variability. Here the large (or field) scale corresponds to the dimensions affected by releases from a low-level waste repository -- tens to thousands of meters in the horizontal and meters to hundreds of meters in the vertical. The small (or local) scale corresponds to the dimensions of a typical laboratory experiment (centimeters to meters). For clarity in further discussions, the bulk, large scale, mean, or "effective" parameters are defined as follows:

- H = mean tension
- Θ = mean moisture content
- $\hat{K}$ = effective hydraulic conductivity
- $\hat{C}$ = effective specific moisture capacity

It should be clear from the illustrations of Figures 2-1 through 2-3 that soil hydraulic properties are heterogeneous and that it would be extremely difficult to have complete knowledge of the variations from location to location except at those locations where measurements are available. It can also be envisioned, however, that the variability has a certain degree of structure to it and that properties at one location are related to those at another location. In this manner, knowledge of the heterogeneity can be viewed in a probabilistic fashion in that a limited amount of spatially varying information can be utilized to characterize spatial structure through an analysis of statistical moments. The soil properties are represented as random fields and the expected value of a spatially varying property is represented by the mean or average of the random field (the first moment). The second moment characterizes the expected deviation around the average behavior, including the degree of spatial persistence of the deviation. In the work presented here it is assumed that the second moment, which quantifies the correlation between the values of the random field at two spatial locations, depends only on the separation distance of the two points. That is, the field is stationary or statistically homogeneous. Such a statistical characterization approach has a wide applicability and is discussed in detail in publications such as Vanmarcke (1983) or Bras and Rodriguez-Iturbe (1985).

It has been observed, and it can be shown analytically, that large-scale unsaturated flow phenomena are significantly affected by the small-scale variation of the characteristic properties

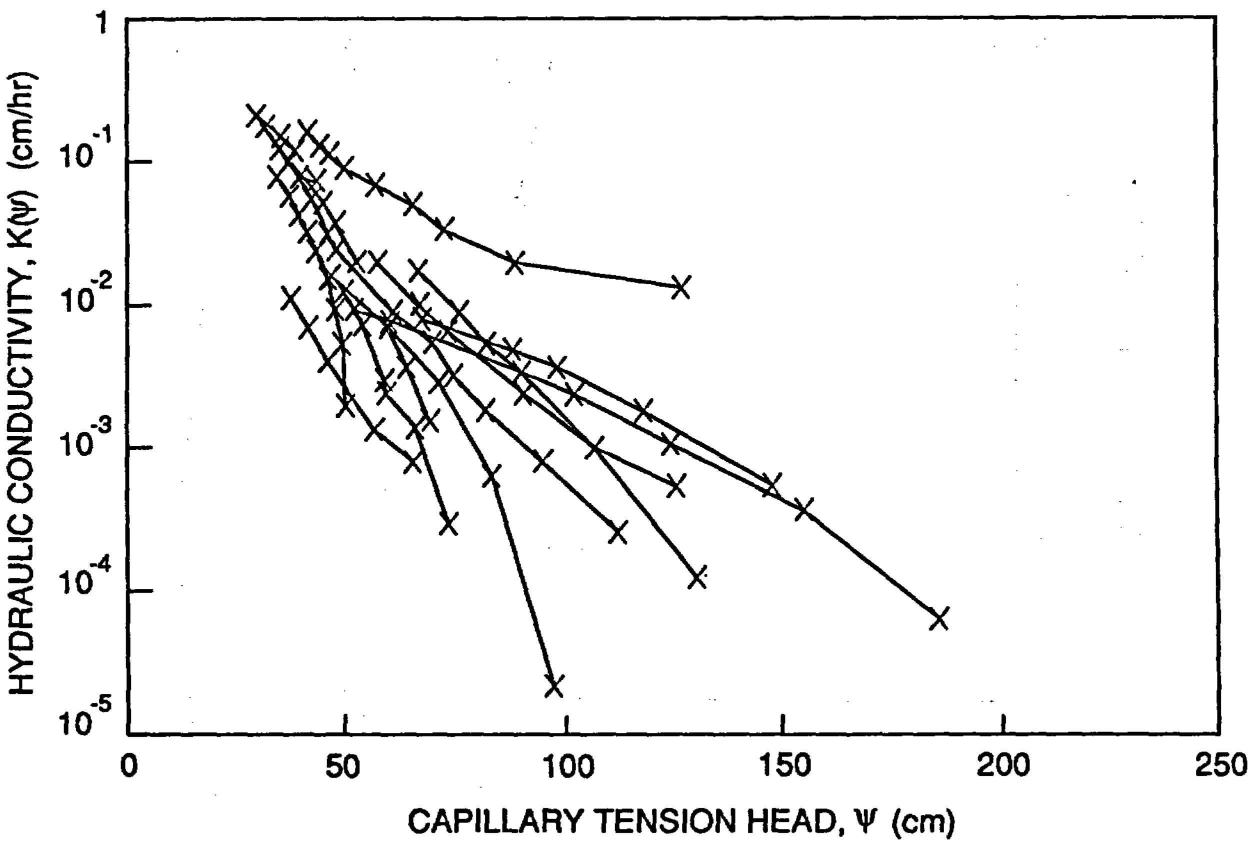

Figure 2-1. **Unsaturated hydraulic conductivity versus capillary tension head for the Maddock sandy loam. Each curve corresponds to a different spatial location. (Reproduced from Mantoglou and Gelhar, 1985)**

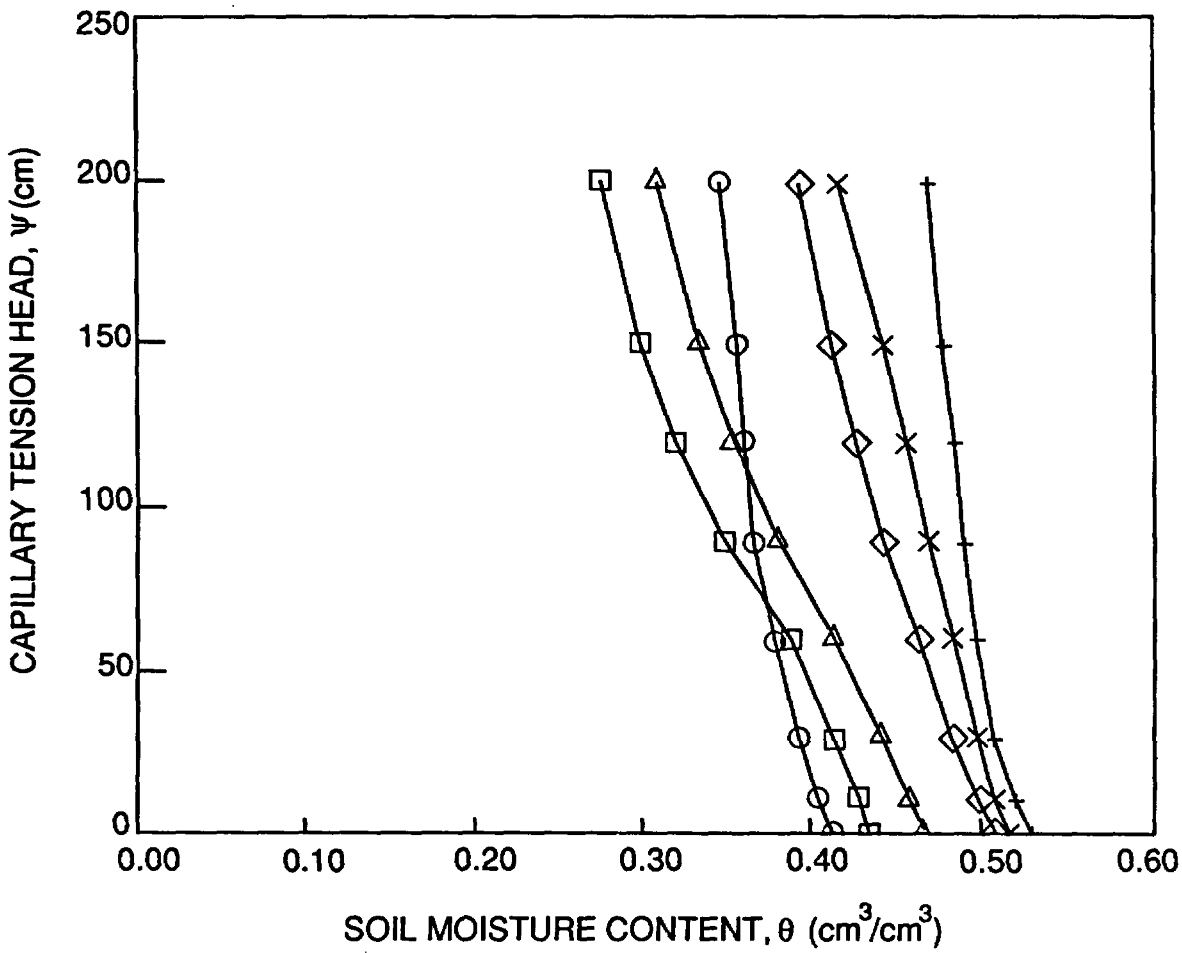

Figure 2-2. Capillary tension head versus soil moisture content for the Panoche silty clay loam. Each curve corresponds to a different spatial location. (Reproduced from Mantoglou and Gelhar, 1985)

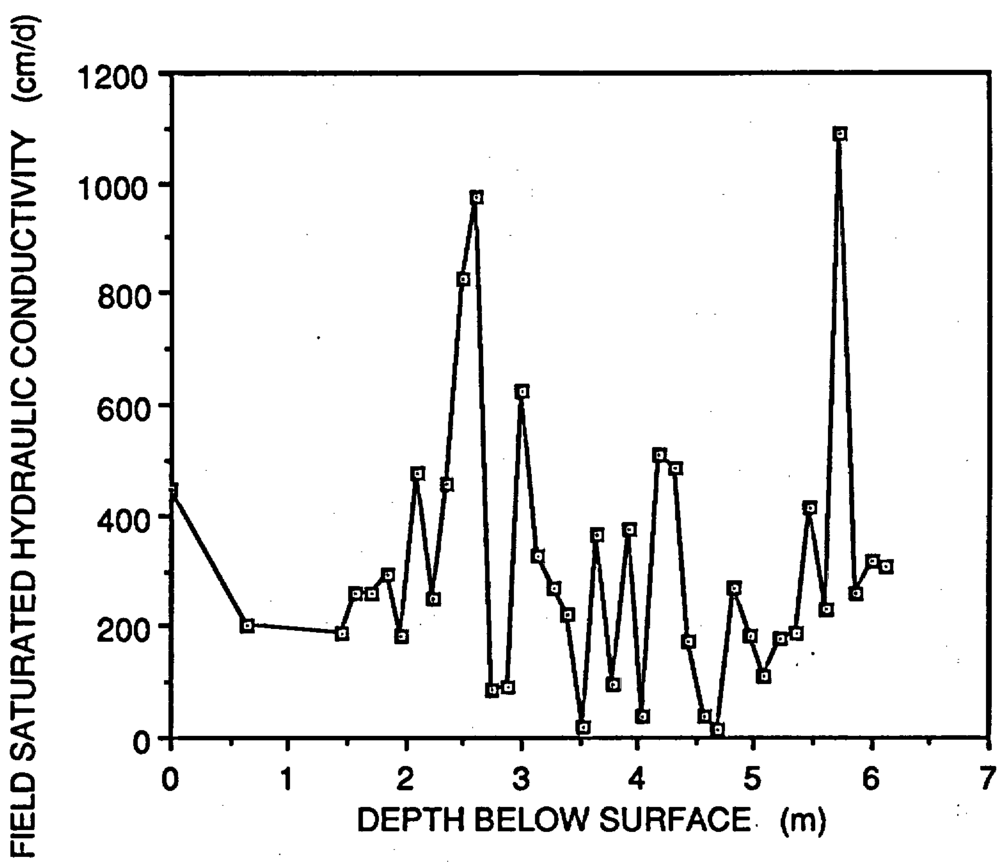

Figure 2-3. **Saturated hydraulic conductivity versus depth at the Las Cruces trench site 3.4 m from the west trench wall. Data collected using a Guelph permeameter. (Reproduced from Wierenga et al., 1986a)**

of the medium. Recognizing this influence, it is desirable to incorporate the details of heterogeneity into the modeling effort in order to capture the large-scale effects of local spatial variability and uncertainty. There is little doubt that if the spatial variation of local parameters was fully known large-scale phenomena could in principal be predicted, since the mechanisms and equations underlying the local behavior are quite well understood. However, this requires that one be able to (1) acquire the small-scale information, and (2) manipulate that information. The former implies collection of an enormous database of material, and clearly this is a very difficult and impractical requirement to satisfy. The latter refers to computational capabilities, which are rapidly increasing but are in general still not adequate to make detailed three-dimensional simulations feasible in practice. With these concepts in mind, a stochastic description of porous media offers an efficient mechanism to capture the essence of heterogeneity and spatial variability, based on a realistic data set. The spectral solution approach described in Mantoglou and Gelhar (1985, 1987a, b, c) offers a methodology to analyze the effects of small-scale parameter variability on large-scale phenomena.

2.2 Stochastic Unsaturated Flow Theory

2.2.1 Brief review of related work

Soil is spatially variable on scales as small as the size of a pore or as large as a soil formation. No two pore spaces or sand grains are exactly the same; nor do two lenses or layers have exactly the same physical properties. Soil scientists and groundwater hydrologists have long recognized this fact, and the trend in research is to develop ways to incorporate heterogeneity into models of soil systems. This section reviews some of the methods which have been used to include spatial variability and associated uncertainty into the modeling of unsaturated flow.

Effective soil properties

Subsurface flow can be modeled using deterministic methods, but because of the heterogeneous nature of the material, it is difficult to envision the complete knowledge of conductivity and moisture content implied by the use of a deterministic model. This brings hydrologists to ask if it is possible to define an *equivalent homogeneous system* that will provide a satisfactory representation of the heterogeneous system present in the real world. In other words, can "effective parameters" for the soil properties be defined that will display the mean behavior of the heterogeneous system? The development and applicability of effective parameters has been examined in the literature, primarily for the case of saturated flow systems [Warren and Price (1961); Freeze (1975); Gutjahr et al (1978); Smith and Freeze (1979); El–Kadi and Brutsaert (1985)] but with some discussion of unsaturated flow. The following literature review focuses on the unsaturated case.

Dagan (1982) analyzed the effective conductivity for unsteady saturated flow, showing that the effective conductivity is time dependent. This behavior could be interpreted as a kind of hysteresis although Dagan did not discuss his results in that way. Dagan and Bresler (1983) and Bresler and Dagan (1983) investigated effective parameters for one-dimensional vertical unsaturated flow, finding that the result was not a single parameter but rather an effective expression that represented the mean behavior. In the case of steady gravitational flow, the effective unsaturated conductivity was defined by an expression which varied between the geometic mean for the case of no ponding to the arithmetic mean for the case of flooding. In the unsteady flow case, these expressions were highly non-linear. Bresler and Dagan found that, in general, expressions for the effective parameters could not be derived and considered that a non-linear expression for the unsaturated effective conductivity was of no practical use. They concluded that, except for steady gravitational flow, effective parameters could not easily be defined and the concept of an equivalent porous medium was an invalid one in unsaturated systems. Of course these conclusions apply only to the rather artificial vertically homogeneous one-dimensional flow system which was analyzed.

Yeh et al (1982, 1985a, b, c) used stochastic perturbation methods to derive theoretical relationships for the effective conductivity for the steady unsaturated flow case in one, two and three dimensions, with the saturated hydraulic conductivity assumed to be log-normally distributed. They investigated the influence on effective parameters of flow normal and parallel to stratification for the case of multi-directional flow. It was found that when flow was parallel to the stratification, the effective conductivity approached the arithmetic mean and when flow was perpendicular to the stratification, the effective conductivity approached the harmonic mean. When the product of the vertical correlation scale and the slope of the logarithm of unsaturated hydraulic conductivity versus tension was large, however, both cases approached the geometric mean as a value of effective conductivity. One important discovery of the Yeh et al (1982, 1985a, b, c) analyses is the fact that *the anisotropy of effective conductivity in unsaturated flow is dependent on the mean tension.* Yeh et al (1985c) discuss several field observations and laboratory experiments which show qualitatively similar anisotropy effects, but this predicted behavior has not been investigated quantitatively. Mualem (1984) has analyzed anisotropy of the effective conductivity by assuming that the degree of anisotropy can be determined by taking the ratio of arithmetic and harmonic means.

Stochastic modeling

In one of the early attempts to account for the heterogeneous nature of unsaturated soils, Bouwer (1969) applied a Green-Ampt model of one-dimensional infiltration to a medium that had a variable unsaturated hydraulic conductivity. In essence, Bouwer simulated a one-dimensional soil column as a layered medium; each layer was assigned a different, but not a random, value of unsaturated hydraulic conductivity. A modified Green-Ampt model was used to calculate the infiltration rate and depth to the front in each layer. This model recognized the importance of heterogeneity in unsaturated flow but treated only heterogeneity in the vertical, not in the horizontal. The vertical variability was treated as deterministic rather than random, so although Bouwer recognized the variability of the medium, he did not take into account the uncertainty associated with that variability.

Warrick and Amoozegar-Fard (1979, 1981) presented a technique which used a similar media concept to develop a scaled version of the unsaturated flow equation. This scaled version was solved for infiltration using the quasi-analytical method of Philip (1969), and for drainage using a numerical technique developed by Rubin and Steinhardt (1963). The resulting equations for infiltration and drainage were written in terms of the scaling parameter. Warrick and Amoozegar-Fard also performed Monte-Carlo simulations of infiltration and drainage by treating the scaling parameter as an independent random variable. This introduced randomness, but not spatial correlation. Layering in the vertical was ignored; the models were one-dimensional and homogeneous in the vertical once the random scaling factor was chosen.

Philip (1980) studied unsteady unsaturated one-dimensional flow in a stochastic sense by using scaled values of hydraulic conductivity and tension based on a characteristic length scale of the medium. Flow was simulated through a layered one-dimensional system where layers were restricted to one of two types of soil, each with a characteristic length scale, with a probability of occurrence of either soil of 1/2. Thus the characteristic length became the random variable. The flow system was solved using the Philip (1969) solution to examine the resulting sorbtivity, S, an integrated parameter which appears in this quasi-analytic analysis. Sorbtivity could be thought of as a single parameter incorporating the effects of capillarity on transient flow processes. Philip found the effective sorbtivity of the column to be less than the individual sorbtivity of the layers; it was also less than the arithmetic or geometric mean of the sorbtivity of the layers. This model attempted to treat the spatial nature of the variability, at least in the flow direction. It was limited, however, by its one-dimensionality and by the fact that the variability was restricted to the length scale parameter only.

Dagan and Bresler (1983) and Bresler and Dagan (1983) studied stochastic modeling of one-dimensional unsteady unsaturated flow beginning with the Richards equation and a set of deterministic boundary and initial conditions and using empirical, non-hysteretic models for the unsaturated conductivity and moisture content relationships. The empirical relationships were written as a function of six soil parameters, one of which was the saturated hydraulic conductivity. Although all of these parameters could be considered spatially variable, only the saturated hydraulic conductivity was treated as a random variable and in particular a log-normal random variable. Conductivity was written in terms of a scaling parameter; a probability density function was assigned to the scaling factor, thus making the saturated hydraulic conductivity variable. The Richards equation was solved approximately using a Green-Ampt procedure. This yielded saturation as a function of depth and time for selected values of saturated hydraulic conductivity. Means and variances of the soil parameters such as moisture content and tension were calculated using statistical averaging and the given probability density function. This analysis showed good results in estimating the means and variances of the soil parameters, but did not model the actual flow system very well. The major limitation here was that the model assumed each one-dimensional column to be homogeneous with an assigned saturated hydraulic conductivity. In other words, the analysis considered spatial variation in the horizontal plane but not in the vertical.

Andersson and Shapiro (1983) investigated one-dimensional steady unsaturated flow using both Monte-Carlo simulations and a perturbation method with a goal of obtaining output means and variances of moisture content. The analysis began with the Richards equation and empirical relations for unsaturated hydraulic conductivity and moisture content as functions of tension and space. For the Monte-Carlo technique, a nearest neighbor random field generator adopted from Smith and Freeze (1979) was used to create a set of spatially correlated conductivity values. Using these values as inputs, the Richards equation was solved numerically, output values of moisture content were calculated, and means and variances of moisture content were determined. For the perturbation technique, a stochastic differential moisture content were determined. For the perturbation technique, a stochastic differential equation was developed and solved where the hydraulic conductivity was the input random field. A solution for tension was the result, which was converted into a value of moisture content using an empirical relationship. From this, closed–form expressions for the mean and variance of moisture content were derived. Several test cases were examined, and the means and variances determined using both methods were compared. In all cases examined, a good comparison was found between the Monte-Carlo results and the perturbation results. Recall that for this study, only one-dimensional steady unsaturated flow was examined.

As can be seen by this review, much of the work done in stochastic modeling of the unsaturated zone has involved only one-dimensional soil columns. Often these columns were assumed to be homogeneous in the vertical once a random value of either conductivity or a scaling parameter had been assigned to it. Most of the analyses were for steady flow; little has been done for the case of unsteady unsaturated flow. Note that the variable of interest to investigators was most often the hydraulic conductivity. The majority of work has involved Monte-Carlo simulations, though some work has used analytical procedures such as perturbation techniques. It is clear from this overview that further studies into stochastic modeling of unsaturated flow would enhance present understanding, especially in the area of unsteady multi-dimensional flow.

2.2.2 Stochastic description of unsaturated soil hydraulic properties

As mentioned earlier, the soil properties used to describe unsaturated flow, the hydraulic conductivity $K(\psi)$ and the moisture content $\theta(\psi)$, both depend on the soil water tension head ψ. The stochastic description of spatial variability adopted here requires that the functions $K(\psi)$ and $\theta(\psi)$ be expressed in terms of a small number of measurable parameters. Mantoglou and Gelhar (1985) adopt the hydraulic conductivity parameterization proposed by Gardner (1958)

$$\ln K(\psi) = \ln K_s - \alpha\psi \qquad (2\text{–}1)$$

This parameterization makes the analysis that Mantoglou and Gelhar (1985, 1987a) follow more tractable and it provides a reasonably good description of observed $K(\psi)$ characteristics in soils over a certain range of tension values (see Figure 2-1). Its implications about the $K(\psi)$ values for high tensions will be examined in Section 2.2.5. In general, the parameter α depends on the actual tension head value. Furthermore if local parameters exhibit hysteresis, $\ln K$ and α will also depend on the time history of the tension (i.e., wetting or drying conditions).

Various parameterizations may also be adopted for the moisture content $\theta(\psi)$ or, equivalently, for the specific moisture capacity $C(\psi)$, defined as $C(\psi) = -\partial\theta/\partial\psi$. Mantoglou and Gelhar (1985, 1987a) suggest, for example, a linear approximation for $\theta(\psi)$. Since we do not adopt a stochastic description for $\theta(\psi)$ in this report, we do not need to parameterize the moisture content function. We will, therefore, retain the general functional notation $\theta(\psi)$.

It is assumed that the local soil properties $\ln K_s(x)$ and $\alpha(x)$ are realizations of three-dimensional, spatially correlated random fields composed of two components

$$
\begin{aligned}
\ln K_s &= F + f \\
\alpha &= A + a
\end{aligned}
\tag{2–2}
$$

where F and A are large-scale components and f and a are small-scale components of $\ln K_s$ and α, respectively. The large-scale components F and A are assumed to be smooth deterministic spatial functions that represent "mean" behavior, while the small-scale components f and a are realizations of three-dimensional zero mean second-order stationary random fields which represent "fluctuations" from the mean.

The decomposition suggested by (2-2) implies that there is a distinct disparity between the scales of variation of the two components and will not be valid in cases where these scales overlap. For the developments that will be presented in the following sections it is implied that the mean properties F and A are practically constant at the scale of the flow domain under consideration, while the local fluctuations have a scale of variation much smaller than the scale of the flow domain.

2.2.3 Derivation of large-scale models and effective parameters

One of the objectives of the stochastic approach to heterogeneous unsaturated flow is to develop equations that apply at large scales and which take into consideration the local variability of the unsaturated hydraulic soil properties. The effects of variability are expressed in the governing equations through effective parameters. The starting point is the local-scale flow equation. On a local scale, conservation of mass for soil moisture of constant density moving in a rigid soil matrix leads to

$$
-\frac{\partial \theta}{\partial t} = \frac{\partial q_i}{\partial x_i} \qquad i = 1,2,3 \tag{2–3}
$$

where θ is the soil moisture content (in cm^3/cm^3) and q_i is the specific discharge in the direction x_i (in centimeters per second); x_1, x_2, x_3 are the coordinates of a Cartesian system and repeated indices are understood to be summed so, for example, the divergence operator is written as

$$
\frac{\partial q_i}{\partial x_i} = \frac{\partial q_1}{\partial x_1} + \frac{\partial q_2}{\partial x_2} + \frac{\partial q_3}{\partial x_3} \tag{2–4}
$$

It is further assumed that the local specific discharge can be expressed as a Darcy equation

$$
q_i = K(\psi)\,\frac{\partial(\psi + z)}{\partial x_i} \tag{2–5}
$$

Then the conservation of mass equation can be rewritten as

$$
-\frac{\partial \theta}{\partial t} = C\,\frac{\partial \psi}{\partial t} = \frac{\partial}{\partial x_i}\left[K(\psi)\,\frac{\partial(\psi + z)}{\partial x_i}\right] \tag{2–6}
$$

where ψ is the (positive) capillary tension head (in centimeters of water), K is the local unsaturated hydraulic conductivity (in centimeters per second), z is the vertical position with z increasing downward (in centimeters), and $C = -\partial\theta/\partial\psi$ is the specific moisture capacity. Note that the local hydraulic conductivity is assumed to be isotropic (i.e., $K_1 = K_2 = K_3 = K$).

If the decomposition presented in (2-2) is followed, the local flow equation (2-6) can be viewed as a partial differential equation with stochastic parameters and therefore a stochastic output ψ. It is then possible to express ψ as

$$\psi = H + h \tag{2-7}$$

where H is the mean of ψ and h represents fluctuations around the mean. Taking the expected value of (2-6) with respect to f and a yields

$$-\frac{\partial}{\partial t}\left\{E[\theta]\right\} = \frac{\partial}{\partial x_i}\left\{E\left[K\frac{\partial(\psi + z)}{\partial x_i}\right]\right\} \tag{2-8}$$

Equation (2-8) would be more useful if the expected values within the brackets could be expressed in terms of the mean soil properties, the mean flow characteristics and the statistical parameters of f and a. In the left hand side, $E[\theta]$ represents the mean soil moisture content $\Theta \equiv E[\theta]$. Mantoglou and Gelhar (1987a) propose a local linearization of θ around the mean tension head (assuming that the perturbation h is "small") which yields, for deterministic $\theta(\psi)$

$$\Theta = E\,[\theta(\psi)] = E\left[\theta(H) + \left.\frac{\partial\theta}{\partial\psi}\right|_{\psi=H} \cdot h\right] = \theta(H) \tag{2-9}$$

and the effective specific moisture capacity is then defined by

$$\hat{C} = -\,\partial\Theta/\partial H = C(H) \tag{2-10}$$

Note that $\theta(H)$ is known since the $\theta(\psi)$ relationship is known.

In the right hand side of (2-8), the term in square brackets is equivalent to the flux (2–5) which in the general case is a three-dimensional vector. The system of axes (x_1, x_2, x_3) is oriented in the direction of the principal statistical anisotropy axes of the random fields f and a where it is assumed that these axes coincide for f and a. This assumption could be relaxed if information about the orientation of the two different fields was available. Incorporating the decompositions (2-2) and (2-7) into (2-1), the expected value in the right hand side of (2-8) can be written as

$$E[q_i] = K_M\, E\left[\exp(f - Ah - Ha - ah + E[ah])\left(J_i + \frac{\partial h}{\partial x_i}\right)\right] \tag{2-11}$$

where the parameters

$$K_M = e^{F-AH-E[ah]} = K_G\, e^{-AH-E[ah]}$$

$$J_i = \frac{\partial(H+z)}{\partial x_i} \qquad (2\text{–}12)$$

The terms E[ah] included in the exponential terms of (2-11) and (2-12) have opposite sign and thus combine to multipy the right side of (2-11) by unity. These terms have been deliberately included in this manner so that the arguments of the exponential in (2-11) are zero-mean. The fact that the perturbation terms are small suggests an expansion of the exponential in a series around zero, and thus a zero-mean argument is desired. The incorporatioin of the E[ah] terms to facilitate zero-mean arguments is the approach used by Mantoglou and Gelhar (1987a) and represents a correction to the analysis of Mantoglou and Gelhar (1985).

In order to evaluate the expected value in (2-11), Mantoglou and Gelhar (1987a) expand the exponential in a Taylor series and keep only second order terms to obtain

$$E[q_i] = K_M\left\{J_i\left[1+\frac{1}{2}E[(f-Ah-Ha)^2]\right] + E\left[(f-Ah-Ha)\frac{\partial h}{\partial x_i}\right]\right\} \qquad (2\text{–}13)$$

Equation (2-13) provides the basis for defining an effective hydraulic conductivity tensor. Such a tensor should have the property $E[q_i] = \hat{K}_{ij}J_j$ and be symmetric. A separation of (2–13) into components of this form is not possible, because as will be seen in Section 2.2.4 the terms inside the brackets depend on the spatial, as well as temporal, gradients of the mean tension head in a complex and nonlinear manner. However, if the additional assumption is made that the principal axes of $\hat{K}_{ij}$ are oriented in the principal statistical anisotropy axes of f and a [Mantoglou and Gelhar (1987a)], then one can define

$$\hat{K}_{ii} = \frac{E[q_i]}{J_i} \qquad i = 1,2,3 \qquad \text{no sum on i} \qquad (2\text{–}14)$$

while $\hat{K}_{ij} = 0$ for $i \neq j$, where x_i are the common principal statistical anisotropy axes. Admittedly, other definitions of the effective hydraulic conductivity tensor are possible and, in terms of the effect on the governing equation, they would be similar since it is the expected value of the specific discharge that enters in (2-8); however, the above definition of $\hat{K}_{ij}$ facilitates expressing the mean flow equation (2-8) in a form similar to the local governing equation (2–6). Also, this is consistent with the orientation of the effective hydraulic conductivity tensor principal axes that have been found for steady state saturated flow [Gelhar and Axness (1983)] and for steady unsaturated flow [Yeh et al (1985a, b, c)].

Using (2-13) in (2-14) one can find

$$\hat{K}_{ii} = K_M\left[1 + \frac{\sigma_\varepsilon^2}{2} + \frac{\tau_i}{J_i}\right] \qquad i = 1,2,3 \tag{2-15}$$

where

$$\sigma_\varepsilon^2 = E\,[(f - Ah - Ha)^2] = \sigma_f^2 + A^2\,E[h^2] + H^2\,\sigma_a^2$$
$$- 2A\,E[fh] - 2H\,E[fa] + 2AH\,E[ah] \tag{2-16a}$$

$$\tau_i = E\left[(f - Ah - Ha)\,\frac{\partial h}{\partial x_i}\right] = E\left[f\frac{\partial h}{\partial x_i}\right] - H\,E\left[a\frac{\partial h}{\partial x_i}\right] \tag{2-16b}$$

Recall that *these expressions are derived from a Taylor series expansion of the exponential in (2-11) and will only be valid when the exponent values are relatively small.* As mean tension increases, for example, (2-15) may predict values which lack any physical meaning. In order to alleviate such problems, Gelhar and Axness (1983) and Yeh et al (1985a, b, c) have proposed an "exponential generalization" for the effective hydraulic conductivities. It is assumed that the terms in the brackets of (2-15) are essentially the first two terms of a Taylor series expansion of an exponential, which can be reconstructed as follows:

$$\hat{K}_{ii} = K_M \exp\left(\frac{\sigma_\varepsilon^2}{2} + \frac{\tau_i}{J_i}\right) \qquad \text{no sum on i} \tag{2-17}$$

Substituting (2-10) and (2-17) into (2-8), the large-scale transient unsaturated flow model becomes

$$-\frac{\partial \Theta}{\partial t} = C(H)\frac{\partial H}{\partial t} = \frac{\partial}{\partial x_i}\left[\hat{K}_{ij}\,\frac{\partial (H + z)}{\partial x_j}\right] \tag{2-18}$$

which is of the same form as the local governing equation (2-6).

It is apparent from (2-15) and (2-16) that the effective hydraulic conductivity function appearing in (2-18) depends on a number of second-order moments of the fluctuations f, a, and h {i.e., σ_f^2, $E[h^2]$, σ_a^2, $E[fh]$, $E[fa]$, $E[f(\partial h/\partial x_i)]$, and $E[a(\partial h/\partial x_i)]$} as well as the mean quantities A and H. Although σ_f^2, σ_a^2, and A may be assumed to be *known* input statistics, and H is given by (2-18), the remaining moments needed to evaluate the effective conductivity are *unknown*. These moments can be evaluated, however, from the perturbation equation which is obtained if the *mean* flow equation is subtracted from the *perturbed* flow equation. In particular, if (2-18) is subtracted from (2-6) and if the fluctuations f and a are small, second order terms such as

$$fa - E[fa] \tag{2-19}$$

can be neglected compared to first-order terms, resulting in

$$\frac{\partial h}{\partial t} + \frac{K_M}{C(H)}\left(-\frac{\partial^2 h}{\partial x_i \partial x_j} + AC(H)Gh + AL_i \frac{\partial h}{\partial x_i}\right)$$

$$= \frac{K_M}{C(H)}\left[\left(J_i \frac{\partial f}{\partial x_i} + C(H)Gf\right) - \left(J_i H \frac{\partial a}{\partial x_i} + ba\right)\right] \qquad (2\text{–}20)$$

where

$$G = \frac{1}{K_M} J_t$$

$$J_t = \frac{\partial H}{\partial t}$$

$$L_i = J_i + \frac{\partial H}{\partial x_i}$$

$$b = J_i \frac{\partial H}{\partial x_i} + HC(H)G \qquad (2\text{–}21)$$

Based on arguments similar to those presented above in the development of (2–13) from (2–11), applied here for consistency in the linearization process, the term (-E[ah]) within K_M is included in the perturbation equation (2-20). Note that this term was not included by Mantoglou and Gelhar (1985, 1987a, b, c). The present analysis is consistent with the discussion provided by Mulford (1986), and represents a correction to the analysis of Mantoglou and Gelhar.

The procedure used to derive the required moments from (2-20) works with spectral representations of the fluctuations f, a, and h rather than with the fluctuations themselves. If the original fluctuations f, a, and h are viewed as realizations of stationary random fields, the corresponding Fourier-Stieltjes spectral amplitudes dZ_f, dZ_a, and dZ_h are defined as follows:

$$f(x) = \iiint_{-\infty}^{\infty} \exp(ik \cdot x)\, dZ_f(k)$$

$$a(x) = \iiint_{-\infty}^{\infty} \exp(ik \cdot x)\, dZ_a(k)$$

$$h(x,t) = \iiint_{-\infty}^{\infty} \exp(ik \cdot x)\, dZ_h(k,t) \qquad (2\text{–}22)$$

where $i = (-1)^{1/2}$, x is the vector spatial coordinate (x_1,x_2,x_3) and k is the corresponding wave number vector (k_1,k_2,k_3). The spectral amplitudes introduced here can be viewed as new random fields which are functions of wave number rather than location. Equation (2-22) states that the random perturbations f(x) and a(x) are the Fourier-Stieltjes transforms of the spectral amplitudes. This *spectral representation* of the random fluctuations is convenient because it allows (2-20) to be readily solved in the wave number domain. This is accomplished by substituting the individual components of (2-22) directly into (2-20) to yield

$$\frac{\partial(dZ_h)}{\partial t} + \frac{K_M}{C(H)}\left[k_1^2 + k_2^2 + k_3^2 + AC(H)G + iAL_jk_j\right]dZ_h$$

$$= \frac{K_M}{C(H)}\left[(i\, J_jk_j + C(H)G)\, dZ_f - (iHJ_jk_j + b)\, dZ_a\right] \qquad (2\text{–}23)$$

In principle, (2-23) can be formally solved for dZ_h; it is a first-order ordinary differential equation with dZ_h the dependent variable and k a parameter. Mantoglou and Gelhar (1987a) present the general solution. However, as will be seen later, it is not dZ_h but the various spectra constructed with dZ_h [S_{hh}, S_{hf}, S_{ha}] that are sought. For present purposes, it is sufficient to note that the general solution of (2-23) can be written as

$$dZ_h(k) = W_f(k)dZ_f(k) + W_a(k)dZ_a(k) \qquad (2\text{–}24)$$

where it has been assumed that time t is relatively large, W_f and W_a are three-dimensional system response functions [defined in a precise way by Mantoglou and Gelhar (1987a)], and the dependence of $dZ_h(k)$, W_f and W_a on time is implied.

The wave number solution summarized in (2-24) may be used to derive the moments included in the effective conductivity expressions given in (2-15) and (2-16). The derivation is based on several spectral representation properties which will now be discussed briefly. Consider two cross-correlated stationary random fields u(x) and v(x). If $dZ_u(k)$ and $dZ_v(k)$ are the corresponding random Fourier-Stieltjes amplitudes of the real random fields u(x) and v(x), the following property holds [Lumley and Panofsky (1964)]:

$$\begin{aligned} E[dZ_u(k_1)\, dZ_v^*(k_2)] &= S_{uv}(k)dk \qquad && \text{if } k_1 = k_2 \\ &= 0 && \text{otherwise} \end{aligned} \qquad (2\text{–}25)$$

where $S_{uv}(k)$ is the cross-spectral density function of u and v. The expected value of u(x)v(x) can be evaluated as

$$E[uv] = E\left[\iiint_{-\infty}^{\infty} e^{ik_1x}\, dZ_u(k_1) \iiint_{-\infty}^{\infty} e^{-ik_2x}\, dZ_v^*(k_2)\right]$$

$$= \iiint_{-\infty}^{\infty} S_{uv}(k)dk \qquad (2\text{–}26)$$

Replacing u and v with h, f, a, and $\partial h/\partial x_i$ as required, the moments appearing in (2-16) are

$$E[h^2] = \sigma_h^2 = \iiint_{-\infty}^{\infty} S_{hh}(\mathbf{k})d\mathbf{k} \qquad (2\text{–}27)$$

$$E[fh] = E[hf] = \iiint_{-\infty}^{\infty} S_{hf}(\mathbf{k})d\mathbf{k} \qquad (2\text{–}28)$$

$$E[ah] = E[ha] = \iiint_{-\infty}^{\infty} S_{ha}(\mathbf{k})d\mathbf{k} \qquad (2\text{–}29)$$

$$E\left[f\frac{\partial h}{\partial x_i}\right] = E\left[\frac{\partial h}{\partial x_i}f\right] = \iiint_{-\infty}^{\infty} (ik_i)\, S_{hf}(\mathbf{k})d\mathbf{k} \qquad (2\text{–}30)$$

$$E\left[a\frac{\partial h}{\partial x_i}\right] = E\left[\frac{\partial h}{\partial x_i}a\right] = \iiint_{-\infty}^{\infty} (ik_i)\, S_{ha}(\mathbf{k})d\mathbf{k} \qquad (2\text{–}31)$$

The various spectra needed to evaluate these moment expressions can be found from (2-24) and (2-25) if the spectra of the input processes f and a are given. An important special case is analyzed in detail in the next subsection.

Of particular note among the moment expressions presented here is (2-27), which represents the variance of the mean tension head. In addition to its contribution to the evaluation of effective conductivity [see (2-15) and (2-16)], the tension head variance provides a means to analyze uncertainty within the mean tension prediction provided by the solution of (2-18). As discussed below, the variance has been found to depend on various factors, including mean tension and the spatial gradient of tension.

2.2.4 The stratified soil case

Mantoglou and Gelhar (1987b, c) have developed closed–form solutions for the capillary tension head variance (σ_h^2), the mean soil moisture content (Θ), the effective specific soil moisture capacity ($\hat{C}$), and the effective hydraulic conductivity tensor ($\hat{K}_{ij}$) for transient unsaturated flow in stratified soils. Note that stratification of a soil that is modeled as a random field can be expressed through the ratio of the vertical and horizontal correlation scales of the log hydraulic conductivity field. If x_1 is aligned perpendicular to the stratification (pointing downwards) and along one of the principal axes of orientation of f where the correlation scale is λ_1, then x_2 and x_3 correspond to the horizontal coordinate axes with λ_2 and λ_3 the correlation scales along these directions, respectively. A stratified soil has correlation scale aspect ratios λ_1/λ_3 and λ_1/λ_2 smaller than one and a perfectly stratified soil has $\lambda_1/\lambda_3 \to 0$, $\lambda_2/\lambda_3 \to 1$. In the following developments, the correlation scales enter the equations through the correlation function, or more precisely through its Fourier transform, the spectrum. It is assumed here that f and a both follow an exponential covariance function with identical correlation lengths. The corresponding spectral density functions may be written as

$$S_{ff}(k) = \frac{\sigma_f^2 \lambda_1 \lambda_2 \lambda_3}{\pi^2 (1 + \lambda_1^2 k_1^2 + \lambda_2^2 k_2^2 + \lambda_3^2 k_3^2)^2} \tag{2-32}$$

$$S_{aa}(k) = \frac{\sigma_a^2 \lambda_1 \lambda_2 \lambda_3}{\pi^2 (1 + \lambda_1^2 k_1^2 + \lambda_2^2 k_2^2 + \lambda_3^2 k_3^2)^2} \tag{2-33}$$

The assumption of identical correlation lengths is considered a reasonable one made in the absence of sufficient information about the form of the correlation function of a; it can easily be changed if more information is available.

The assumption of perfect stratification introduced into (2-23) leads to

$$\frac{\partial(dZ_h)}{\partial t} + \frac{K_M}{C(H)}\left[k_1^2 + AC(H)G + iAL_1k_1\right]dZ_h$$

$$= \frac{K_M}{C(H)}\left[(i\,J_1k_1 + C(H)G)dZ_f - (iHJ_1k_1 + b)dZ_a\right] \tag{2-34}$$

Comparing (2-34) to (2-23) it can be observed that as a consequence of the stratification, $dZ_h(k,t)$ depends only on the k_1 wave number. Mantoglou and Gelhar (1987b, c) investigate the case where $\partial(dZ_h)/\partial t$ is small compared to the other terms, which gives

$$dZ_h = \frac{i\,J_1k_1 + C(H)G}{k_1^2 + AC(H)G + i\,AL_1k_1}\,dZ_f$$

$$- \frac{i\,HJ_1k_1 + b}{k_1^2 + AC(H)G + i\,AL_1k_1}\,dZ_a \tag{2-35}$$

The assumption of $\partial(dZ_h)/\partial t$ being small is reasonable, according to Mantoglou and Gelhar (1985), only when the mean capillary tension head H is relatively large (dry soils).

Mantoglou and Gelhar (1987b) obtained general and approximate asymptotic solutions for the capillary tension head variance, the mean soil moisture content and the specific soil moisture capacity using the simplified spectral equation (2-35) and assuming spectral density functions corresponding to an exponential covariance function for the fluctuations. They investigated two extreme cases of soil property interactions:

- f and a uncorrelated
- f and a perfectly correlated

The general solutions involve integrals which can be evaluated analytically, as shown in the Appendix of Mantoglou and Gelhar (1987b). The asymptotic expressions, which reveal in a simpler manner the interaction among the various parameters, are obtained by examining the magnitude of variable G, given by

$$G = e^{-F + AH + E[ah]} \frac{\partial H}{\partial t} \tag{2-36}$$

In the transient case when H is large (relatively dry soil), G tends to $+\infty$ or $-\infty$ depending on the sign of $\partial H/\partial t$. In the steady-state case, or in the case of H being small (wet soil) and $\partial H/\partial t$ being small (almost steady-state), $G \rightarrow 0$.

Mantoglou and Gelhar (1987b) show that the most important flow characteristics that affect the variance, particularly at high tension, are H and J_t ($= \partial H/\partial t$). For this reason they investigated the dependence of σ_h^2 on H and J_t, fixing the spatial derivatives at $J_1 = 1$, $J_2 = J_3 = 0$ (conditions that approximately hold near the core of a soil moisture plume in a horizontally stratified formation). The soil parameters correspond to Panoche clay loam and Maddock sandy loam [Nielsen et al (1973); Carvallo et al (1976)]. Using past information about soil property variability in natural soil formations [e.g., Gelhar and Axness (1983)], an approximate correlation length $\lambda_1 = 100$ cm in the direction perpendicular to stratification was assumed (and, of course, $\lambda_2, \lambda_3 \gg \lambda_1$). The dependence of σ_h^2 on H and J_t is shown in Figure 2-4 where σ_h^2 is plotted as a function of H for a set of discrete values of J_t. The values of σ_h^2 predicted using the asymptotic expressions for $G \rightarrow \pm\infty$ and $G \rightarrow 0$ are also plotted for comparison. Some general remarks on these results are:

- for H and/or J_t small, σ_h^2 follows closely the asymptotic curve predicted for $G \rightarrow 0$
- σ_h^2 increases much faster with respect to H than with respect to $|\partial H/\partial t|$
- for a fixed H, σ_h^2 increases as $|\partial H/\partial t|$ increases. In addition, σ_h^2 tends to be larger for $\partial H/\partial t < 0$ (wetting vs. drying)
- for high $|\partial H/\partial t|$ values, the general expressions for σ_h^2 approach the asymptotic ones, as H increases, much faster than for low $|\partial H/\partial t|$
- the dependence of σ_h^2 on the time history of H implies a hysteresis of the variance σ_h^2. The variance is larger in the case of wetting than it is in the case of drying.

The effective hydraulic conductivities of transient unsaturated flow in stratified soils are presented by Mantoglou and Gelhar (1987c). Using the "exponential generalization" assumption, the general form describing $\hat{K}_{ii}$ was given in (2-17). Evaluation of terms in (2–16), required for the determination of $\hat{K}_{ii}$ is discussed by Mantoglou and Gelhar (1987b, c). These terms involve integrals which are evaluated analytically. Figure 2-5 demonstrates the dependence of $\hat{K}_{11}$ and $\hat{K}_{22}$ on H and J_t, which are considered to have a pronounced effect. The soil properties assumed correspond to the Maddock soil, and the spatial gradients are held contant [$J_1 = 1$, $J_2 = J_3 = 0$]. Some remarks on this result are as follows:

- the horizontal conductivity ($\hat{K}_{22}$) is larger than the vertical conductivity ($\hat{K}_{11}$)
- $\hat{K}_{11}$ and $\hat{K}_{22}$ depend on the sign of J_t (drying or wetting), especially at high tension
- the effective hydraulic conductivity perpendicular to stratification ($\hat{K}_{11}$) is smaller for decreasing H (wetting) than it is for increasing H (drying)

a.) Wetting Case

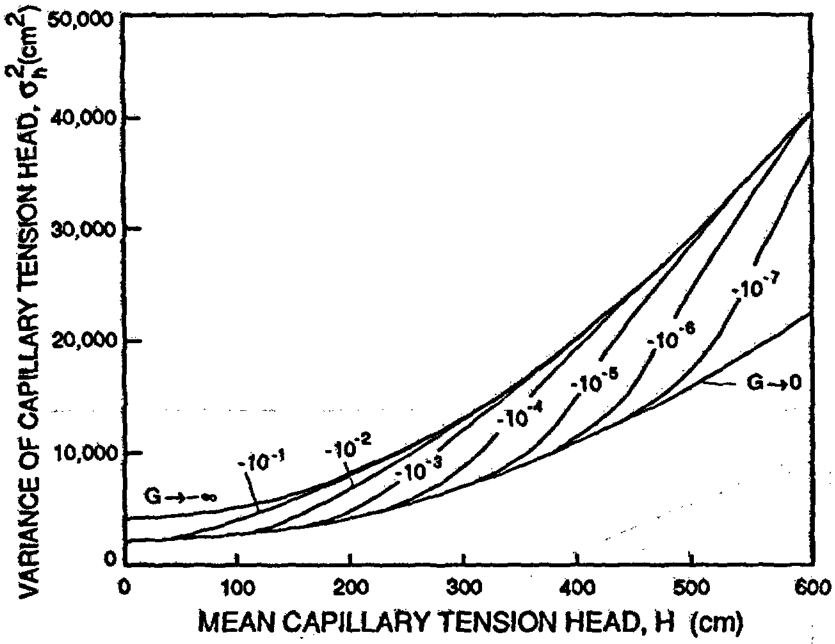

b.) Drying Case

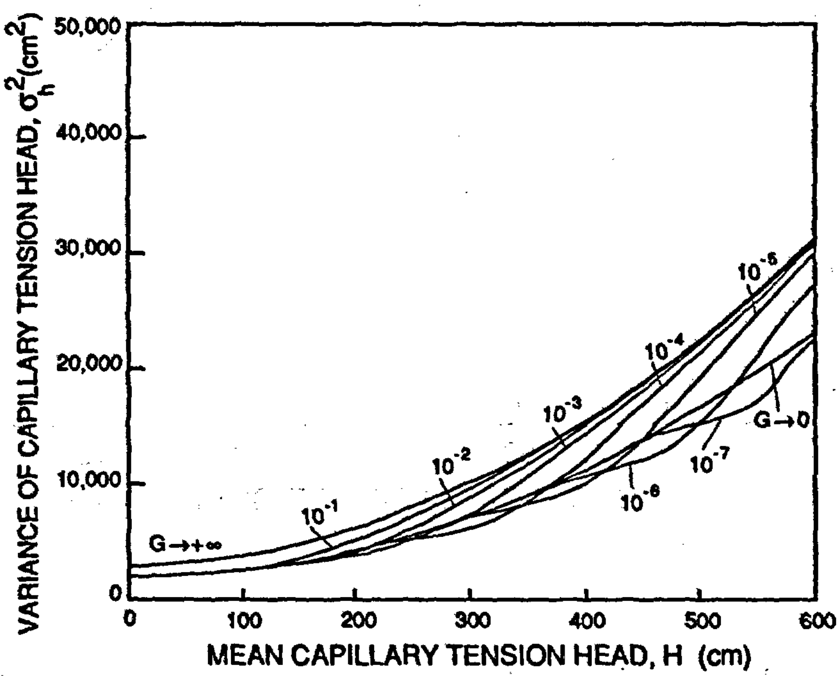

Figure 2.4 **Variance of capillary tension head versus mean capillary tension head for the Panoche silty clay loam. The curves correspond to different values of J_t. The asymptotic curves for G→ 0 and G→ ± ∞ are also shown. (Reproduced from Mantoglou and Gelhar, 1985)**

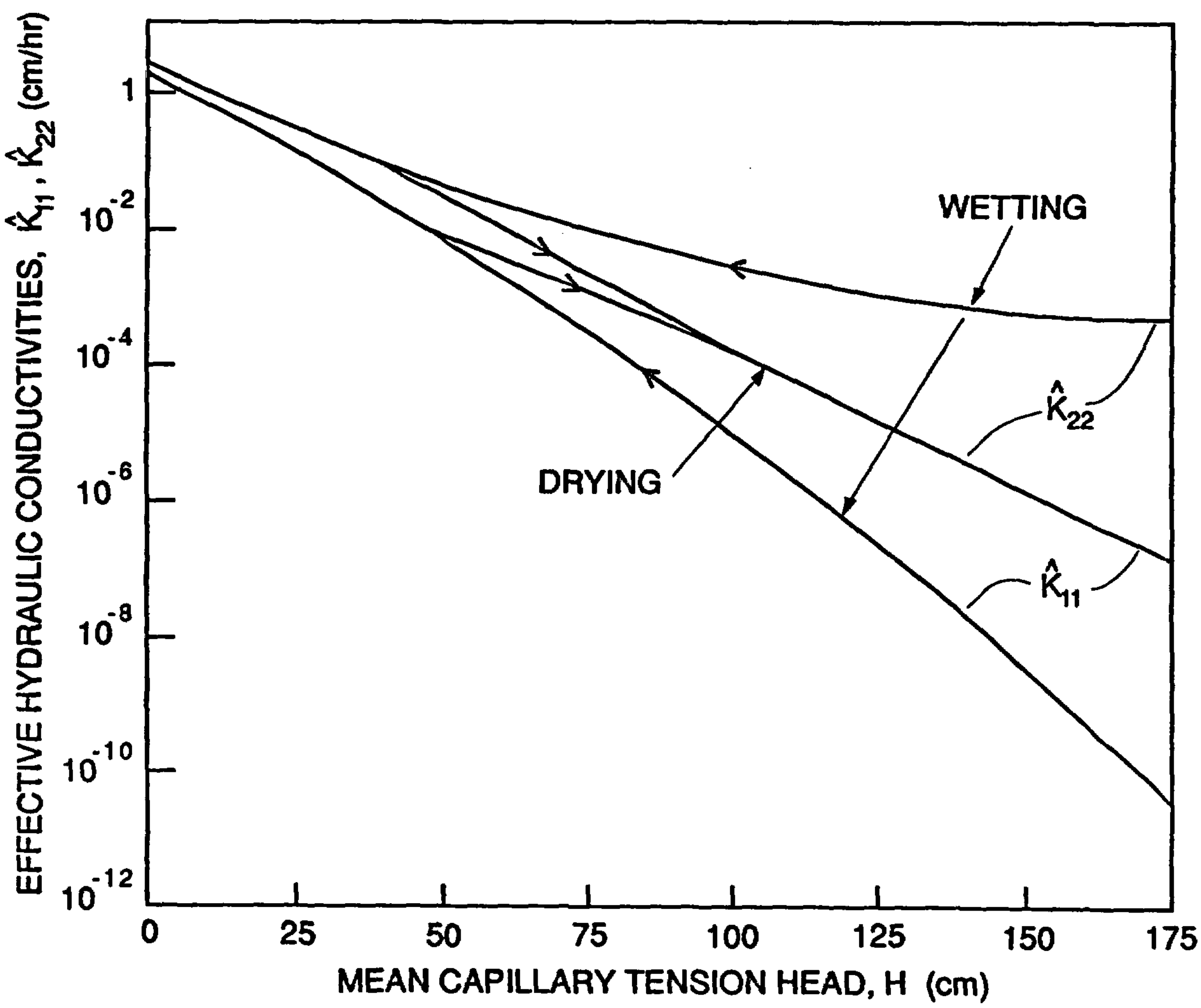

Figure 2-5. **Vertical and horizontal hydraulic conductivities versus mean capillary tension head for the Maddock sandy loam with $J_t = \pm\ 0.01$ cm/s, illustrating hysteresis and anisotropy of the effective hydraulic conductivities. (Reproduced from Mantoglou and Gelhar, 1985)**

- the horizontal effective hydraulic conductivity ($\hat{K}_{22}$) is larger for decreasing H (wetting) than it is for increasing H (drying)
- the anisotropy ratio in the case of wetting is large, particularly for dry soils

Note that Figure 2-5 does not correspond to an actual flow situation, since in such a case the H and $\partial H/\partial t$ are time dependent and can be determined by a simultaneous solution of the large-scale mean flow equation (as will be done in Chapter 4). Some of the remarks above are also applicable to the approximate asymptotic evaluations of Mantoglou and Gelhar (1987c). For the case of deterministic moisture content, the asymptotic expressions are

for wetting ($G \rightarrow -\infty$)

$$\hat{K}_{11} = K_G \exp\left[-AH - \frac{\sigma_f^2}{2}\left(\frac{1+\zeta^2 H^2}{AL_1\lambda_1}\right) + \frac{\sigma_a^2 H}{A}\right]$$

$$\hat{K}_{22} = K_G \exp\left[-AH + \frac{\sigma_f^2}{2}\left(\frac{1+\zeta^2 H^2}{AL_1\lambda_1}\right) + \frac{\sigma_a^2 H}{A}\right] \qquad (2\text{–}37)$$

for drying ($G \rightarrow +\infty$)

$$\hat{K}_{11} = K_G \exp\left(-AH + \frac{\sigma_a^2 H}{A}\right)$$

$$\hat{K}_{22} = K_G \exp\left(-AH + \frac{\sigma_a^2 H}{A}\right) \qquad (2\text{–}38)$$

for steady-state ($G \rightarrow 0$)

$$\hat{K}_{11} = K_G \exp\left[-AH - \frac{\sigma_f^2}{2}\left(\frac{1+\zeta^2 H^2}{1+AL_1\lambda_1}\right) + \sigma_f^2 \frac{J_1\lambda_1\zeta^2 H}{1+AL_1\lambda_1}\right]$$

$$\hat{K}_{22} = K_G \exp\left[-AH + \frac{\sigma_f^2}{2}\left(\frac{1+\zeta^2 H^2}{1+AL_1\lambda_1}\right) + \sigma_f^2 \frac{J_1\lambda_1\zeta^2 H}{1+AL_1\lambda_1}\right] \qquad (2\text{–}39)$$

where $\zeta^2 = \sigma_a^2/\sigma_f^2$. For $G \rightarrow -\infty$, the anisotropy ratio can be estimated from

$$\frac{\hat{K}_{22}}{\hat{K}_{11}} = \exp\left[\frac{\sigma_f^2 + \sigma_a^2 H^2}{AL_1\lambda_1}\right] \qquad (2\text{–}40)$$

The degree is anisotropy increases as σ_f^2 and/or σ_a^2 increases and/or $AL_1\lambda_1$ decreases. For drying ($G \rightarrow +\infty$), $\hat{K}_{11} = \hat{K}_{22}$. Finally, for steady-state ($G \rightarrow 0$)

$$\frac{\hat{K}_{22}}{\hat{K}_{11}} = \exp\left[\frac{\sigma_f^2 + \sigma_a^2 H^2}{1 + AL_1\lambda_1}\right] \tag{2-41}$$

which shows that the anisotropy ratio increases as H increases, but is smaller than that in the wetting case, particularly for small $AL_1\lambda_1$ (i.e., fine and or small-scale variable soil).

Two features of large-scale unsaturated flow which have been identified in these analyses are of significant practical importance:

- the large-scale hysteresis
- the tension-dependent and time-history-dependent anisotropy of the effective hydraulic conductivities

The reader can find further discussions of the physical meaning and the practical implications of these results in Mantoglou and Gelhar (1987a, b, c).

2.2.5 Operational modifications to the basic theory

The generalized model to be analyzed in solving the large-scale mean flow problem is (2-18), repeated here for convenience:

$$C(H)\frac{\partial H}{\partial t} = \frac{\partial}{\partial x_i}\left[\hat{K}_{ij}\,\frac{\partial(H+z)}{\partial x_j}\right] \tag{2-42}$$

This equation is the same as the traditional Richards equation, except for the use of an *effective conductivity function* obtained from a stochastic analysis of heterogeneity. By assuming that the soil moisture retention is not variable, input variability is confined to the saturated hydraulic conductivity [K_s in (2-1)] and to the slope of the log hydraulic conductivity versus tension curve [α in (2-1)]. This allows closer examination of the effects caused by variability in the conductivity-based parameters, which are often the parameters of most interest (see Section 2.2.1). By analyzing (2-42), the effects of the variability in conductivity-based parameters and the consequences of using an effective conductivity function based on stochastic theory can be explored while still enabling the use of solution techniques which are well established and reliable.

As seen above, the effective conductivity is a complicated function of several variables. For the stratified case analyzed in Section 2.2.4, this function can be represented by: $\hat{K}_{ij} = \hat{K}_{ij}$ (F, A, C(H), σ_f^2, σ_a^2, λ_1, H, $\partial H/\partial x_i$, $\partial H/\partial t$). Note that $\hat{K}_{ij}$ is a function of both the soil parameters F, A, C(H), σ_f^2, σ_a^2, λ_1, and of the mean flow characteristics H, $\partial H/\partial x_i$ and $\partial H/\partial t$.

In the numerical simulations described in Chapter 4, the inclusion of the spatial gradient of tension, $\partial H/\partial x_i$, in the calculation of the effective conductivity proved to be problematic. This seemed to interfere significantly with convergence during the iterative solution step. To address this issue, recall the assumption in the development of the linear fluctuation equations (see section 2.2.3) that mean values vary slowly in space; in other words, they change very little within a correlation scale. In some of the numerical simulation experiments that were performed, if the mean did change rapidly over a small spatial distance (i.e., if the gradient $\partial H/\partial x_i$ was not small) iteration to a final value of effective conductivity was not possible. Thus to expedite iterative convergence and to ensure calculation of a final value of effective conductivity, an approximation was invoked that the gradient of tension in space is equal to zero *within the solution step which evaluates and updates the effective conductivity.* The approximation that $\partial H/\partial x_i = 0$ appears to significantly improve the ability of the numerical technique to iterate to final solutions, and this approximation was adopted in all simulations discussed in Chapter 4. Ideally, the stochastic mean equation and effective parameters should only be applied to model simulations where the mean values vary slowly in space, in accordance with the assumptions of the theory. In such cases, the approximation above is likely reasonable. This assumption should receive further attention in future studies.

The asymptotic expressions for $\hat{K}_{ii}$ given above [equations (2-37), (2-38) and (2-39)] are obtained from equations (34a, b, c) of Mantoglou and Gelhar (1987c) for the case of deterministic moisture content. These expressions were derived from (2-17) for the case J_i $\partial H/\partial x_i \approx 0$; the terms σ_ε^2 and τ_i are given by Mantoglou and Gelhar (1987c) in equations (32a) through (33c). Using these expressions in the case of deterministic moisture content, τ_1 can be expressed as $-J_1\sigma_\varepsilon^2$ and $\tau_2 = 0$ from which (2-17) can be written as

$$\hat{K}_{11} = K_M \exp\left(-\frac{\sigma_\varepsilon^2}{2}\right) = K_G \exp\left(-AH - E[ah] - \frac{\sigma_\varepsilon^2}{2}\right) \qquad (2\text{–}43)$$

$$\hat{K}_{22} = K_M \exp\left(\frac{\sigma_\varepsilon^2}{2}\right) = K_G \exp\left(-AH - E[ah] + \frac{\sigma_\varepsilon^2}{2}\right) \qquad (2\text{–}44)$$

Equations (2-43) and (2-44) are used in the simulations discussed in Chapter 4; σ_ε^2 is given by (2-16a), $E[h^2]$ is given by equations (17) and (20) of Mantoglou and Gelhar (1987b), E[fh] is given by equations (12) through (15a) of Mantoglou and Gelhar (1987c), E[ah] is given by equations (17) and (18a) of Mantoglou and Gelhar (1987c), and E[fa] = 0 since f and a are assumed uncorrelated. In regions of the simulated domain where $G \approx 0$ (approximately steady-state), (2–39) is used for $\hat{K}_{ii}$ and $E[h^2]$ is given by equation (28) of Mantoglou and Gelhar (1987b).

An additional assumption made to facilitate calculation of the effective conductivity involves the parameter E[ah]. This parameter is a function of itself and its own gradient in space; E[ah] = F{ E[ah], $\partial E[ah]/\partial x_i$ }. Thus E[ah] must be evaluated iteratively during each solution step. As mentioned in the previous paragraph, the development of the stochastic model assumed that mean values vary slowly in space. E[ah] can be thought of as a mean value and the gradient of E[ah] in space, $\partial E[ah]/\partial x_i$, should be small. This is consistent with the stationarity assumption of the theory. Since the assumption that $\partial E[ah]/\partial x_i = 0$ seems to aid significantly in convergence, it was adopted in all simulations discussed in Chapter 4. This assumption may be inadequate in the case of wetting with a sharp front and should be examined in greater detail in future studies. In the numerical simulations discussed in Chapter 4, a chord-slope Newton-

Raphson type iteration scheme is used to calculate E[ah]. It converges quickly as long as the spatial gradient of E[ah] is neglected. One option for future studies, in an effort to ivestigate the importance of including spatial gradient terms, may be to write E[ah] as a differential equation to be solved at each time step, instead of viewing E[ah] as a non-linear function.

The widely used conductivity relationship of van Genuchten (1980) [see (3-5)] indicates that the local log conductivity function $\ln K(\psi)$ will be nonlinear or, equivalently, that the parameter α defined in (2-1) depends on the tension ψ. Such tension dependence of α is substantiated by both laboratory and field experiments [Stephens and Rehfeldt (1985); Wierenga et al (1986a, b)]. Generally speaking, α tends to decrease at higher tensions, giving significantly larger values of conductivity at high tensions than would be obtained if the low-tension value of α applied over the entire range. Simulation experiments conducted as part of the investigation described in Chapter 4 indicated, in fact, that numerical simulations of high-tension conditions is practically impossible if the mean of α [A] is held constant at the value measured in the laboratory under much wetter (low tension) conditions. For this reason, values of A and F used in the simulations of Chapter 4 were obtained from a *local linearization* of the following nonlinear conductivity function [van Genuchten (1980)]:

$$K_{VG}(H) = \frac{K_G[1 - (\alpha_1 H)^{n-1}(1 + (\alpha_1 H)^n)^{-m}]^2}{[1 + (\alpha_1 H)^n]^{m/2}} \qquad (2\text{–}45)$$

This function is plotted in Figure 2-6 (using the parameters $n = 1.982$, $\theta_s = 0.368$, $\theta_r = 0.102$, $\alpha_1 = 0.0334$ and $K_G = 0.0092$ cm/s).

The nonlinear log conductivity function (2-45) may be approximated at any given value of mean tension (H) by a tangent line (see Figure 2-6). The corresponding values of A and F are the slope and intercept of this tangent line, and are thus expressed as

$$\begin{aligned} A(H) &= -\frac{d[\ln K_{VG}(H)]}{dH} = -\frac{1}{K_{VG}(H)}\frac{dK_{VG}(H)}{dH} \\ &= -2T_2^{-1}\left[\alpha_1 nm(\alpha_1 H)^{2n-2}T_1^{-m-1} - \alpha_1(n-1)(\alpha_1 H)^{n-2}T_1^{-m}\right] \\ &\quad + \alpha_1 nm(\alpha_1 H)^{n-1}T_1^{-1} \Big/ 2 \end{aligned} \qquad (2\text{–}46)$$

where

$$\begin{aligned} T_1 &= 1 + (\alpha_1 H)^n \\ T_2 &= 1 - (\alpha_1 H)^{n-1}(1 + (\alpha_1 H)^n)^{-m} \end{aligned} \qquad (2\text{–}47)$$

and

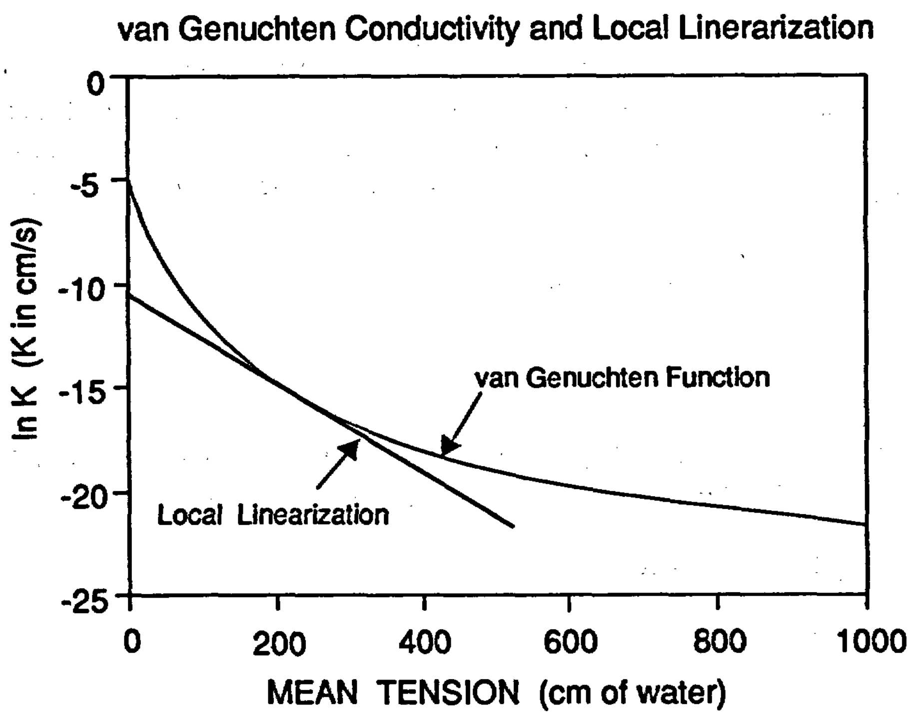

Figure 2-6. **Log hydraulic conductivity versus mean capillary tension head, based on a van Genuchten-type function of conductivity versus mean tension. [see equation (2-45)].**

$$F(H) = \ln K_{VG}(H) + A(H)H \tag{2-48}$$

Note that F has no particular physical significance in this case since it is only a fitting parameter. It must, however, be included in the effective conductivity expressions in order to insure that the linear approximation does, in fact, describe the desired tangent line.

When the values F and A used in the simulation are calculated from the linearization approach outlined above, the variance parameters σ_f^2 and σ_a^2 must also be adjusted in the simulation. It is reasonable to expect a relatively constant relation between the variability of the parameter and its mean value as the mean value changes over a range of tension. For example, as A decreases with an increase in tension σ_a^2 should also decrease. This suggests that the standard deviations σ_a and σ_f used in the simulations should be computed by multiplying the fitted values A and F by constant coefficients. These constant coefficients can be estimated from soils data measured over a range of tension which is narrower than the range encountered in the actual simulation. For the two-dimensional simulations described in Chapter 4, the following relations were used:

$$C_F = \frac{\sigma_f}{K_G} = \text{constant} \tag{2-49}$$

$$C_A = \frac{\sigma_a}{A} = \text{constant} \tag{2-50}$$

where σ_f, σ_a, K_G and A are based on available soils data. In the simulation, σ_f^2 and σ_a^2 vary with tension as do the fitted values of K_G and A. The following relations were used:

$$\sigma_f(H) = C_F K_G(H) \tag{2-51}$$

$$\sigma_a(H) = C_A A(H) \tag{2-52}$$

Of course, the assumption that the coefficients C_F and C_A are constant is somewhat arbitrary and should be examined in future studies.

2.3 Stochastic Unsaturated Transport Theory

2.3.1 Derivation of large-scale models and effective parameters

Perturbation analysis

The large-scale transport model is derived following the same steps that were presented for the large-scale flow model. The analysis of this section was first presented in Mantoglou and Gelhar (1985) and it follows closely the analysis of Gelhar and Axness (1983). The general equation describing transport of an ideal nonreactive conservative solute by unsaturated flow is given by

$$\frac{\partial}{\partial t}(\theta c) = \frac{\partial}{\partial x_i}\left(E_{ij}\frac{\partial c}{\partial x_j} - cq_i\right) \quad i,j = 1,2,3 \tag{2-53}$$

where it is assumed that the liquid density and viscosity are constant, c(x,t) is concentration (mass per volume of water), θ is the moisture content, E_{ij} is the local bulk dispersion coefficient (equal to θD_{ij}), and D_{ij} is the dispersion coefficient tensor (which includes hydrodynamic dispersion and molecular diffusion).

In steady state, (2-53) simplifies to

$$\frac{\partial(cq_i)}{\partial x_i} = \frac{\partial}{\partial x_i}\left(E_{ij}\frac{\partial c}{\partial x_j}\right) \tag{2-54}$$

It is assumed here that the local coefficient of bulk dispersion E_{ij} is constant. It can be shown that, in several cases of interest, the results are not very sensitive to the parameter E_{ij} [Mantoglou and Gelhar (1985)]. Vomvoris (1986) has shown that variations in the local dispersion coefficient have only a minor influence on macrodispersion.

Consider the concentration c as the output of (2-54). Due to spatial variability of the parameters f and a the local specific discharge q_i is spatially variable, resulting in a spatially variable concentration c. As in Section 2.2, it is assumed that the parameters f and a are realizations of three-dimensional stationary random fields. Consequently, through the governing equations, the local specific discharge q_i and the concentration c become realizations of stationary random fields as well. Let

$$\begin{aligned} q_i &= \bar{q}_i + q_i' \qquad i = 1,2,3 \\ c &= \bar{c} + c' \end{aligned} \tag{2-55}$$

where $\bar{q}_i$, $\bar{c}$ are the mean of q_i, c and q_i', c' are the corresponding fluctuations around the mean.

The large-scale model of steady solute transport in unsaturated soils is derived by averaging the local governing equation (2-54) over the ensemble of realizations of the random fields f and a. Taking the expected valued of (2-54) with respect to f and a yields

$$\frac{\partial\{E[cq_i]\}}{\partial x_i} = \frac{\partial}{\partial x_i}\left(E_{ij}\frac{\partial E[c]}{\partial x_j}\right) \tag{2-56}$$

The expected value in the right hand side of (2-56) represents the mean $\bar{c}$. Substituting (2-55), the expected value in the left hand side of (2-56) is written as

$$E[cq_i] = \bar{c}\,\bar{q}_i + E[c'q_i'] \tag{2-57}$$

The term $\bar{c}\bar{q}_i$ represents the convective flux associated with the mean flow while term $E[c'q_i']$ is a macroscopic dispersive flux due to the spatial variation of q_i. Assuming that the macroscopic dispersive flux can be expressed in a Fickian form, it may be written as

$$E[c' q_i'] = -\hat{E}_{ij} \frac{\partial \bar{c}}{\partial x_j} \tag{2-58}$$

where $\hat{E}_{ij}$ is an effective bulk macrodispersion coefficient tensor. Finally, a macrodispersivity tensor may be defined as

$$A_{ij} = \frac{\hat{E}_{ij}}{q} \tag{2-59}$$

where q is the magnitude of the mean specific discharge vector and, generally, A_{ij} may depend on q. Equation (2-56) can then be written as

$$\frac{\partial(\bar{c}\,\bar{q}_i)}{\partial x_i} = \frac{\partial}{\partial x_j}\left[(E_{ij} + A_{ij}q)\,\frac{\partial \bar{c}}{\partial x_j}\right] \tag{2-60}$$

This is the large-scale transport equation and it is of a form similar to the local transport equation (2-54). Note that the total large-scale dispersion coefficient is $E_{ij} + A_{ij}q$, where the bulk macrodispersion coefficient $\hat{E}_{ij} = A_{ij}q$ accounts for the additional dispersion due to the spatial variability of q_i.

A linearized perturbation equation relating c' to q_i' may be derived from the local governing equation of steady transport (2-54). Substitution of (2-55) into (2-54) and expansion of the products yields

$$\frac{\partial}{\partial x_i}[\bar{c}\,\bar{q}_i + \bar{c}q_i' + c'\,\bar{q}_i + c'\,q_i'] \;=\; E_{ij}\,\frac{\partial^2(\bar{c} + c')}{\partial x_i \partial x_j} \tag{2-61}$$

where E_{ij} is assumed to be a constant. Subtracting the mean equation (2-56) from the local equation (2-61) produces

$$\frac{\partial}{\partial x_i}[\,\bar{c}q_i' + c'\,\bar{q}_i + c'\,q_i' - E(c'\,q_i')] \;=\; E_{ij}\,\frac{\partial^2 c'}{\partial x_i \partial x_j} \tag{2-62}$$

Assuming that q_i' and c' are small, the second order term $c'q_i'$ - $E[c'q_i']$ may be neglected, which constitutes the linearization process. The first order approximation describing the concentration fluctuations c' in terms of specific discharge fluctuations q_i' is then

$$\frac{\partial}{\partial x_i}[\,\bar{c}q_i' + c'\,\bar{q}_i] \;=\; E_{ij}\,\frac{\partial^2 c'}{\partial x_i \partial x_j} \tag{2-63}$$

For convenience, the coordinate axis x_1 can be aligned in the direction of the mean fluid flow so that $\bar{q}_1 = q$ and $\bar{q}_2 = \bar{q}_3 = 0$ (see Figure 2-7). Note that this orientation of axes is different than the one in the flow case; the system of axes x_1, x_2, x_3 is now not aligned in the principal statistical anisotropy directions. The local dispersion tensor may then be approximated in the form [Naff (1978)]

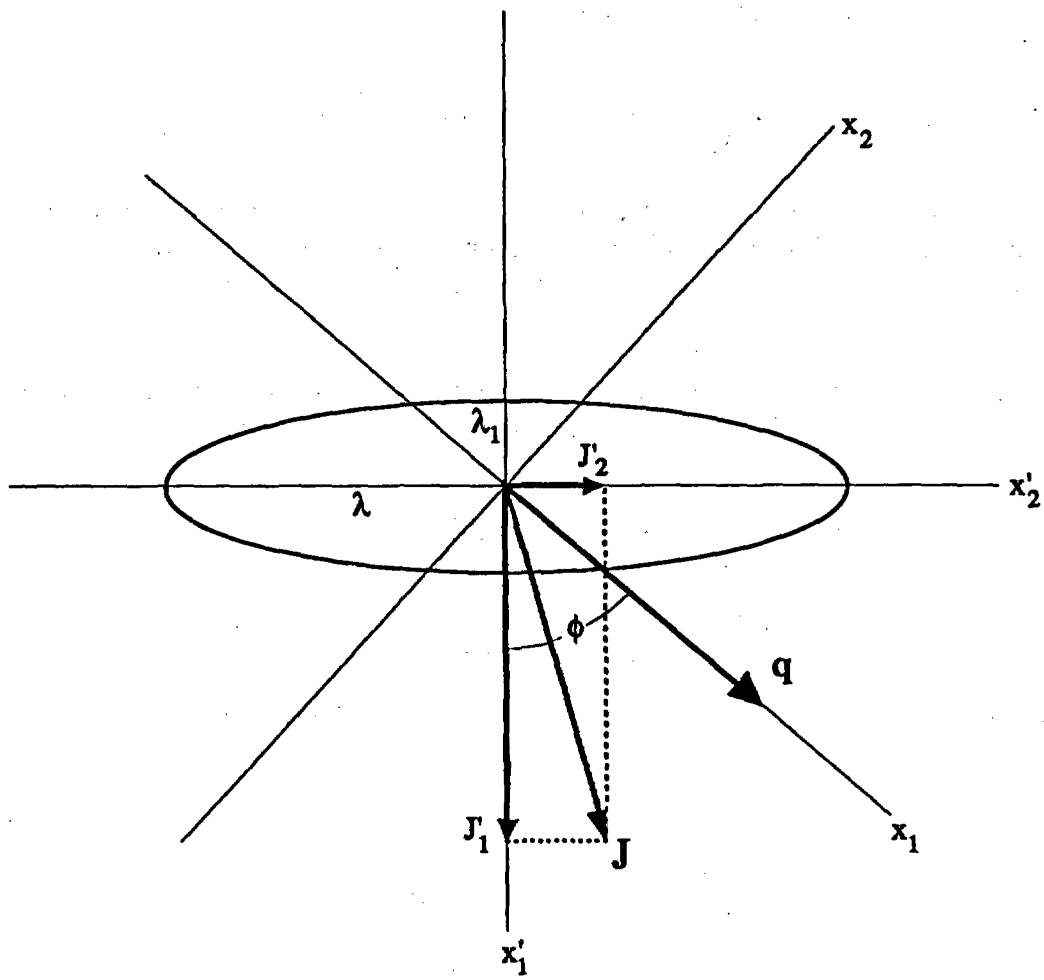

Figure 2-7. Coordinate system (x'_1, x'_2, x'_3) corresponding to the principal anisotropy axes (of f and a). The ellipse represents an equal covariance level. Axis x_1 of the coordinate system (x_1, x_2, x_3) is oriented in the direction of the mean specific discharge. Note that the direction of the mean specific discharge is not the direction of the mean head gradient. (Reproduced from Mantoglou and Gelhar, 1985)

$$[E_{ij}] = \begin{bmatrix} \alpha_L q & 0 & 0 \\ 0 & \alpha_T q & 0 \\ 0 & 0 & \alpha_T q \end{bmatrix} \tag{2-64}$$

where α_L and α_T are the local longitudinal and transverse dispersivities. Expanding the left term of (2-63) and utilizing (2-64), (2-63) reduces to

$$q_i' \frac{\partial \bar{c}}{\partial x_i} + q\frac{\partial c'}{\partial x_1} = q\left[\alpha_L \frac{\partial^2 c'}{\partial x_1^2} + \alpha_T\left(\frac{\partial^2 c'}{\partial x_2^2} + \frac{\partial^2 c'}{\partial x_3^2}\right)\right] \tag{2-65}$$

where the conservation of mass equation $\partial q_i/\partial x_i = 0$ has been used. Equation (2-65) is an approximate linearized partial differential equation relating concentration fluctuations c' and specific discharge fluctuations q_i'. The mean specific discharge q is a parameter to this equation.

Assuming that q_i' and c' are realizations of three-dimensional stationary random fields, it is possible to express q_i' and c' in the wave number domain as follows:

$$q_i'(\mathbf{x}) = \iiint_{-\infty}^{\infty} \exp(i\mathbf{k}\cdot\mathbf{x})\, dZ_{q_i}(\mathbf{k})$$

$$c'(\mathbf{x}) = \iiint_{-\infty}^{\infty} \exp(i\mathbf{k}\cdot\mathbf{x})\, dZ_c(\mathbf{k}) \tag{2-66}$$

Substituting into (2-65) the random spectral amplitude may be written

$$dZ_c = -\frac{\dfrac{\partial \bar{c}}{\partial x_j}\, dZ_{q_j}}{q\,[ik_1 + \alpha_L k_1^2 + \alpha_T (k_2^2 + k_3^2)]} \tag{2-67}$$

where the repeated index j corresponds to summation.

One additional step is required, namely the expression of dZ_{q_j} in terms of the statistical parameters of f and a, which are the quantities more easily measured. The specific discharge is given by

$$q_i = K(\psi)\,\frac{\partial(\psi+z)}{\partial x_i} = K(\psi)\left[J_i + \frac{\partial h}{\partial x_i}\right] \tag{2-68}$$

where

$$K(\psi) = K_M \exp(\,f - Ah - aH - ah + E[ah]) \tag{2-69}$$

with K_M given by (2-12). Expanding the exponential and assuming products of fluctuations are small, (2-69) gives

$$K(\psi) \approx K_M\,(1 + f - Ah - aH) \tag{2-70}$$

Using (2-70), (2-68) gives

$$q_i = K_M\left(J_i + J_i f - J_i Ah - J_i aH + \frac{\partial h}{\partial x_i} + f\frac{\partial h}{\partial x_i} - Ah\frac{\partial h}{\partial x_i} - aH\frac{\partial h}{\partial x_i}\right) \tag{2-71}$$

Taking the expected value of (2-71), subtracting the resulting equation from (2-71) and assuming that products of fluctutations are negligibly different from their mean values yields the following linearized equation

$$q_i' = q_i - E[q_i] = K_M\left[\left(\frac{\partial h}{\partial x_i} - J_i Ah\right) + J_i\,(f - aH)\right] \tag{2-72}$$

Equation (2-72) relates the specific discharge fluctuations to the capillary tension head and soil property fluctuations. Using the representation theorem of this equation yields

$$dZ_{q_i} = K_M\left[\,(ik_i - AJ_i)dZ_h + J_i\,(dZ_f - HdZ_a)\right] \tag{2-73}$$

For the perfectly stratified case examined in Section 2.2.4, the spectral amplitudes dZ_h are related to dZ_f and dZ_a by (2-35). As an example, in the case of steady-state flow $\partial h/\partial t$ and G are zero and (2-35) simplifies to

$$dZ_h = \frac{i\,(dZ_f - HdZ_a)J_jk_j - \left(J_j\frac{\partial H}{\partial x_j}\right)dZ_a}{k^2 + iAL_jk_j} \tag{2-74}$$

and substituting into (2-73)

$$dZ_{q_i} = W_i dZ_f + V_i dZ_a \tag{2-75}$$

where

$$W_i = K_M\,\frac{J_j(\delta_{ij}k^2 - k_ik_j) + iAJ_i(L_j - J_j)k_j}{k^2 + iAL_jk_j} \tag{2-76}$$

$$V_i = K_M\,\frac{-HJ_j(\delta_{ij}k^2 - k_ik_j) - iAHJ_i(L_j - J_j)k_j - (ik_i - AJ_i)\left(J_j\frac{\partial H}{\partial x_j}\right)}{k^2 + iAL_jk_j} \tag{2-77}$$

Equations (2-67) and (2-75) relate fluctuations c' and q_i' to soil property fluctuations f and a. These equations are used below for the evaluation of $E[c'q_i']$ and the corresponding A_{ij}.

Evaluation of macrodispersivities

Using the steady-state linearized equations just derived and the spectral representation theorem, term $E[c'q_i']$ is given by

$$E[c'q_i'] = \iiint_{-\infty}^{\infty} S_{cq_i}(\mathbf{k})\, d\mathbf{k} = -A_{ij}\, q \frac{\partial \bar{c}}{\partial x_j} \tag{2–78}$$

where, from (2-67) and $S_{cq_i}\, d\mathbf{k} = E[dZ_c dZ_{qi}^*]$,

$$S_{cq_i}(\mathbf{k}) = -\frac{S_{q_iq_j} \frac{\partial \bar{c}}{\partial x_j}}{q\left[ik_1 + \alpha_L k_1^2 + \alpha_T(k_2^2+k_3^2)\right]} \tag{2–79}$$

From (2-79) in (2-78) it is evident that the macrodispersive flux is Fickian, i.e., proportional to the mean concentration gradient if $\partial\bar{c}/\partial x_j$ is constant or slowly varying; the resulting macrodispersivity is then

$$A_{ij} = \frac{1}{q^2} \iiint_{-\infty}^{\infty} \frac{S_{q_jq_i}(\mathbf{k})d\mathbf{k}}{ik_1 + \alpha_L k_1^2 + \alpha_T(k_2^2+k_3^2)} \tag{2–80}$$

Using (2-75) as a generic form of the dZ_{q_i} with (2-25), the cross-spectral density function $S_{q_j}S_{q_i}$ is given by

$$S_{q_jq_i} = W_j W_i^* S_{ff} + V_j V_i^* S_{aa} + W_j V_i^* S_{fa} + V_j W_i^* S_{af} \tag{2–81}$$

Note that the form of (2-80) is identical to the result for the saturated flow case [Gelhar and Axness (1983), Equation 28']. However, the mean specific discharge and the spectrum of the specific discharge fluctuations are different in the unsaturated flow case.

Mantoglou and Gelhar (1985) calculated macrodispersivities in steady-state solute transport and steady-state flow for the following three cases:

- statistically isotropic soil with one-dimensional steady vertical infiltration
- statistically anisotropic soil with the mean flow perpendicular to stratification
- statistically anisotropic soil with arbitrary orientation of mean flow

For case (a), analytical expressions were developed for A_{11} and A_{22} using an approximate solution based on the fact that $\varepsilon = \alpha_L/\lambda \ll 1$. For case (b), using the assumption that $\varepsilon \to 0$, approximate analytical expressions were evaluated for A_{11} and A_{22} under a condition of mild stratification and also for strong stratification. Details of these analyses are discussed in Mantoglou and Gelhar (1985). For case (c), Mantoglou and Gelhar (1985) evaluated A_{ij} in the case of a horizontally stratified soil with $\partial H/\partial x_j$ ($j = 2, 3$) being relatively small. Note that in statistically anisotropic soil, even small lateral gradients may produce significant lateral flow due to large lateral hydraulic conductivities. Mantoglou and Gelhar (1985) developed expressions for A_{ij} in case (c) which require numerical integration for application to a given problem. These expressions have been incorporated into the analysis presented in Chapter 5 of this report. Further details of this application are presented in the Appendix.

Some Examples

Mantoglou and Gelhar (1985) evaluated the macrodispersivities A_{ij} as a function of the mean capillary tension head and the mean specific discharge for the Panoche clay loam and Maddock sandy loam soil. The case of a statistically isotropic soil, with flow perpendicular to bedding, is mentioned here with the soil property fluctuations f and a assumed uncorrelated.

Figure 2-8 plots the longitudinal macrodispersivity A_{11} as a function of the mean capillary tension head H for $\alpha_L = \alpha_T = 1$ cm, and isotropic hydraulic conductivity with $\lambda = 100$ cm. This figure shows that as H increases (i.e., soil desaturates), A_{11} initially increases. After reaching a maximum value, A_{11} starts to monotonically decrease for increasing H. This behavior is explained as follows. With the soil matrix initially saturated (H = 0), when H increases the coarser regions of the soil start to desaturate and the flow follows finer soil paths. As a result, flow follows a more tortuous path than in the saturated case, which increases A_{ij}. As the soil matrix continues to desaturate, however, the finer soil volumes also desaturate. It is then likely that the continuity of flow paths is interrupted (i.e., volumes of fine soil may contain stagnant water masses). It is thus expected that, at large H, the macrodispersivities A_{ij} decrease for increasing H.

Figure 2-8 shows that for small H, the longitudinal macrodispersivity for the Maddock soil is larger than the one for Panoche soil. This tendency can be ascribed to the larger variability of the saturated hydraulic conductivity in the Maddock soil. As H increases however, A_{11} of the Maddock soil drops rapidly while A_{11} of the Panoche soil remains relatively constant. This behavior is probably due to the larger variety of textures in the Maddock soil compared to the Panoche soil. It is expected that as the Maddock soil desaturates the coarser pore volumes empty quickly, which generates immobile water masses in the finer soil volumes. This may explain the fast decrease of A_{ij} for increasing H. In the relatively uniform Panoche soil the soil desaturates more uniformly and immobile soil water volumes are less likely to be generated.

Additional examples based on the Maddock and Panoche soils, for both longitudinal and transverse dispersivity, are presented by Mantoglou and Gelhar (1985).

2.3.2 The equations for the mean transport model

In the simulations that are presented in Chapter 5, the mass transport equations are unsteady and therefore a more general form than (2-60) is required. Starting with the mass conservation equation (2-53), expanding c and q_i as in (2-55) and θ in a similar manner [$\theta = \bar{\theta} + \theta'$], the equation becomes

$$\frac{\partial}{\partial t}(\bar{\theta}\bar{c}) + \frac{\partial}{\partial t}E[\theta'c'] + \frac{\partial}{\partial x_i}(\bar{q}_i\bar{c}) = -\frac{\partial}{\partial x_i}E[c'\,q_i'] + \frac{\partial}{\partial x_i}\left(E_{ij}\frac{\partial \bar{c}}{\partial x_j}\right) \quad (2\text{-}82)$$

It is easy to verify for the steady-state case that time derivatives disappear and (2-82) is similar to (2-56) and (2-57). The dispersive term $E[c'q_i']$ is assumed to be of a Fickian form, similar to (2-58). Physically, it is expected that since the macrodispersivities result from the complicated paths that the flow field follows in a natural heterogeneous medium, they will start

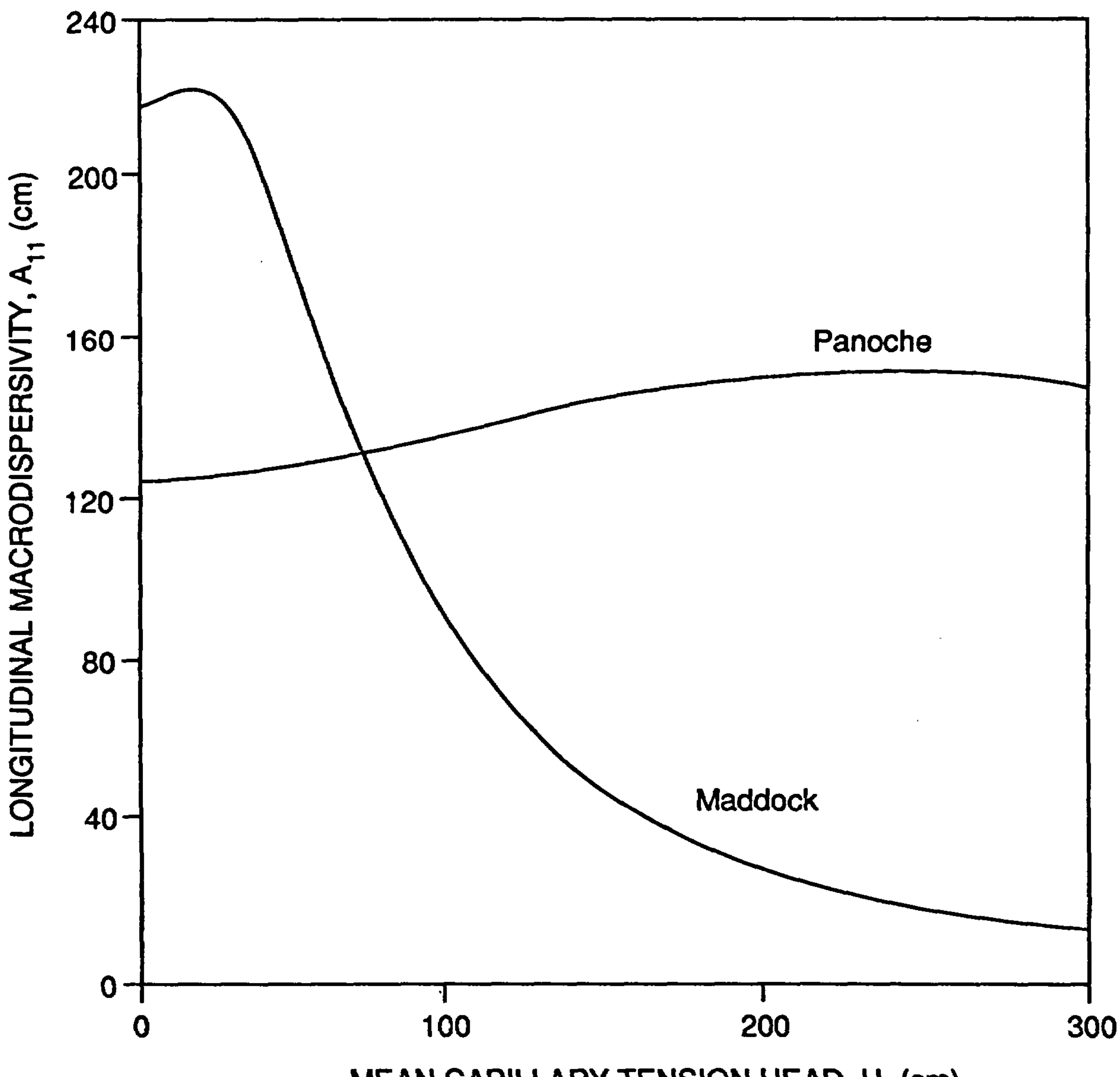

Figure 2-8. Longitudinal macrodispersivity versus mean capillary tension head for two isotropic soils with λ = 100 cm and $\alpha_L = \alpha_T$ = 1 cm. (Reproduced from Mantoglou and Gelhar, 1985)

from a zero value (when flow is at the very early stages) and reach an asymptotic value as time passes or as the plume travels through the heterogeneous medium and "samples" increasing scales of heterogeneity. The macrodispersivities reach their asymptotic value when the plume has "sampled" the larger scale of heterogeneity, which is on the order of the correlation scale. Note that the macrodispersivities calculated by Mantoglou and Gelhar (1985) under an assumption of steady-state are equivalent to the asymptotic values. Theoretical results which describe the transition period are given in Gelhar (1987). In recent work involving simulations, Tompson et al (1988) present a type of validation of this transition which is based on numerical experiments.

For the simulations performed in Chapter 5 it is assumed that the macrodispersivities have reached their asymptotic value. Clearly this is an approximation (a zero-th order approximation of the actual value) and will result in concentration distributions at the early stages of simulation which are smoother than otherwise would be expected. Further theoretical work is required to provide operational expressions for the "developing" part of the macrodispersivities (i.e., the transition from the zero value to the asymptotic). For the current modeling efforts, the dispersive flux in the mean transport model will be given by a Fickian form

$$E[c'\,q_i'] = -\bar{q}A_{ij}\frac{\partial \bar{c}}{\partial x_j} \tag{2–83}$$

where A_{ij} are the steady-state asymptotic values derived in Mantoglou and Gelhar (1985). It should be mentioned that, since the mean flow field analyzed in Chapter 4 is unsteady, the flow factor that enters in the macrodispersivity calculations in Chapter 5 is also time and space varying. However, such dependence should not be confused with the temporal dependence that is expected in the developing macrodispersivity (the transition period) since this has a different origin. As Gelhar et al (1979) show, the transition feature of the macrodispersivity exists even in the case of a steady-state flow field.

The additional term $E[\theta'c']$ in (2-82) can be analyzed using the approach of Garabedian et al (1988), which was developed to treat variable porosity and retardation in saturated flow. The effect of this term in the more complex case of unsaturated flow should be investigated in future work. In the analysis described in Chapter 5, this additonal term has been neglected.

CHAPTER 3

THE EXPERIMENTS AT LAS CRUCES

3.1 Introduction

Field and laboratory studies involving transport of moisture and solutes in unsaturated soils are being conducted at New Mexico State University under the direction of P.J. Wierenga [Wierenga et al (1986a, b)]. Initial experiments pertinent to the present study were conducted in a lysimeter facility on the New Mexico State University College Ranch, which is located approximately 40 km northeast of Las Cruces, New Mexico. Additional moisture and solute transport experiments were conducted in undisturbed soil adjacent to an excavated trench, near the lysimeter facility. These studies have included an extensive program of soil and solute sample collection, field and laboratory evaluation of soil physical and chemical characteristics and hydraulic properties, and data analysis. This work is fully described in a series of reports by Wierenga et al (1986a, b, 1988). This chapter provides an overview of the experiments at Las Cruces and describes their relation to the numerical simulations to be discussed in Chapter 4. Section 3.2 briefly outlines the procedures for soil data collection and analysis and describes the techniques used to develop input parameters for the simulations. Section 3.3 describes the lysimeter facility and a one-dimensional flow experiment which has been used to check the stochastic theory and related simulations. Section 3.4 discusses the large-scale field experiment, which is viewed as a two-dimensional flow system.

The climate in the Las Cruces region is characterized by an abundance of sunshine, low relative humidity, and an average Class A pan evaporation of 239 cm/year. Average annual precipitation is 23 cm, with 52 percent of the total rainfall occurring during July through September. The average monthly maximum air temperature ranges from a high of 36° C in June to a low of 13° C in January [Wierenga et al (1986a)]. Under these warm, arid conditions the unsaturated soil profile is areally extensive and deep, extending to tens or hundreds of meters below the ground surface. The natural soil moisture content is low, typically less than 10 percent and as low as several percent by volume [Wierenga et al (1986a, b, 1988)].

3.2 Procedures for collection and analysis of soils data

3.2.1 Lysimeter soils

During construction of the lysimeter facility, soil samples were collected from the exposed wall of the excavation from ground surface to a depth of 6 m, and by bucket auger from 6 m to 8.2 m depth. Particle-size distributions and selected soil chemical characteristics were determined by standard methods. Moisture content of the natural soils at the lysimeter site were determined gravimetrically for selected depths from 1.2 to 9.2 m; water content values ranged from 0.066 to 0.037 g/g during September 1985 [see Wierenga et al (1986a)].

Two different soils were used in the lysimeter experiments -- Berino loamy fine sand and Glendale silty clay loam. The Berino soil was determined to consist of 93 percent sand, 2 percent silt and 5 percent clay; the Glendale soil was determined to be 15 percent sand, 63 percent silt and 22 percent clay. The Berino soil was collected at a site on the NMSU College Ranch and the Glendale soil was taken from an NMSU site located south of Las Cruces [Wierenga et al (1986b)].

The relationship between water content and pressure potential (i.e., capillary tension) for the two soils was determined in the laboratory using disturbed samples. For the pressure range 0 to 0.4 bar (408 cm of water), a pressure chamber was used. Soil was packed into a core ring and/or placed into a Buchner funnel and saturated from below with 0.01N $CaCl_2$ solution. The samples were then subjected to step-increases of pressure in the chamber, and the outflow at each pressure was measured volumetrically. A small sieved, air-dried soil sample was used in a 5-bar pressure plate extractor apparatus for the pressure range 0.4 to 5 bar, and a 15-bar ceramic plate extractor was used for the range 5 to 15 bar. The water held at each pressure step was calculated based on the outflow volumes and the final water content. The experiment was repeated for 20 samples of each soil type. Further details of the experiments and their results are presented by Wierenga et al (1986a, 1986b).

To determine the saturated hydraulic conductivity of the Berino and Glendale soils, cylindrical cores were packed with each of the soils to a known (dry) density. The cores were saturated from below with 0.01N $CaCl_2$ solution. The saturated water content was determined gravimetrically. A constant pressure head differential was then established and the volumetric flux through the core sample was determined. This procedure was repeated for several samples of each soil type. The average saturated conductivity was 541 cm/day for the Berino soil, and 13.1 cm/day for the Glendale soil [Wierenga et al (1986a, b)].

A nonlinear least-squares curve-fitting algorithm was used in a computer program to fit a known function to the measured soil water retention data for the Berino and Glendale soils. The program is a modification of an earlier program by van Genuchten (1980) [see Wierenga et al (1986a), for reference to a personal communication]. The soil water retention curve proposed by van Genuchten (1980) has the form

$$\theta = \theta_r + (\theta_s - \theta_r)\left[\frac{1}{1 + (\alpha_1\psi)^n}\right]^m \tag{3-1}$$

where θ_r is the residual water content; θ_s is the saturated soil water content; ψ is the tension; and α_1, m and n are unknown parameters. Mualem (1976) developed a model to predict the hydraulic conductivity from the soil moisture retention curve, having the form

$$K = K_s\ S_e^p\left[\frac{f(S_e)}{f(1)}\right]^2 \tag{3-2}$$

where K is the unsaturated hydraulic conductivity, K_s is the saturated hydraulic conductivity, and p is a parameter. The effective saturation, S_e, is given by

$$S_e = \frac{(\theta - \theta_r)}{(\theta_s - \theta_r)} \tag{3-3}$$

and

$$f(S_e) = \int_0^{S_e} \frac{1}{\psi(S_e')} \, dS_e' \tag{3-4}$$

Based on expressions (3-1) through (3-4) and assuming that m = (1 - 1/n) and p = 0.5, van Genuchten (1980) derived a solution for the unsaturated hydraulic conductivity in terms of capillary pressure head given by

$$K(\psi) = K_s \frac{\{1 - (\alpha_1\psi)^{n-1} [1 + (\alpha_1\psi)^n]^{-m}\}^2}{[1 + (\alpha_1\psi)^n]^{m/2}} \tag{3-5}$$

The available laboratory soil water retention data for the Berino and Glendale soil samples were used with laboratory values for θ_s and θ_r to estimate the parameters α_1 and n in (3-1) (under the assumption that m = 1 - 1/n). The residual moisture content was assumed to be represented by the measured moisture content at a pressure of 15 bar. Detailed results of the curve-fitting procedures are presented by Wierenga et al (1986a, b) [see, for example, Figures A-10 through A-13 (1986a) and Figure 1 (1986b)]. The conductivity function (3-5) can be used to estimate the parameter α of (2-1) by using laboratory values of K_s and plotting log conductivity versus tension [see, for example, Figure 2 of Wierenga et al (1986b)]. Based on preliminary data, estimates of α for the Glendale and Berino soils were provided by Dr. Wierenga for the one-dimensional numerical simulations described in Section 4.5.

3.2.2 Field soils

During excavation of the trench, relatively undisturbed soil cores were collected by driving metal core rings into the natural soil. In addition, small grab samples were collected at the core locations for analysis of particle size distribution. Core samples were collected along the length of the trench within each identified soil horizon on the wall opposite the irrigation area (see Section 3.4 for discussion of the field experiment). Based on visual observations of the soil profile, nine strata were identified. Core samples were taken at horizontal intervals of 0.5 m within each strata, for a total of 50 samples, except within the third horizon where 100 samples were collected at intervals of 0.25 m. In addition, soil cores were collected at three vertical transects, across all strata, at depth intervals of approximately 20 cm from near ground surface to a depth of 6.1 m.

The bulk density for each soil core sample was determined based on oven-dry weight. The wet range of the soil water retention curves was determined using a pressure chamber after saturating the relatively undisturbed cores in Buchner funnels, similar to the procedure used for the Berino and Glendale samples (see Section 3.2.1). The drier portion of the moisture retention curve for each sample was determined using a pressure plate apparatus for the range of 0.5 to 15 bar, as described in Section 3.2.1. The saturated hydraulic conductivity of each sample was determined using the relatively undisturbed cores in a method described by Elrick et al (1980); the soil cores were slowly saturated in a water bath and then the rate of upward flow through each core was measured volumetrically under a constant head differential. This procedure provided an efficient means to analyze the large number of samples collected at the trench site.

For each soil sample collected at the trench site, the laboratory analyses described above provided the saturated hydraulic conductivity and eleven data points of moisture content versus tension. The van Genuchten parameters of (3–1) and (3–5) were fit to these data to develop a moisture retention curve and an unsaturated hydraulic conductivity curve for each sample (see discussion in section 3.2.1). In addition, all data for each soil layer (50 values of K_s and 550 data for moisture retention versus tension) were lumped together and the same fitting procedure was used to develop "composite" curves for each soil strata. Further details and results are presented by Wierenga et al (1986b, 1988).

Estimates of the saturated hydraulic conductivity (the field saturated conductivity, K_{fs}) were determined *in situ* using the Guelph permeameter method [Elrick et al (1984); Reynolds et al (1984)]. Tests were performed adjacent to each field location where soil cores were collected in the nine horizontal transects. For this test, an uncased hole was drilled by hand into the undisturbed soil. The Guelph permeameter was then used to maintain a constant water level in the hole and to measure the rate of water flow out of the hole. The test was repeated at each site. Based on these results, a value of K_{fs} was estimated and associated with each of the core samples collected [see Wierenga et al (1986b)]. These data were used to estimate the vertical correlation length of the saturated conductivity field, required for the two-dimensional numerical simulation the stochastic theory (see Section 4.6). Preliminary comparisons of the K_{fs} data to the laboratory K_s data reveal differences among the saturated conductivity estimates from the two methods. Note that the two tests were not performed on identical samples at each site; the Guelph permeameter test was typically offset from the soil core sampling location by approximately 20 cm. In addition, Elrick et al (1984) and Reynolds et al (1984) note that K_{fs} values are typically less than K_s values. An evaluation of the correlation between these two data sets requires further analysis.

Unsaturated hydraulic conductivities were estimated for each soil core sample using the fitted equations (3-1) and (3-5). The linear slope [α] of the semi-log plot of the exponential hydraulic conductivity model was then determined for each sample as follows: at the 95 percent relative water content [RW95] {given by RW95 = $\theta_r + 0.95\ (\theta_s - \theta_r)$}, the tension, ψ, for the given sample was determined using (3-1). The conductivity was then determined using (3-5), based on the given value of ψ. This procedure was repeated for RW80 for each sample. From these two derived values of $K(\psi)$, the slope [α] of $\ln K(\psi)$ versus ψ [see equation (2-1)] was calculated for each sample, and statistics of α for each layer were compiled. Results are presented by Wierenga et al (1986b, 1988) [see, for example, Table 9 (1986b)]. Data for only the first soil layer were used to determine the required statistical inputs of α for the two-dimensional simulation of Section 4.6, as these were the only soil testing results available at the time of the simulation. The mean A and the variance σ_a^2 determined from these data enter the simulation using equation (2-48) to define the constant coefficient C_A, which is used in the relinearization approximation.

3.3 Lysimeter experiment

Several lysimeters are installed at the NMSU College Ranch near Las Cruces. The lysimeter of interest to the present study is located in an array of six such devices, which have been designed for a variety of unsaturated soil experiments. The facility consists of one 2.44 m diameter central access lysimeter, surrounded by two 2.44 m and four 0.95 m diameter lysimeters (see Figure 3-1). All lysimeters are 6.1 m in length and are buried vertically into the soil. The lysimeters rest on a concrete slab. Horizontal access holes cut into the smaller lysimeters at 1-m vertical intervals connect these lysimeters to the central access area.

The present study is concerned with experiments conducted in lysimeter "C" (see Figure 3–1), which was designed to study effects of soil layering on flow and transport. Lysimeter C was filled with alternating 20-cm-thick layers of Berino loamy fine sand and Glendale silty loam. The soil was air dried, sieved and packed into the lysimeter at a known density (see Figure 3–2). Suction tubes with porous cups were installed through the access holes to allow soil solution samples to be withdrawn for chemical analyses. Other suction tubes were installed near the bottom to remove drainage water. Two tensiometers were placed into each soil layer, installed through the lysimeter wall in a horizontal position and located 10 cm apart. An access tube for a neutron probe was installed vertically in the center of the lysimeter. Irrigation water was supplied from a needle-embedded plate which was installed just above the soil surface. During the experiment, this plate was rotated at a constant speed to evenly distribute a known flux of water and solute uniformly over the surface. A vapor trap was installed over the top of the lysimeter to prevent evaporation of water.

Water and solute were added to lysimeter C at a rate of 2 cm/day. The rate of downward water movement was determined from neutron probe readings and also from tensiometer data. A comparison of the measured moisture profile with numerical simulation results based on the stochastic theory is presented in Section 4.5. Further details of the lysimeter facility and experimental results can be found in Wierenga et al (1986a, b, 1988).

3.4 Large-scale field experiment

A trench which measures approximately 26 m long, 5 m wide and 6 m deep was dug into a naturally-layered undisturbed soil near the lysimeter facility. A field experiment was designed to study the large-scale multi-dimensional movement of water and solutes into the initially dry soil. This experiment involved the uniform application of a known flux of water and solute within a large rectangular area at one side of the trench. A brief overview of the experiment is presented here. Further details and experimental results are presented by Wierenga et al (1986a, b, 1988). A numerical analysis based on the stochastic theory was designed to simulate the evolving moisture profile; this is presented in Section 4.6.

The rectangular irrigation area was located adjacent to the excavated trench and measured approximately 4 m by 9.9 m (see Figure 3-3). The irrigation system consisted of parallel

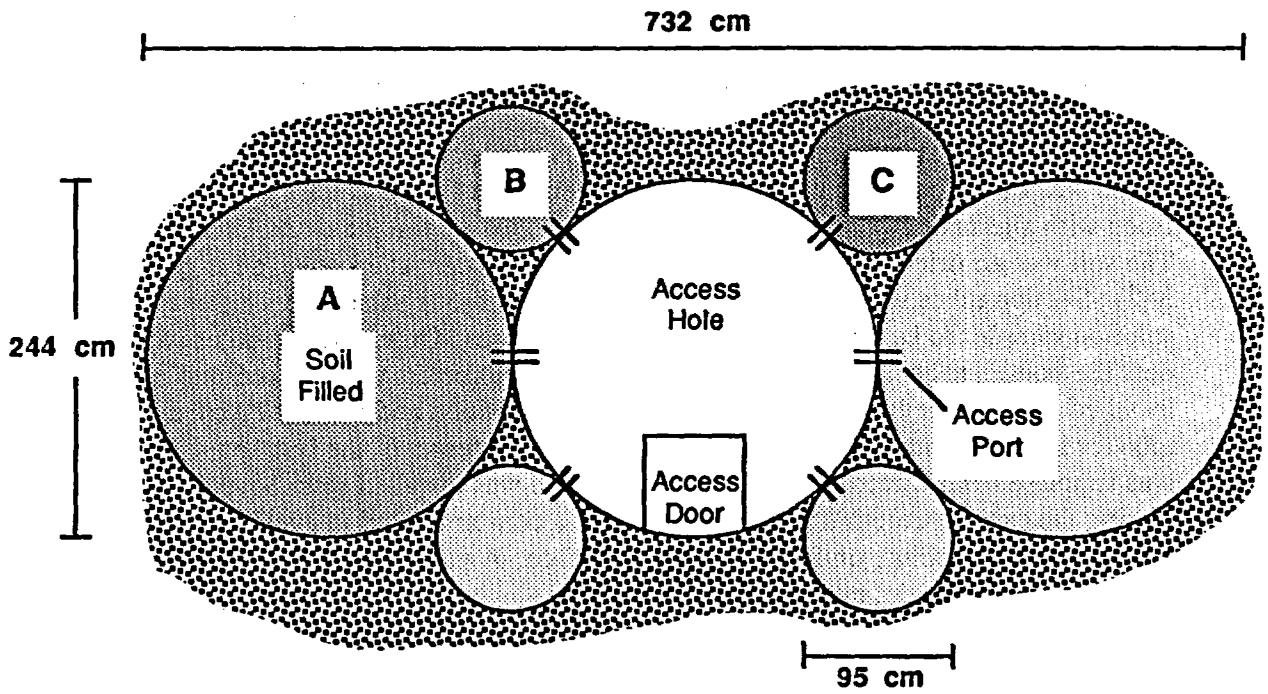

Figure 3-1. Top view of lysimeter [Reproduced from Wierenga et al. (1986a)]

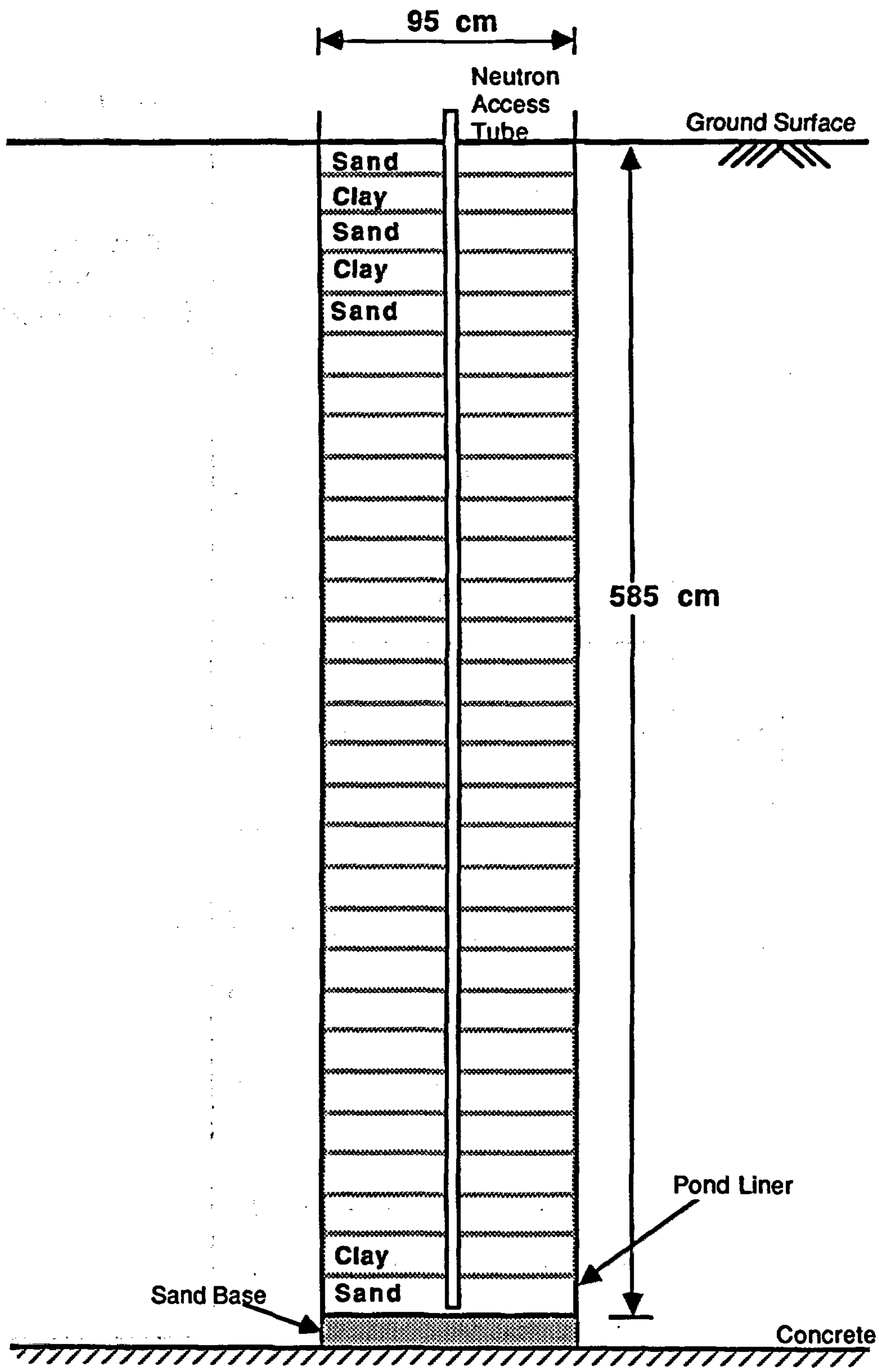

Figure 3-2. Schematic view of lysimeter filled with alternate layers of Berino loamy fine sand and Glendale clay loam [Reproduced from Wierenga et al (1986a)]

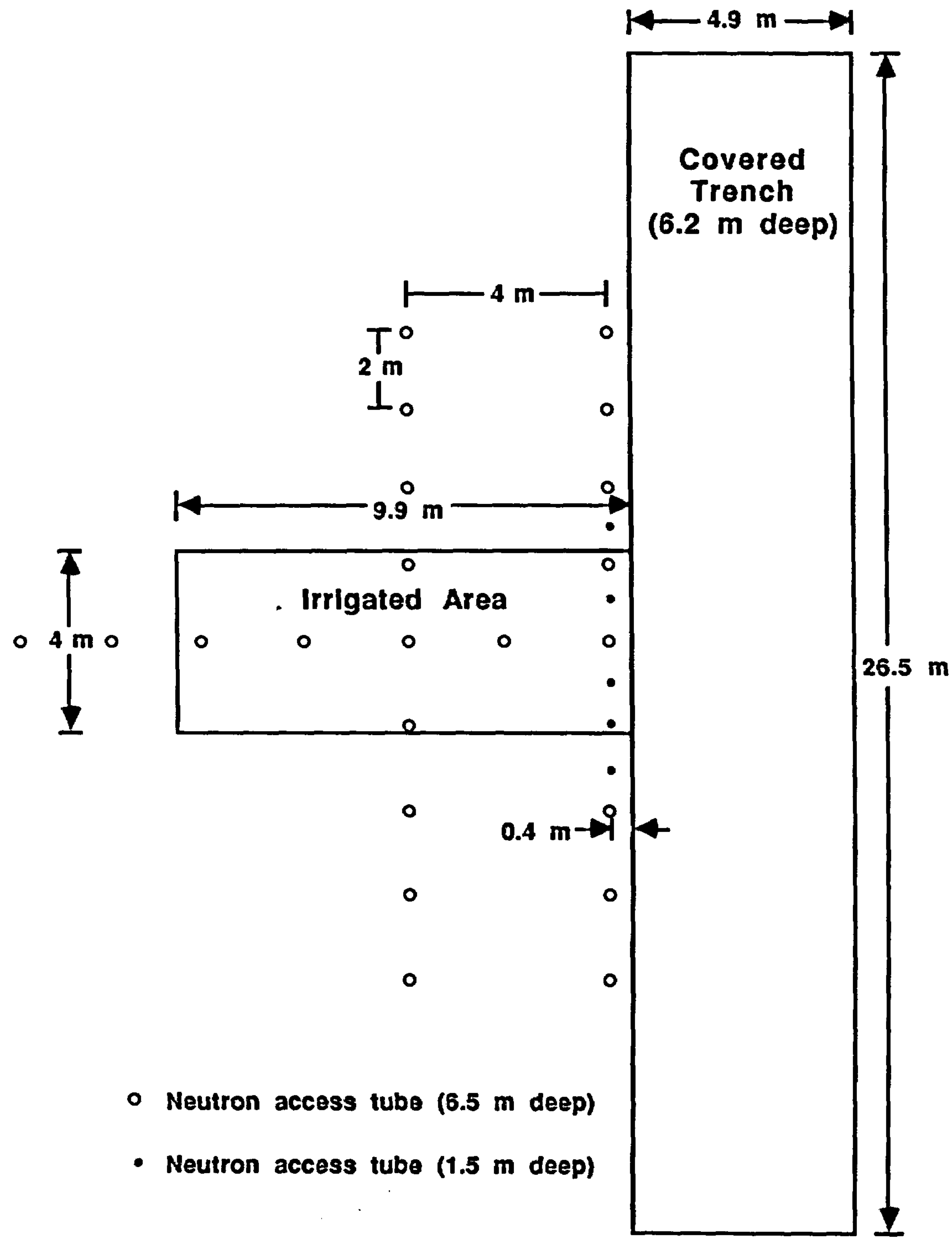

Figure 3-3. Top view of trench and irrigated area [Reproduced from Wierenga et al (1986b); revised based on personal communication, P.J. Wierenga (1987)]

trickle lines laid out on a fixed frame suspended several inches above the soil surface. Drip holes were located approximately 6 inches apart in a square grid over the entire irrigation area. A known flux of water and solute were supplied from a timer-controlled pump and storage tank system designed for intermittent irrigation during several periods throughout the day. The intended application rate was 2 cm/day. Due to several instances of mechanical/electrical problems, however, the average irrigation rate for the application period of about 80 days was determined to be approximately 1.8 cm/day. The irrigation plot and surrounding areas, including the trench, were covered with plastic and other materials to prevent evaporation from the soil surface and to eliminate the input of rainfall or storm runoff water. To minimize evaporation from the exposed face of the trench adjacent to the irrigated area, humidified air was circulated inside the covered trench and the wetted face was covered with plastic.

A total of 26 vertical neutron probe access tubes were installed within and adjacent to the irrigated area to depths ranging from 1.5 to 6.5 m below ground surface. These access tubes were arranged in three rows (see Figure 3-3), providing for the collection of three-dimensional data. Prior to the start of irrigation, *in situ* moisture content determinations, based on the neutron probe readings, were made in all access tubes. Readings were then taken in all access tubes on a daily basis (with few exceptions and occasionally excluding weekends) for approximately the first two months of the irrigation period. The frequency was then reduced to an interval of several days. Vertical resolution (interval spacing) for the neutron probe readings was 25 cm in all cases. Details of the apparatus and the experimental data are discussed in Wierenga et al (1986a, b, 1988).

Suction tubes with ceramic porous cups were installed into the trench face into undisturbed soil to a horizontal distance of 0.5 m. These provided a two-dimensional array of sampling points over a vertical plane beneath and (laterally) adjacent to the irrigation area. The suction tubes were arranged in a square grid over the vertical plane, placed approximately 0.5 m apart (see Figure 3-4). A total of 103 suction cups were installed; during the experiment, 79 were used to measure tension and 24 were used to collect soil solution samples (see Figure 3-4). Tension was measured using a hand-held electronic tensiometer in those suction tubes located at or behind the advancing wetting front, with the number of sampling points increasing as the propagating front expanded in space. Tension measurements were made at a frequency of one to several days throughout the experimental period. The two-dimensional tension profiles determined during the experiment provide a basis to compare numerical simulation results using the stochastic theory and traditional deterministic analysis (see Section 4.6).

A tracer (tritium) was applied as a finite pulse of 10-day duration at the initiation of the irrigation experiment. Soil solution samples were collected from the suction tubes, using a vacuum system, at a frequency of one to several days during the course of the experiment. Samples were taken from the two-dimensional array to track both the leading and trailing fronts of the solute plume. Details of the analyses and experimental results are presented by Wierenga et al (1988).

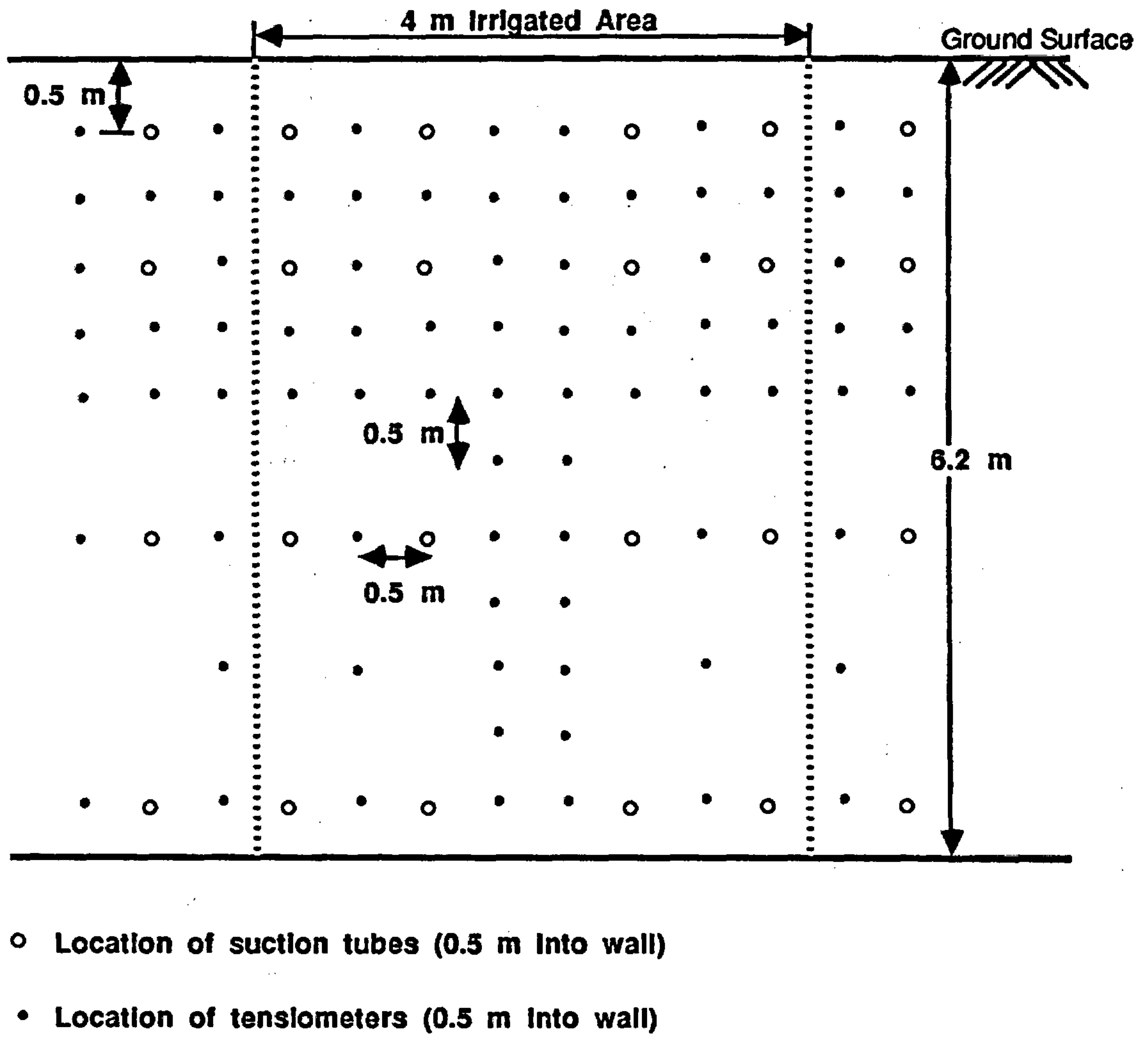

Figure 3-4. Side view of trench with location of tensiometers and suction tubes [Reproduced from Wierenga et al (1986b); revised based on personal communication, P.J. Wierenga (1987)]

CHAPTER 4

THE MEAN FLOW MODEL

4.1 Introduction

This chapter discusses the implementation and testing of a numerical technique to solve the large-scale mean unsaturated flow equation (2-18), and the application of this technique to one-dimensional (1D) and two-dimensional (2D) examples. The numerical formulation for the 1D and 2D cases is presented first, followed by a summary of numerical tests which were performed to evaluate the computer codes and example results from the applications.

A flow model for the 1D version of (2-18) was developed first and much of the work on this case was completed before proceding to the study of multi-dimensional aspects of the mean flow problem. There were several reasons for this. The 1D case is simpler to develop and significantly less demanding to solve. Thus, it provides an efficient setting to examine various solution techniques and, more important, to explore new concepts of the flow problem inherent in the stochastic theory. In many ways, studies here were preliminary both in developing an understanding of the unique aspects of the stochastic theory and in comparison to field tests. At the time simulations were performed, the input data for field parameters were incomplete and estimates were required for some cases. The goal of the 1D model simulations was to compare predicted flow results to deterministic analyses and to lysimeter experiments at the Las Cruces, New Mexico field site. Selected tests and comparisons are discussed.

The flow model of the 1D version of (2-18) was extended to two dimensions to investigate the anisotropic character of the effective hydraulic conductivity, in addition to large-scale hysteresis (also evident in the 1D case). Analyses were constrained with a particular set of geometry, boundary and initial conditions in order to evaluate aspects of sensitivity to the statistical inputs. An early goal of this work was to assist in the design of the Las Cruces, New Mexico trench experiment, based on preliminary understandings of the field soil parameters and their variability. The sensitivity analyses are discussed in detail and a preliminary comparison with field results is presented.

Operational modifications for numerical simulation, as compared to the original derivation of the stochastic theory, are discussed in Section 2.2.5. These were developed as experience accrued with the 1D and 2D models, and as the sensitivity analyses revealed the roles of the soil parameter inputs. As a result of this model development process, the 2D case presented here utilizes functional forms different from the 1D case. In particular, the hydraulic conductivity-tension relation in 1D is an exponential function which is linear in log conductivity over the full range of tension [see equation (2-1)]. In the 2D case, the log linear function is applied locally over a limited range of tension and a van Genuchten-type relation is used as a means of varying the slope of this function and re-linearizing as the mean tension changes [see (2-45), which is used as a mean version of (3-5)]. Also, the moisture content-tension relation in 1D is a linear function over the full range of tension, leading to a constant specific moisture capacity. In the 2D case, the van Genuchten function is used to provide a variable specific moisture capacity. This continuous form can be viewed as an extrapolation of a locally linear moisture retention curve which has a constant slope over a given range of tension. The importance of these modifications is reviewed in Section 4.7.

4.2 Numerical Implementation

The model to be analyzed for the case of one-dimensional flow is a version of (2–18):

$$C(H)\,\frac{\partial H}{\partial t} = \frac{\partial}{\partial z}\left[\hat{K}_{11}\frac{\partial(H+z)}{\partial z}\right] \tag{4–1}$$

The flow domain is discretized and an implicit finite-difference procedure is utilized in writing a solution scheme as follows:

$$C(H)\frac{(H_i^{n+1} - H_i^n)}{\Delta t} = \left[\frac{\hat{K}_{i+1/2}^{n+1}}{\Delta z^2}\,(H_{i+1}^{n+1} - H_i^{n+1}) - \frac{\hat{K}_{i-1/2}^{n+1}}{\Delta z^2}\,(H_i^{n+1} - H_{i-1}^{n+1})\right] - \frac{(\hat{K}_{i+1/2}^{n+1} - \hat{K}_{i-1/2}^{n+1})}{\Delta z} \tag{4–2}$$

where $t = n\Delta t$ with $n = 0, 1, 2...$ is the time discretization and $z = i\Delta z$ with $i = 0, 1, 2...$ is the spatial discretization. The mid-nodal conductivities are formed by the geometric mean [i.e., $K_{i+1/2} = (K_i \bullet K_{i+1})^{1/2}$]. The system (4-2) is generally a nonlinear system of equations because the conductivity is dependent on the mean tension. However, if the conductivity at a given space-time step is interpreted as a known value which is updated within that step through an iterative scheme, then (4-2) is viewed as a linear system and can be represented by a tridiagonal coefficient matrix. Such a system is readily solved by a band solver technique; in this application, the Thomas algorithm [Huyakorn and Pinder (1983)] was chosen as a solution procedure for the equation set (4-2).

The discretized system (4-2) is solved using a Picard iteration method [see, for example, Huyakorn and Pinder (1983)]. The use of other iteration schemes such as a chord-slope type Newton-Raphson [Huyakorn and Pinder (1983)] was investigated, but Picard was chosen based on its reliability in converging to solutions for the cases examined. This method was found to take longer to converge to solutions at early times in the simulation as compared to later; this is typical of many other solution techniques as well. Improved convergence to a solution for the H field at each time step was found by a simple modification to the general iterative procedure. Within each time step, the value of the tension field from the last iteration step is saved, and while advancing through the iterative scheme, the current value of tension and the old iterate value are averaged; this average value is used to calculate an updated value of effective conductivity. The updated conductivity is then used to solve (4-2) in the subsequent iterative step. Based on the example cases analyzed, it appears that use of this averaging technique increased the rate of convergence of the iterative procedure. In most cases, the number of iterations required per time step was decreased significantly. A more detailed discussion of the 1D simulations is available in Mulford (1986).

The operational modifications and assumptions described in Section 2.2.5 were applied to both the 1D and 2D simulations except with regard to the re-linearization of functional forms, as noted in Sections 2.2.5 and 4.1. In the 2D case, the gradient of H in both the horizontal and vertical directions was assumed to be zero *in the evaluation of the effective conductivity*. Also, the gradient of E[ah] in both directions was assumed to be zero. For the 2D case, the large-scale unsaturated equation (2-18) was used as the flow model in the form

$$C(H)\,\frac{\partial H}{\partial t} = \frac{\partial}{\partial z}\left[\hat{K}_{11}\frac{\partial (H+z)}{\partial z}\right] + \frac{\partial}{\partial x}\left[\hat{K}_{22}\frac{\partial H}{\partial x}\right] \tag{4-3}$$

Note that cross terms in the conductivity tensor are equal to zero because of the assumption that the conductivity is aligned with the principle axes of the statistical anisotropy. An implicit finite difference technique was again chosen as the solution method; the discretization used is:

$$\begin{aligned} C(H)\,\frac{(H_i^{n+1} - H_i^n)}{\Delta t} = &\left[\frac{\hat{K}^{n+1}_{22\ i+1/2,j}}{\Delta x^2}\,(H^{n+1}_{i+1,j} - H^{n+1}_{i,j}) - \frac{\hat{K}^{n+1}_{22\ i-1/2,j}}{\Delta x^2}\,(H^{n+1}_{i,j} - H^{n+1}_{i-1,j})\right] \\ &+ \left[\frac{\hat{K}^{n+1}_{11\ i,j+1/2}}{\Delta z^2}\,(H^{n+1}_{i,j+1} - H^{n+1}_{i,j}) - \frac{\hat{K}^{n+1}_{11\ i,j-1/2}}{\Delta z^2}\,(H^{n+1}_{i,j} - H^{n+1}_{i,j-1})\right] \\ &+ \frac{(\hat{K}^{n+1}_{11\ i,j+1/2} - \hat{K}^{n+1}_{11\ i,j-1/2})}{\Delta z} \end{aligned} \tag{4-4}$$

where $t = n\Delta t$ with $n = 0, 1, 2...$ is the time discretization, $x = i\Delta x$ with $i = 0, 1, 2...$ and $z = j\Delta z$ with $j = 0, 1, 2...$ are the spatial discretizations. For the 2D system in (4-4) a band solver technique is used to obtain values for H at each point in space for the given time step. This is a simple but effective solution method. As with the 1D simulations, an updated conductivity field is determined based on an average value of the current and previous iterates for H, and the system (4-4) is re-solved. The procedure is repeated until a convergence criterion is met, and then the system is stepped to the next time value. For the simulations described here, the criterion for convergence is a specified maximum relative error. That is, for a particular time step, convergence to the correct tension field is assumed when the magnitude of change from the previous iterate, divided by the previous time step nodel value, is less than a specified numerical value at all nodes in the field.

4.3 Verification of the Numerical Solution Technique

The general iterative solution procedure used in the unsaturated-flow simulation program was tested by comparing selected results to those of other solution techniques for both one-dimensional and two-dimensional cases. Numerical simulations were performed to: (i) verify satisfactory convergence for the iterative solver and, (ii) explore the importance of spatial grid and time-step resolution. To facilitate direct comparison to other available methods, these test simulations utilized deterministic unsaturated conductivity – tension relations and moisture content – tension relations and selected initial and boundary conditions. The specific constitutive relations and auxiliary conditions used for these tests are discussed by Celia et al (1987).

Comparison of the solution technique of the present model to other methods for 1D is presented in Figure 4-1. In this case comparison is based on position of the moisture front at a given time. The "exact" finite-difference solution is described by Celia et al (1987) as earlier work performed by van Genuchten using extremely fine discretizations in space and time. The collocation model result is from the alternating-direction collocation method of Celia et al (1987). Both cases of the present model in Figure 4-1 used a time step of 1 minute, with case (b) having a ten-times finer spatial resolution. The collocation model used a spatial discretization of 2.5 cm.

Comparisons for the 2D flow model are presented in Figure 4-2. In this case, comparison is based on the two-dimensional position of contours of equal tension at a given time. The collocation model result is that of Celia et al (1987) and utilizes a horizontal discretization ranging from 2.5 to 20 cm and a vertical discretization ranging from 5 to 20 cm. Both cases of the present model in Figure 4-2 used a constant horizontal spacing of 2 cm and a constant vertical spacing of 1 cm, with case (b) having a six-times finer temporal resolution.

The numerical results, expressed as moisture content or tension distributions, are quite sensitive to the choice of spatial discretization and time-step size. Over the range of grid and time-step size examined here, the accuracy of the solution improved when space and/or time resolution was increased. The results presented in Figures 4-1 and 4-2 provide evidence of a satisfactory solution method in the present model. However, it is clear that the space and time discretization should be as fine as practical constraints allow. Based on these results and considerations, the numerical simulations described below, involving effective (stochastic) coefficients, utilized vertical spatial grids of 1 to 5 cm for the 1D case and 2.5 to 5 cm for the 2D case (a fraction of the vertical correlation length, which was 10 to 25 cm), a horizontal spatial grid of 20 cm for the 2D case (approximately the correlation length), and time-step sizes ranging from a minute or less to one hour.

4.4 Availability of Data for Input

Application of the stochastic theory to a model simulation requires knowledge of the soil parameters which characterize the simulated setting. The soil parameters required for the stochastic model presented here are F, the mean of the natural log of saturated conductivity, and its variance, σ_f^2; A, the mean of the slope of the log conductivity versus tension curve, and its variance, σ_a^2; and the correlation length, λ_1. A literature review was performed to identify whether the spatial data required to estimate these parameters (or actual estimates of the parameters) could be found in papers which describe field soil spatial variability experiments. This review considered only papers containing soil spatial variability data applicable to the stochastic model used here. Although many studies involving spatial variability of soil parameters were identified, it was determined that most of the papers did not contain

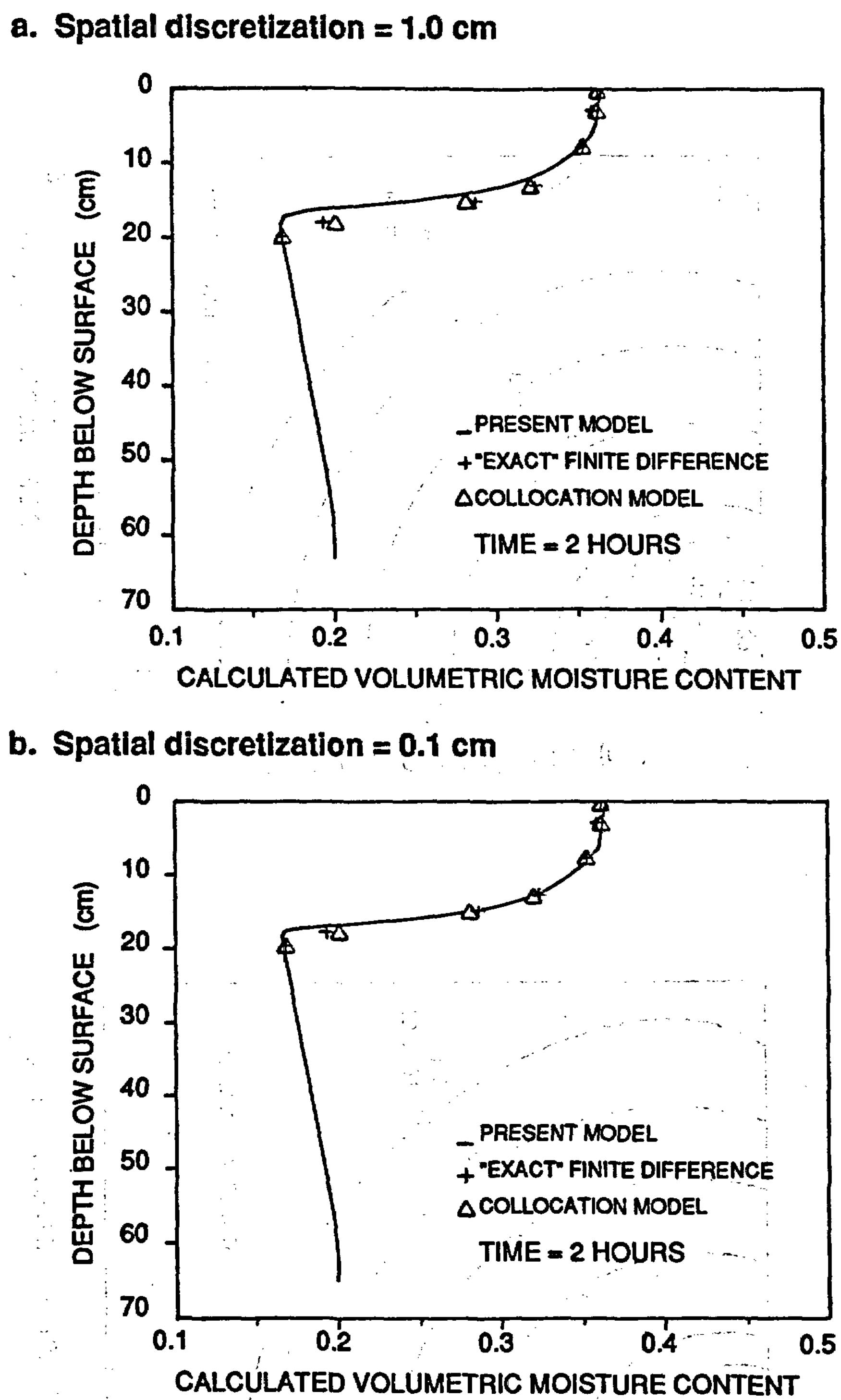

Figure 4-1. Comparison of solution technique to other methods for one-dimensional flow

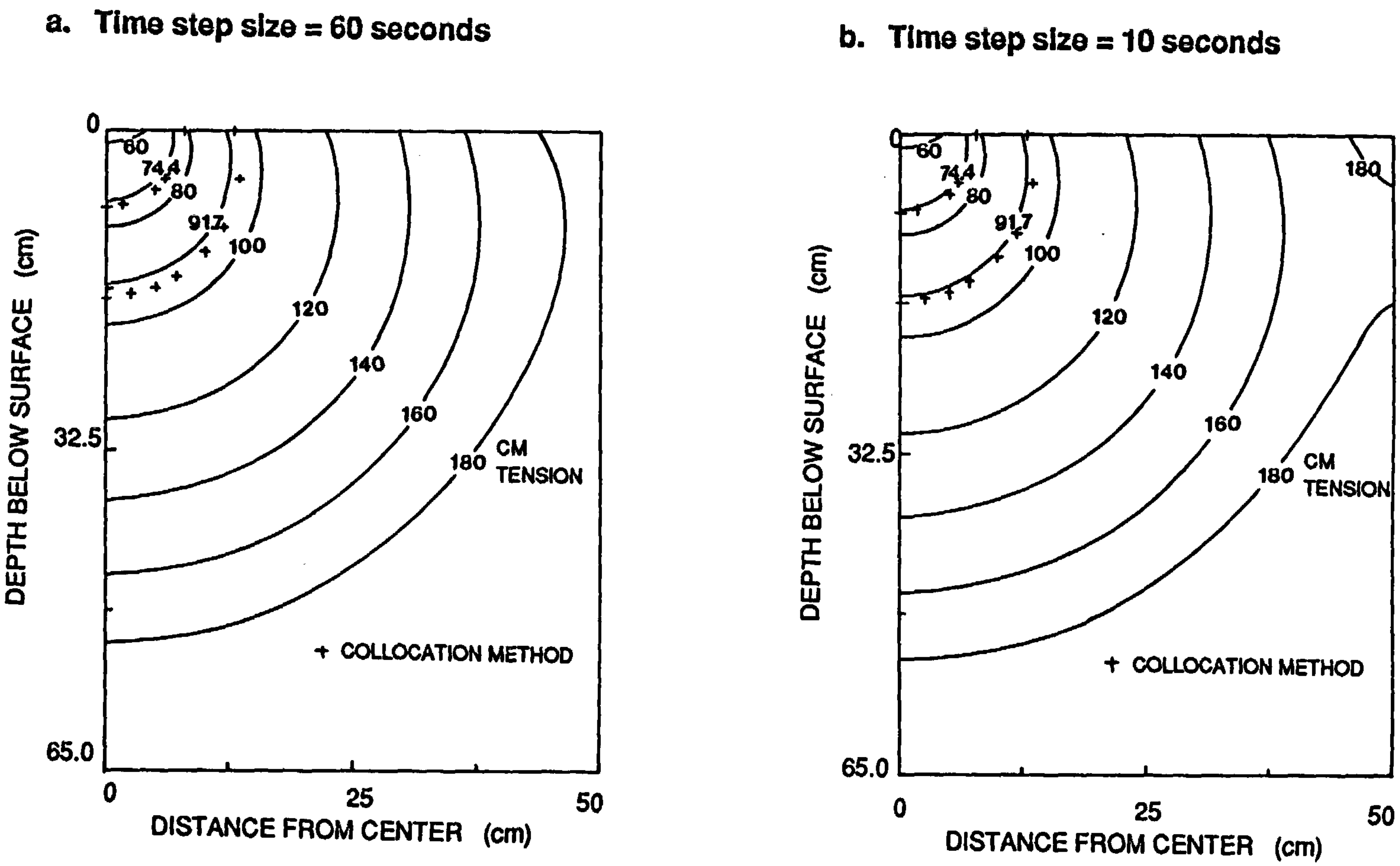

Figure 4-2. Comparison of solution technique to other methods for two-dimensional flow

information on the parameters required for this model. A summary of the literature search is presented in Table 4-1.

It is clear from Table 4-1 that very few of the spatial variability field studies that were reviewed provide all the data required for a stochastic model of the type described in this report. Only one set of A and σ_a^2 values were found, that of Russo (1983). Several values of correlation scales are given; the values reported for vertical correlation scales range from 0.08 meters to 1.8 meters. Horizontal correlation information in the form of covariance or variogram estimates were reported in several studies [Byers and Stephens (1984); Russo (1983)]. Saturated conductivity was the parameter with the most spatial data available. Estimates of F ranged from -2.91 to -9.68 (K_s in cm/s), and the estimates of the variance of f ranged from 0.20 to 0.91.

Information is included in Table 4-1 on the availability of data for mean specific moisture capacity [Γ] and it's variance [σ_γ^2] and also for horizontal correlation scales; these are presented for completeness only. Knowledge of the horizontal correlation scales is not required for the present model due to the stratified soil assumption (see Section 2.2.4). This information would be useful, however, when considering the validity of assuming a large ratio of horizontal to vertical correlation lengths. Specific moisture capacity is assumed deterministic in the present study. However, the variability of this term (expressed through σ_γ^2) is included in the general theory [see Mantoglou and Gelhar (1987a, b, c)]. The importance of this parameter should be addressed in future model simulations which address large-scale flow. No values of Γ or σ_γ^2 are given directly in the literature; however, several studies contain data from which some estimate of these parameters might be derived.

Based on this brief literature review, it is clear that few experiments have been performed which provide the type of data required to apply the stochastic model described here. The study that most nearly contained the data required for the stochastic model was Russo (1983), which provided information on all parameters required for the present model except λ_1. In general, only a minimal amount of spatial data is available to use as inputs to the stochastic model. Availability of such data is a vitally important segment of the stochastic method used here and the data requirements should be carefully considered in future research efforts.

4.5 One-Dimensional Application

4.5.1 Configuration and auxiliary conditions

The flow model to be analyzed numerically for the 1D case is given by (4–2). The boundary and initial conditions chosen for this problem are as follows:

at $z = 0$,	$q = \text{constant}$	$0 \le t \le \infty$;
at $z = L$,	$H = \text{constant}$	$0 \le t \le \infty$;
at $t = 0$,	$H = \text{constant}$	$0 \le z \le L$.

Boundary conditions are depicted in Figure 4–3, which shows a vertical column consisting of alternating layers of two selected soils. The numerical study presented here simulates the

Table 4-1. Survey of Spatial Variability Data Applicable to the Stochastic Model

					PARAMETERS (‡)								
Author(s), Date	Soil Type	Sample Spacing; Irregular (I) Grid (G)	Number of Samples	Parameters Measured and Presented	K_s	σ_f^2	A	σ_a^2	Γ	σ_γ^2	λ_1	λ_2	λ_3
Baker, 1978	nine Wisconsin soils	I	30 samples for each soil; 3 ψ values for each sample	K - ψ graphs; mean $K(\psi)$ values and variances given for different K measurements at single ψ values	3	2	1	1	0	0	0	0	0
Byers and Stephens, 1983	fluvial sand, Socorro, NM	G; 3-d	100 samples each in 2 horizontal directions; 71 samples in vertical	K_s; means and variances of K_s given; 3 correlation lengths given for $\ln(K_s)$	2	3	0	0	0	0	3	3	3
Carvallo et al, 1976	Maddock sandy loam	G	5 plots; 7 depths to 1.5m	θ - ψ data; K - ψ graph, data over 3 dimensions; K_s can be estimated from $K(\psi)$	2	2	1	1	1	1	1	1	1
Cassel, 1983	Norfolk soil	I	4 sites, 3 depths, 3 surface conditions	K_s, θ, n at 3 times; $\psi(t)$ at one location with few θ measurements; means and variances of K_s given for 3 depths	3	3	0	0	0	0	0	0	0
Gatjem et al, 1981	Pima clay loam	G	100 samples each taken on 9 horizontal transects	soil physical and chemical properties; θ; data given; $\theta(\psi)$ for 2 ψ values; areal mean θ at field pressure; "zone of influence" defined	0	0	0	0	0	0	0	2	2
Jury et al, 1982	not available	I	16 plots to monitor vertical flow to 1.5m and transport to 3m	drainage measurments; weekly θ measurements; some K information; data available	1	1	0	0	0	0	1	1	1

(‡) see end of table for explanation of codes

Table 4-1 (continued). Survey of Spatial Variability Data Applicable to the Stochastic Model

Author(s), Date	Soil Type	Sample Spacing; Irregular (I) Grid (G)	Number of Samples	Parameters Measured and Presented	PARAMETERS (‡) K_s	σ_f^2	A	σ_a^2	Γ	σ_γ^2	λ_1	λ_2	λ_3
Kies, 1981	Glendale clay loam	I	1 plot 7m by 7m; 15 locations with 13 depths	K_s data for each depth; $K(\theta)$ curves from core samples; θ measurements, some $\theta(t)$ curves, fitted water release curves	2	2	1	1	1	1	1	0	0
Nielsen et al, 1973; also, Biggar and Nielsen, 1976	Panoche soil	I	20 plots with tension at 6 depths to 1.8m; 5 plots with tension at 3m and suction probes to 6m; 3 cores at 2 sites (6 depths) in each plot used for lab moisture curve	θ - ψ, K - θ data; moisture curve data; areal means and variances of θ, based on moisture curves; means and variances of $K(\theta)$; K_s data; means and variances of flow rates over depths and areas	3	2	1	1	1	1	1	1	1
Russo and Bresler, 1980	Hamra Red Mediterranean soil	I	30 sites in a 2m by 2m area	θ - ψ, K - ψ curves for 3 cores given; mean and variance of K_s given for field	2	3	1	1	1	1	0	1	1
Russo and Bresler, 1981a,b; also Bresler et al, 1984	Hamra Red Mediterranean soil	I	30 sites, each 2.2m by 2.2m; 4 depths to 1.2m	K_s, sorptivity, θ_s, θ_r over 3 dimensions measured; modeling of $\theta(\psi)$ using measured parameters; means and variances of measurements and modeled results; discussion of integral scales	3	3	0	0	0	0	1	2	2
Russo, 1983,	Zofar soil	I	31 sites, each 3m by 3m; tensiometers at 5 depths to 0.5m; neutron probes to 0.6m	$K(\theta)$ and K_s determined for each site; θ measured but no data given; K_s and alpha variances, variograms and integral scales given and discussed; vertical variations not considered	3	3	3	3	0	0	0	3	3

(‡) see end of table for explanation of codes

Table 4-1 (continued). Survey of Spatial Variability Data Applicable to the Stochastic Model

Author(s), Date	Soil Type	Sample Spacing; Irregular (I) Grid (G)	Number of Samples	Parameters Measured and Presented	PARAMETERS (‡) K_s	σ_f^2	A	σ_a^2	Γ	σ_γ^2	λ_1	λ_2	λ_3
Sharma et al, 1980	not available	G	26 sites with surface infiltrometers	soil surface K_s determinations based on steady infiltration tests	3	2	0	0	0	0	0	1	1
Sisson and Lu, 1984	4 soils at Hanford, WA	G; 3-d	1 site; injection test; radial array of wells and neutron probes	4 values of K_s for 4 soils at 4 depths given; 4 $K(\psi)$ curves for each soil; $\theta(t)$ data given for 3 dimensions	2	1	1	1	0	0	1	1	1
Sisson and Wierenga, 1981	Typic Torrifluvent	G	25 large, 125 medium and 625 small infiltrometers	soil surface K_s determinations based on steady infiltration tests	3	3	0	0	0	0	0	3	3
Smith, 1981	Quadra sand	I,G	100 single points; 1- 10 point square; 2- 100 point lines (horizontal and vertical)	K_s, n for each sample; no data given; means and variances for K_s, $\ln(K_s)$ and n; some correlation and spectral calculations given	3	3	0	0	0	0	3	3*	3*
Vieira et al, 1981	Yolo loam	G	1280 infiltrometers	soil surface K_s determinations based on steady infiltration tests; autocorrelograms and variograms given	3	3	0	0	0	0	0	3*	3*

*assumed horizontally isotropic

(‡) Explanation of Parameter Codes:

(3) A direct measurement of the parameter (or some form of it) was made by the authors from data and presented.

(2) Inference of the parameter (or some form of it) should be possible from the data given.

(1) Inference of the parameter (or some form of it) might be possible from the data given; maybe only a guess.

(0) Not possible to estimate parameter based on data of the experiment; not pertinent to the given study.

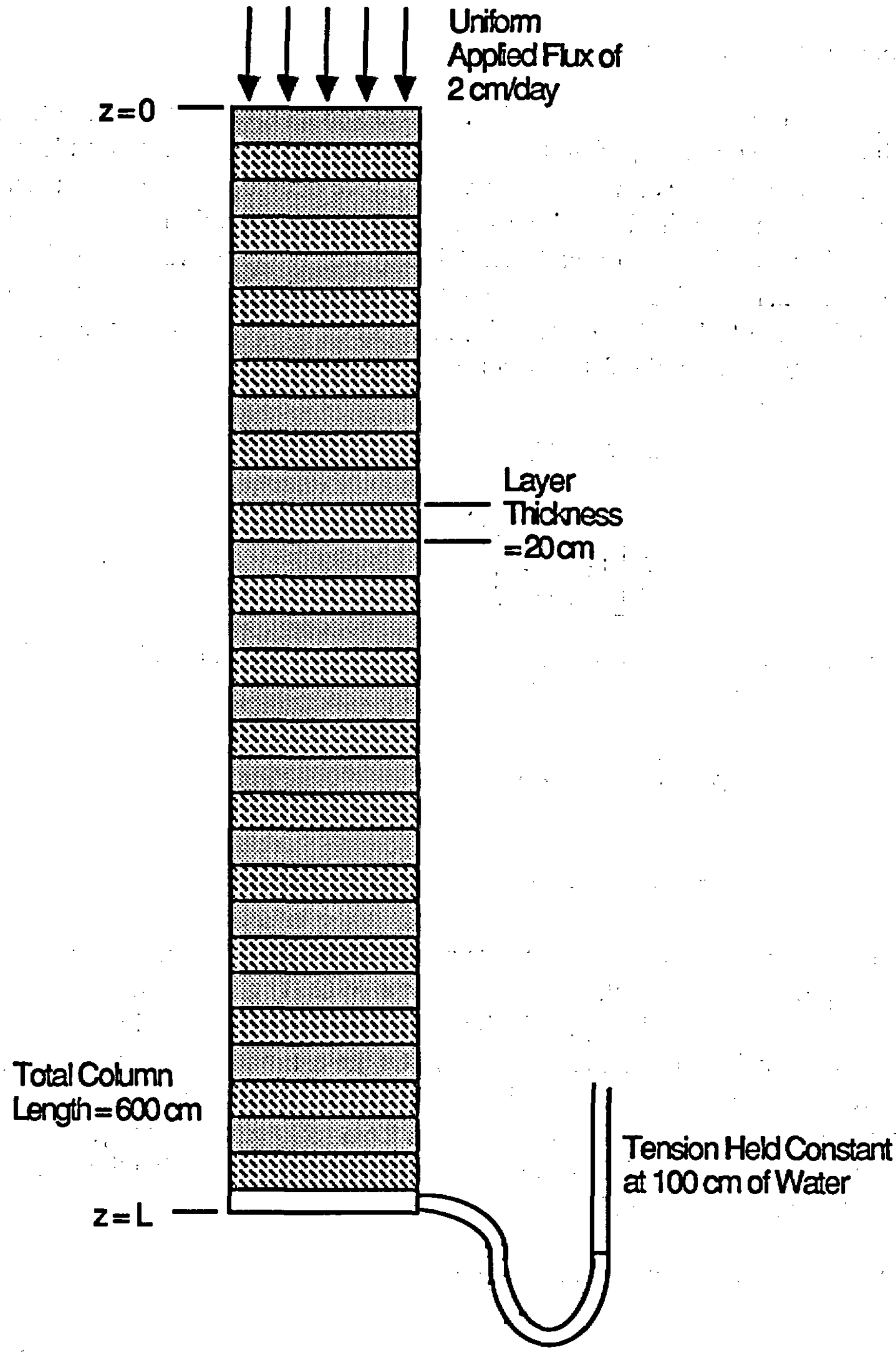

Figure 4-3. Physical structure and boundary conditions for the one-dimensional simulation

layered lysimeter experiment discussed in Section 3.3. The objective of the 1D numerical experiment was to predict the movement of the moisture front through the lysimeter, given a constant flux of 2 cm/day uniformly applied at the top of the column.

4.5.2 Model input parameters

Application of the numerical model requires values for the soil parameters: F, A, and C (mean values for the column); σ_f^2 and σ_a^2 (variances); and λ_1 (the correlation length in the vertical direction). Estimates for these parameters were developed as follows: estimates for the saturated conductivity K_s and the slope of the log conductivity versus tension curve [α] (based on preliminary data) were made available by Dr. Wierenga for both soils in the column (see Section 3.2.1 for discussion). The values of F and σ_f^2 for the column were obtained by assuming that ln K_s takes on two discrete values with equal probabilities. Given the estimates of K_s for both soils, the following formulae were used:

$$F = \ln (K_{s_1} \cdot K_{s_2})^{1/2} \tag{4–5}$$

$$\sigma_f^2 = \frac{1}{4}\left[\ln\left(\frac{K_{s_1}}{K_{s_2}}\right)\right]^2 \tag{4–6}$$

The parameter α was assumed to take on two equally likely values and the following formulae were used for the evaluation of A and σ_a^2:

$$A = \frac{1}{2}(\alpha_1 + \alpha_2) \tag{4–7}$$

$$\sigma_a^2 = \frac{1}{4}(\alpha_1 - \alpha_2)^2 \tag{4–8}$$

Moisture content versus tension data available at the time the simulations were performed were limited to the Berino soil. A constant value of C(H) was determined for the Berino soil by estimating the range through which the moisture content would vary, based on anticipated values of tension during the simulation. Of the estimates used in the simulation, the C estimate is probably the least accurate. The mean saturated moisture content θ_0 was also similarly approximated for the entire column. The final soil parameter is λ_1; it was estimated to equal one half of the layer thickness, the average distance over which the soil parameters are correlated in the layered lysimeter.

The soil parameters used in the simulation are

$$\begin{array}{lll} \text{Glendale} & K_{s_1} = 1.51 \times 10^{-4}\text{cm/s} & \multirow{2}{*}{\Big\}} \quad F = -6.93 \\ \text{Berino} & K_{s_2} = 6.26 \times 10^{-3}\text{cm/s} & \quad \sigma_f^2 = 3.47 \end{array} \tag{4–9}$$

$$\left.\begin{array}{lll} \text{Glendale} & \alpha_1 = 0.0392\ \text{cm}^{-1} \\ \text{Berino} & \alpha_2 = 0.0863\ \text{cm}^{-1} \end{array}\right\} \quad \begin{array}{l} A = 0.0628\ \text{cm}^{-1} \\ \sigma_a^2 = 0.000555\ \text{cm}^{-2} \end{array} \tag{4–10}$$

$$\text{Estimate of C for the entire column} \quad = \quad 0.003\ \text{cm}^{-1} \tag{4–11}$$

$$\text{Estimate of } \theta_0 \text{ for the entire column} \quad = \quad 0.33\ \text{cm}^3/\text{cm}^3 \tag{4–12}$$

$$\text{Estimate of vertical correlation length} \quad = \quad 10\ \text{cm} \tag{4–13}$$

Specific boundary and initial conditions are also required for the simulation. The initial tension in the column was taken to be 100 cm of water. This tension condition was held constant at the bottom boundary. The top condition simulated the lysimeter experiment with an average constant flux of 2 cm/day (see Figure 4-3). A modification was made in the simulation to minimize the difficulty of numerical solution due to sharp fronts at early times in the simulation. The 2 cm/day flux was not applied instantaneously, but rather was applied using a ramp in time, given by the following:

$$Q = \begin{cases} Q_i + \kappa t, & t < t^* \\ \\ 2\ \text{cm/day}, & t > t^* \end{cases} \tag{4–14}$$

where Q_i is the initial flux corresponding to gravity drainage due to the uniform initial tension, and κ is a constant controlling the rate at which Q approaches 2 cm/day. In the simulations described here, κ was $O(4\ \text{cm} \cdot \text{day}^{-2})$.

4.5.3 Hysteresis of effective conductivity

The range of hydraulic conductivities involved in the lysimeter simulation is shown in Figure 4–4 where the log of effective conductivity is plotted versus mean tension at selected values of $\partial H/\partial t$. Note that although curves are presented for only a few values of $\partial H/\partial t$, an infinite number of curves actually exist, bounded by the asymptotic values of effective conductivity for $\partial H/\partial t \rightarrow \pm\infty$ [see expressions for $\hat{K}$ in (2–37) and (2–38)]. As shown in Figure 4–4, the effective conductivity is hysteretic. Its value depends on the rate of change of tension in time and on whether the soil is wetting or drying; thus, it is a multi-valued function at a given tension.

4.5.4 Model results for the stochastic case

The calculated position of the propagating moisture front at selected output times is shown in Figure 4-5 as a plot of mean tension versus depth in the lysimeter. This figure illustrates both wetting and drying conditions. Wetting occurred for 500 hours. At 501 hours, the flux condition at the top was changed from 2 cm/day to zero, and the moisture in the column was

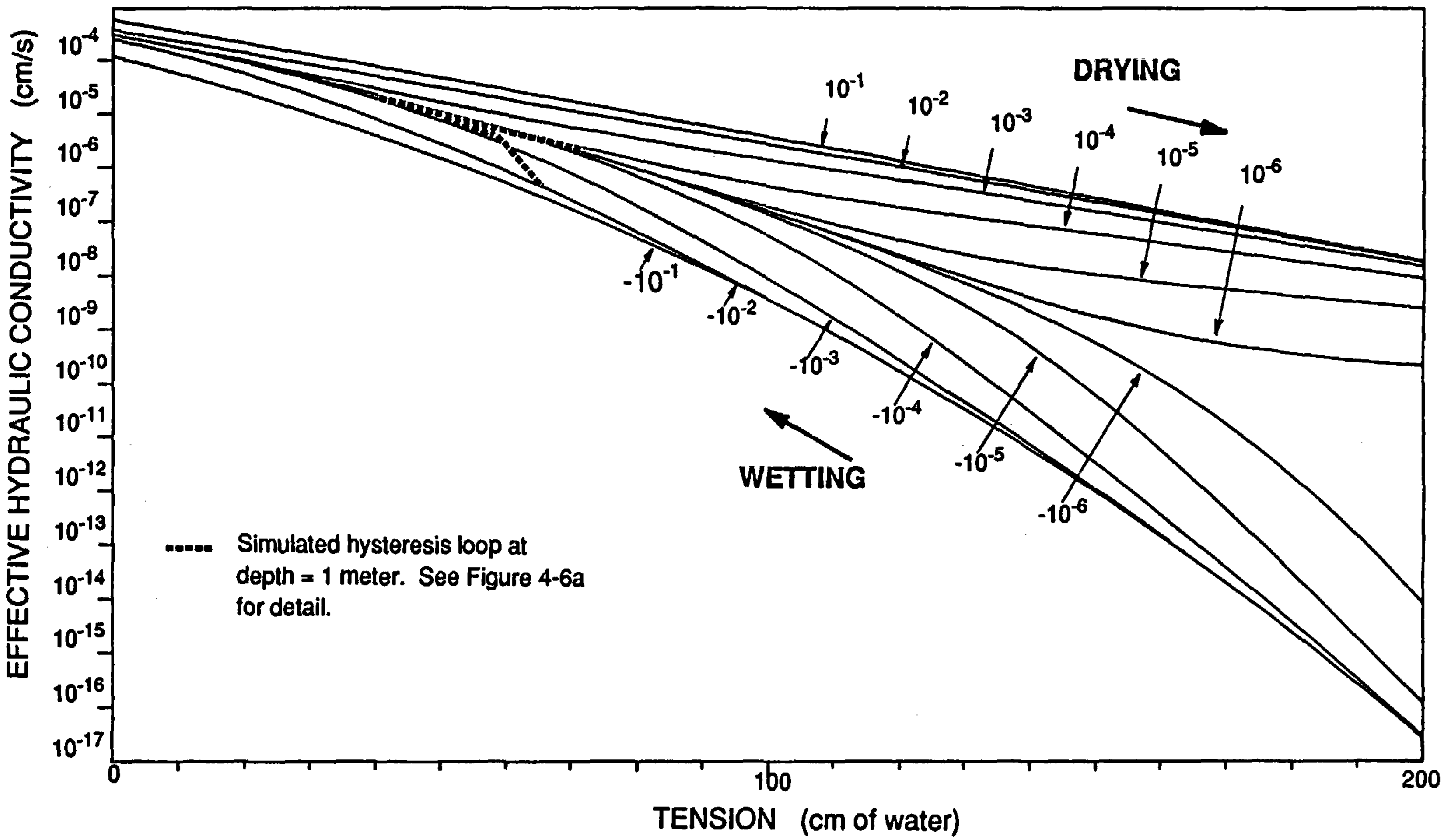

Figure 4-4. Effective hydraulic conductivity versus mean tension for selected values of $\partial H/\partial t$ during one-dimensional flow

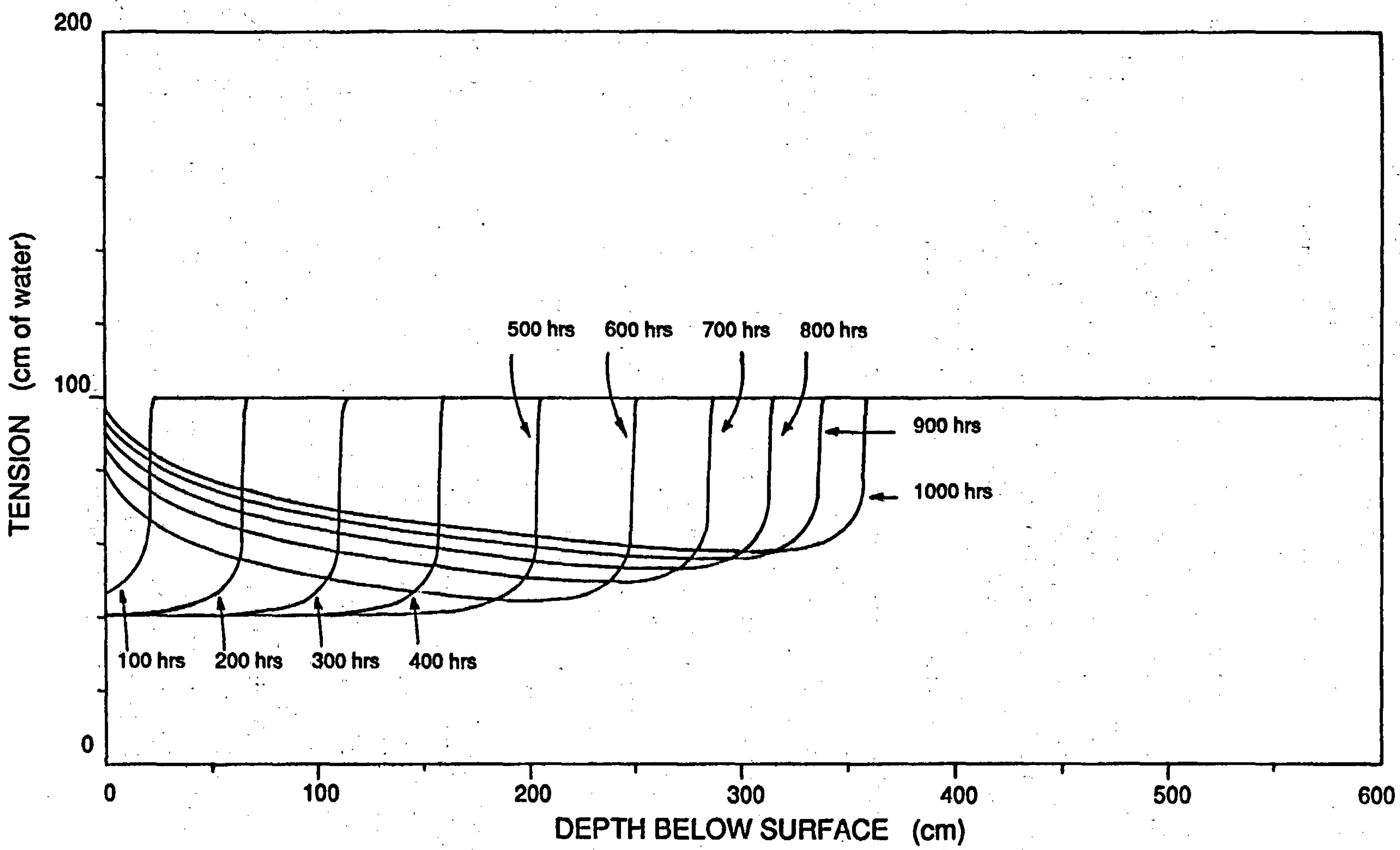

Figure 4-5. Propagation of tension front during wetting/drying cycle in the one-dimensional simulation

allowed to redistribute until 1000 hours had passed. The position of the moisture front is plotted every 100 hours for 1000 hours. The time step used in this simulation was 3600 seconds; the spatial step was 1 cm. Note the smooth nature of the solution and recall that this is a large-scale mean solution where small-scale variations within or across the layers are not represented. Note also, the sharpness of the wetted front. The approximate rate of movement of the front is 0.4 cm/hour, based on the rate of change of position of the "moisture front" lines.

At the one-meter and two-meter depths in the column, hysteresis is illustrated by plotting hydraulic conductivity as a function of tension. This corresponds to a plot of conductivity versus time at a specified point, with time evolution showing the passage of the wetting front. Effective hydraulic conductivity versus tension is plotted for the one-meter depth in Figure 4–6a, and for the two-meter depth in Figure 4–6b. These curves are based on equation (2.15) of Mulford (1986). The curves display the history of conductivity and tension at two locations in the column as infiltration and then redistribution occurred. The effects displayed here are not pore-scale hysteresis, but are developed in the theoretical analysis which incorporates large-scale heterogeneities such as layering. Note that the hydraulic conductivity under wetting conditions is up to an order of magnitude smaller than for drying.

The distribution of moisture content over depth during the simulation is illustrated by plotting this function every 100 hours for infiltration (0–500 hours) and redistribution (501–1000 hours), as shown in Figure 4-7. Moisture content and tension are assumed to be linearly related in the 1D simulations so that this graph is a simple transformation of that given in Figure 4-5. This illustration will be compared to the lysimeter experimental results.

The 1D experiment was also simulated using a uniform spatial discretization of 5 cm, and then again with 10 cm, for comparison to the 1 cm case described above. All other inputs were identical. The tension results for the 5 cm and 10 cm cases are presented in Figures 4–8a and 4–8b, respectively. Note the anomolous tension fluctuations that appear at the wetting front as the larger grid spacings are used in the simulation. Based on this type of result, all other simulations presented here used a spatial discretization of 1 cm for the 1D analyses.

Spatial and temporal changes in the variance of tension σ_h^2 are illustrated by plotting σ_h^2 versus depth at 100-hour intervals for the wetting and drying cycles, as shown in Figure 4-9. These curves are based on equations (17) and (20) of Mantoglou and Gelhar (1987b). The constant variance at depth is consistent with the constant tension at these depths (see Figure 4-5) and is indicative of the initial (dry) condition. The variance under these drier conditions (ahead of the moisture front) is higher than that associated with the wetted region of the column (behind the moisture front). Also, the tension variance increases in regions behind the front during the drying period of the simulation (see times of 600 hours and later in Figure 4-9). The variance increases sharply in the area of the wetting front, as shown by the spiked regions of the curves in Figure 4-9. This indicates a greater uncertainty and less reliability in the solution of mean tension in the vicinity of sharp fronts. This also brings into question the stationarity assumption utilized in the theoretical development, and indicates that the solution procedure may not be valid near sharp fronts due to this inconsistency.

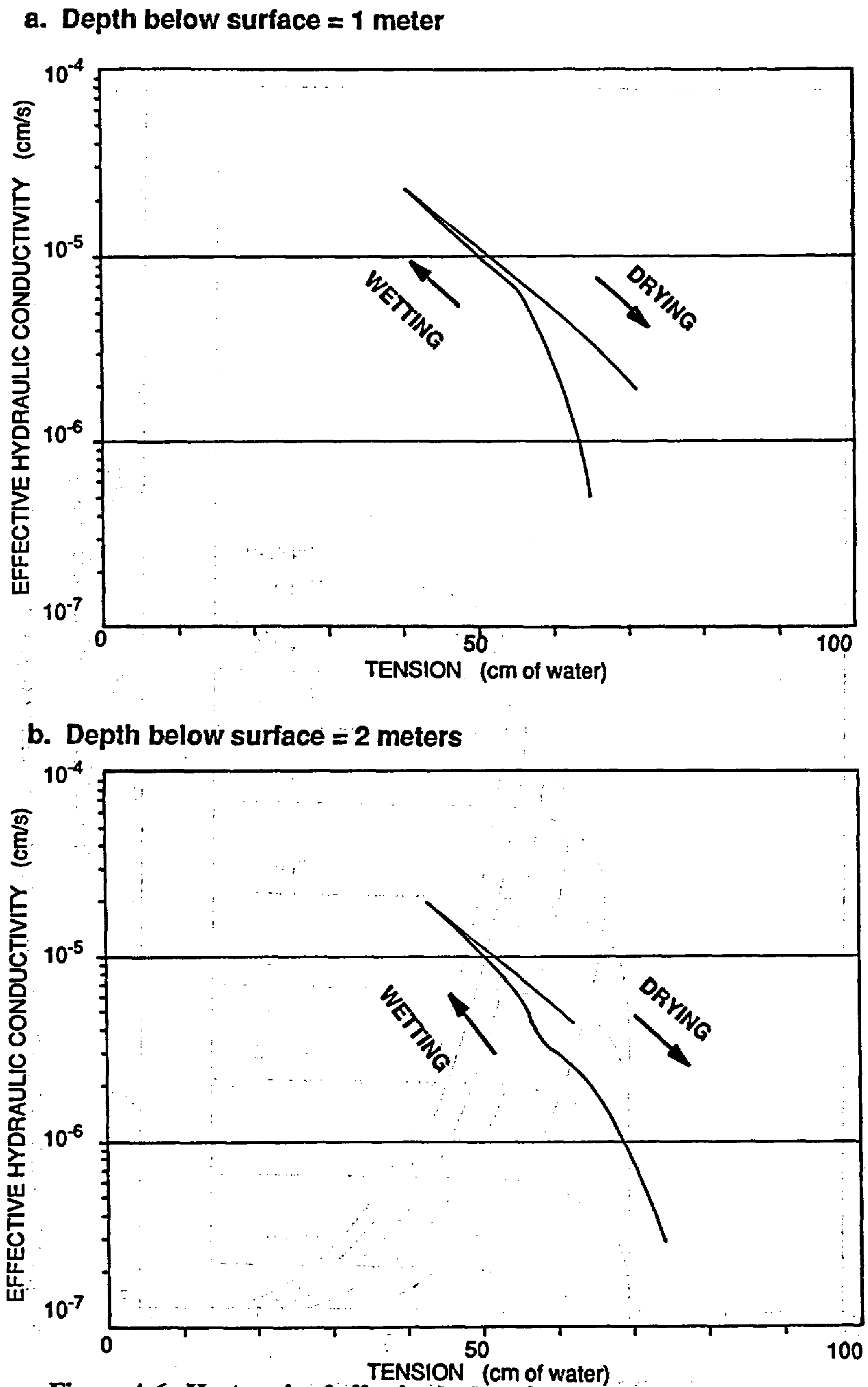

Figure 4-6. Hysteresis of effective hydraulic conductivity during wetting/drying cycle at 1- and 2-meter depths

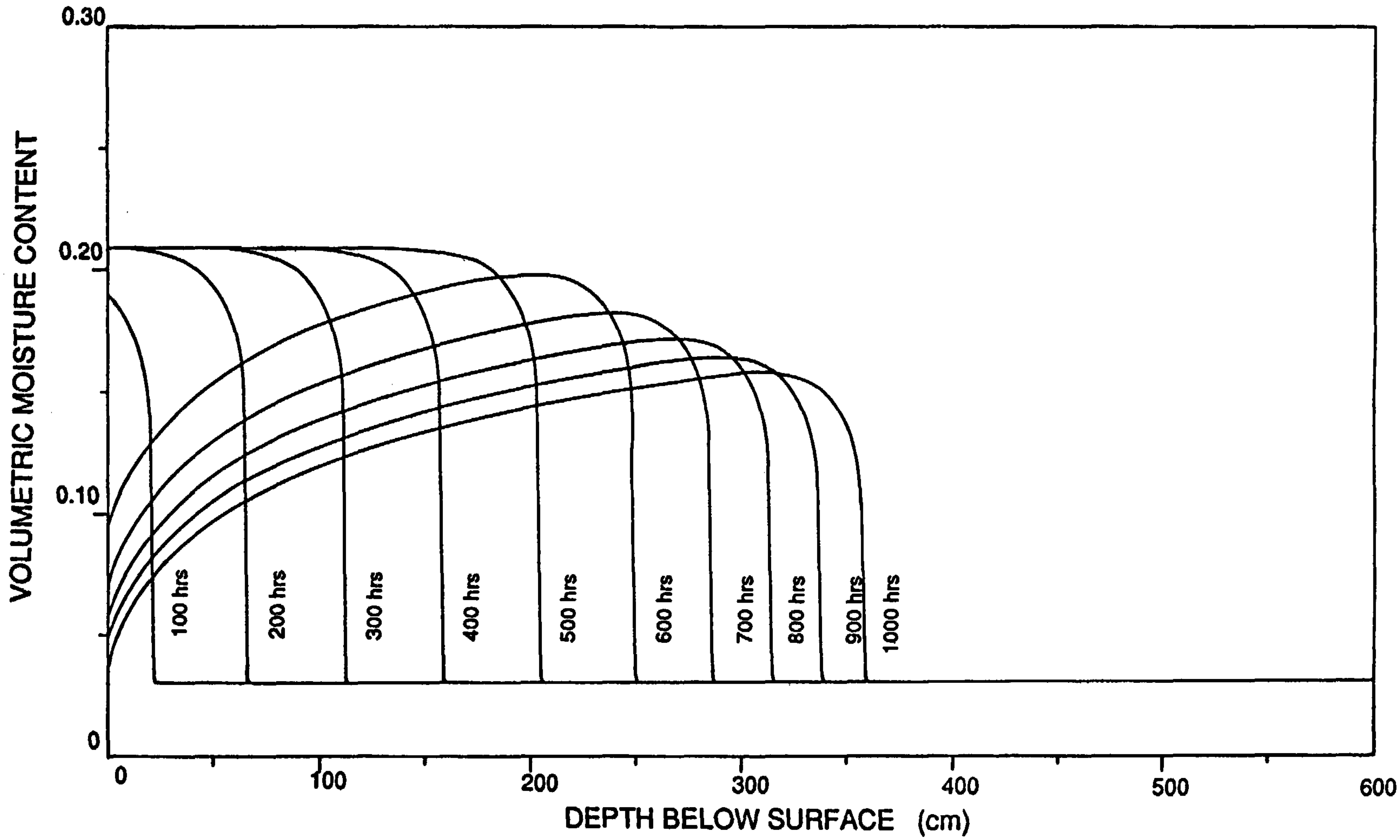

Figure 4-7. Propagation of moisture front during wetting/drying cycle in the one-dimensional simulation

a. Spatial discretization = 5 cm

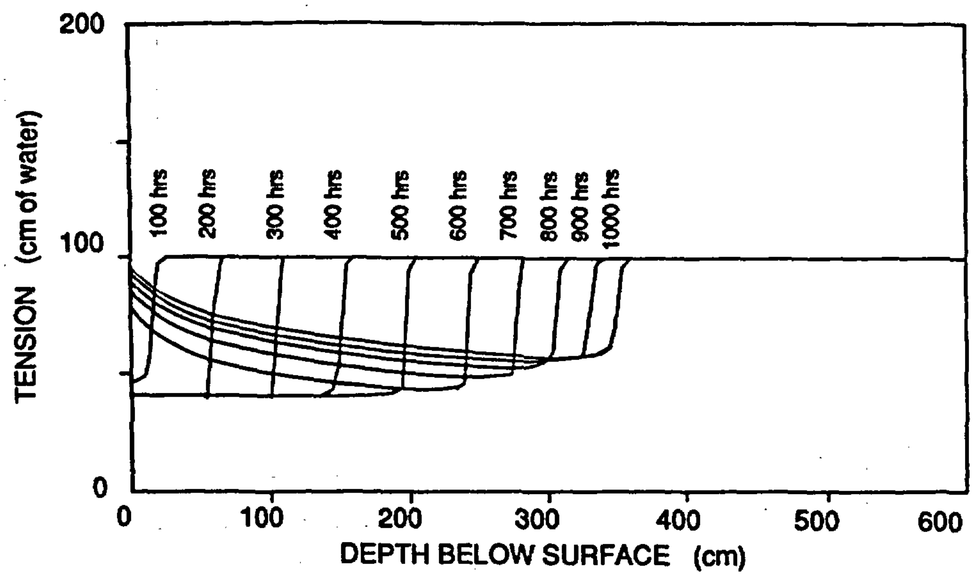

b. Spatial discretization = 10 cm

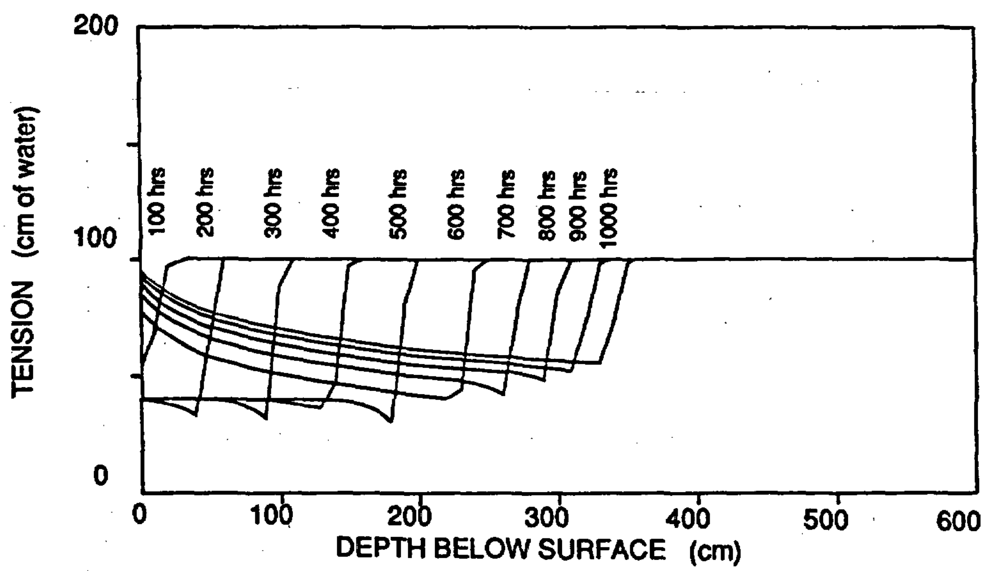

Figure 4-8. Propagation of tension front in the one-dimensional simulation using larger spatial discretization

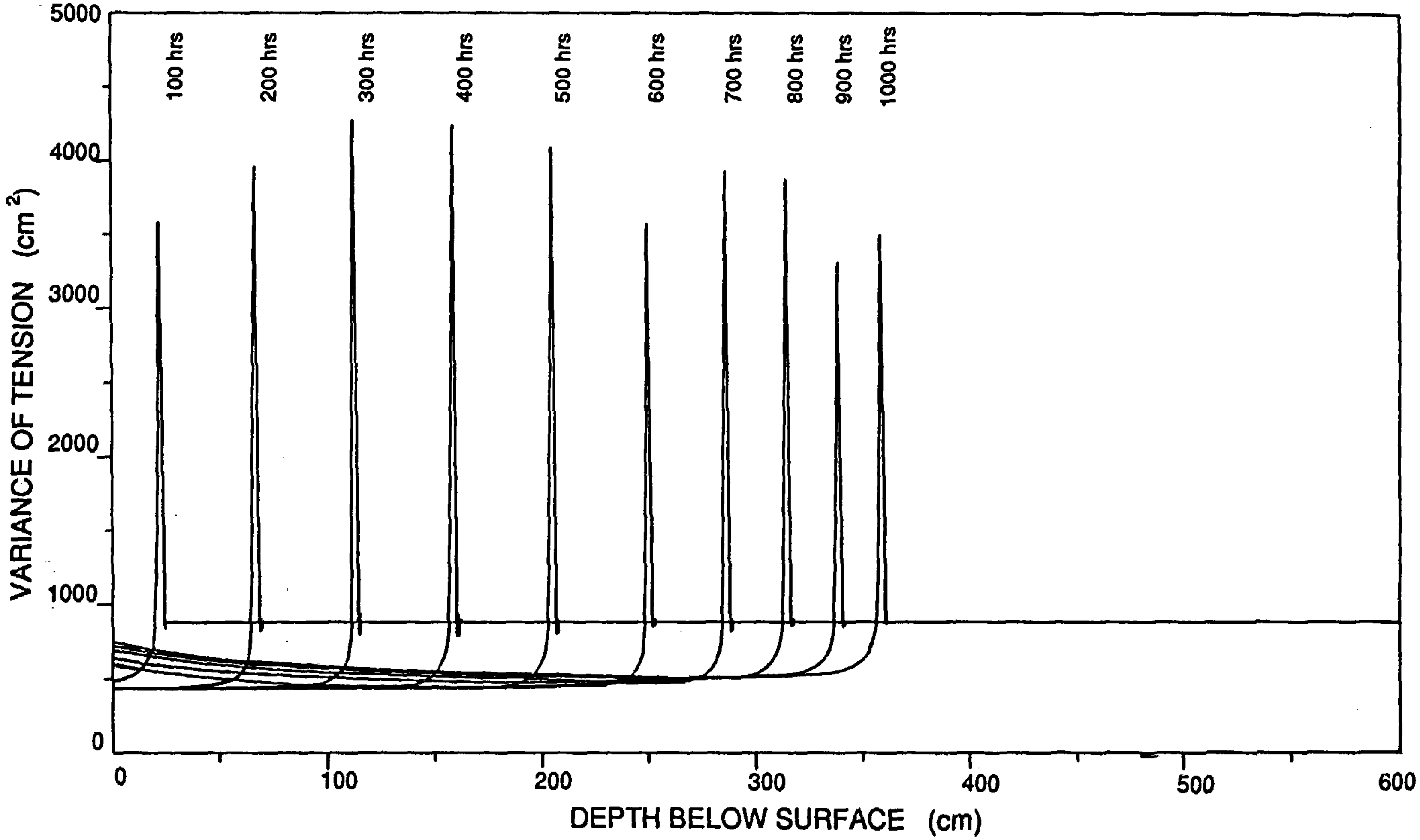

Figure 4-9. Variance of tension versus depth during wetting/drying cycle in the one-dimensional simulation

4.5.5 Model results for a deterministic case

An identical lysimeter geometry and soil layering configuration was also simulated deterministically. Each soil layer was represented individually using the local Richards equation [i.e., (2-6)] and local-scale parameter representations. The hydraulic conductivity function was modeled as a simple exponential, uniquely for each layer, as follows:

Glendale layer	$K(\psi) = K_{s_1} e^{-\alpha_1 \psi}$	(4–15)
Berino layer	$K(\psi) = K_{s_2} e^{-\alpha_2 \psi}$	(4–16)

with K_{s_1}, K_{s_2}, α_1 and α_2 given by (4-9) and (4-10). The local specific moisture capacity was represented by a constant value for both soils, as in (4-11), since information for only one of these soils was available at the time of simulation. This representation is identical to the 1D stochastic simulation described above. It is probably the weakest assumption in the deterministic simulation of the lysimeter since $C(\psi)$ is most likely not constant over the range of tensions simulated.

Results of the 1D deterministic simulation are plotted as tension versus depth at 100–hour intervals for infiltration (0–500 hours) with 2 cm/day surface inflow and for redistribution (501–1000 hours) with zero inflow (see Figure 4–10). In the deterministic case, small-scale spatial variations in hydraulic properties are included directly in the numerical description at the scale of the simulator discretization. In the stochastic case, spatial variations such as layering are incorporated into "effective" functions that are homogeneous over the entire scale of the simulator. This distinction results in a significantly different character of the moisture front between the two cases. Note the presence in the deterministic case of small-scale fluctuations across the soil layers (see Figure 4-10). These are not evident in the simulation of the stochastic model (see Figure 4-5). The rate of movement of the wetting front in the deterministic simulation is approximately 0.55 cm/hour based on the rate of change of position of the wetting front. This rate is somewhat faster than the stochastic simulation, in which the rate of movement of the front was 0.4 cm/hour based on a similar calculation.

4.5.6 Comparison with field data

Field-measured data for moisture content versus depth as a function of time were collected during the actual lysimeter experiment to analyze the movement of moisture in the physical (layered) system. These data were provided by Dr. Wierenga [personal communication (1986); Wierenga et al (1986b)] and are reproduced in Figure 4-11. Note the small-scale fluctuations indicative of the layered structure in the lysimeter, similar to the results obtained in the deterministic simulation (see Figure 4-10). Also note the approximate rate of movement of the wetting front in the physical experiment, which varies from about 0.33 to 0.39 cm/hour. This compares favorably to the propagation rate described by the tension profile of the stochastic simulation (0.4 cm/hour). The moisture content before and after wetting, respectively, for the physical experiment is approximately 0.03 and 0.23 cm^3/cm^3 (see Figure 4-11). These values are similar to those depicted in Figure 4-7 for the stochastic simulation.

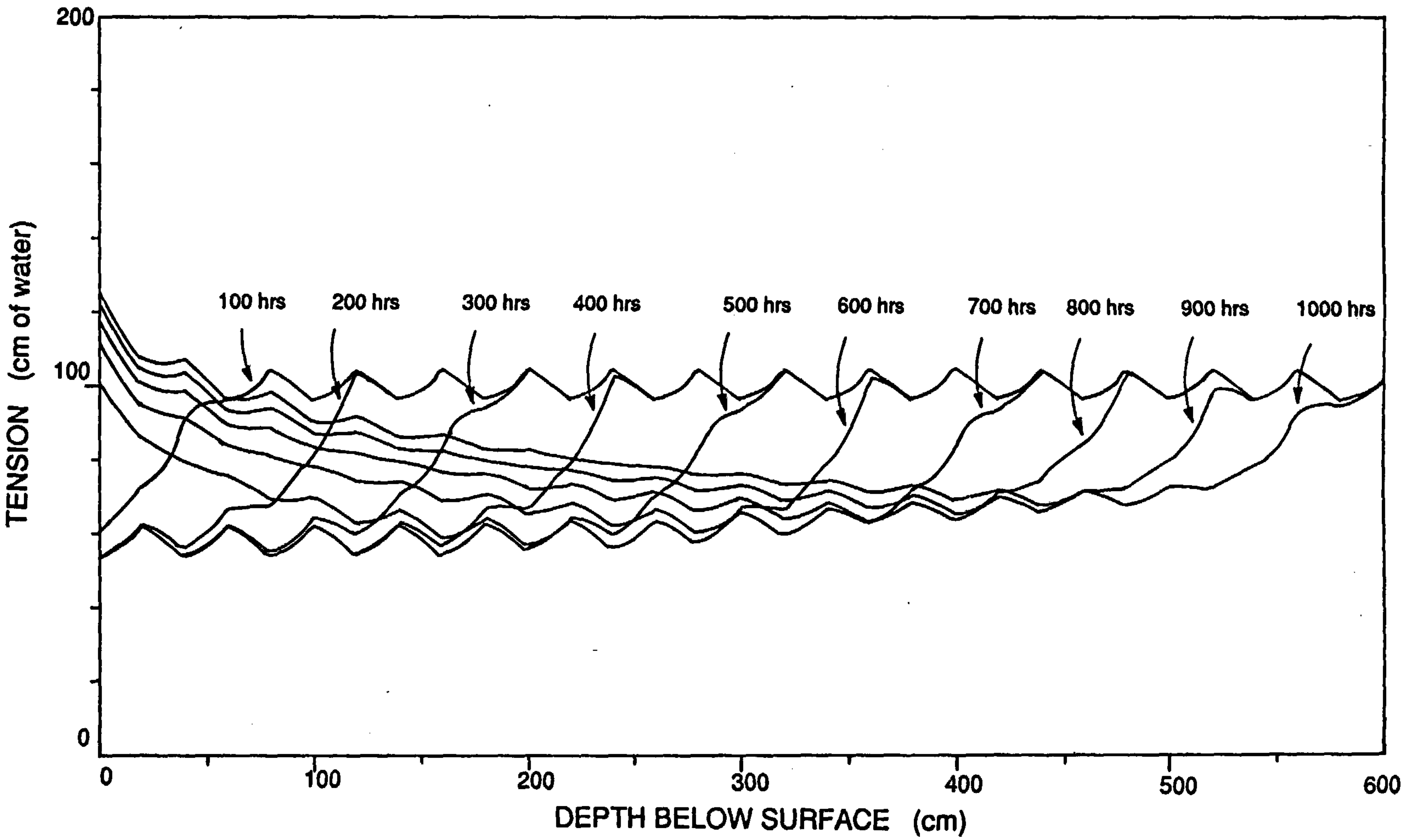

Figure 4-10. Propagation of tension front during wetting/drying cycle in the deterministic, layered one-dimensional simulation

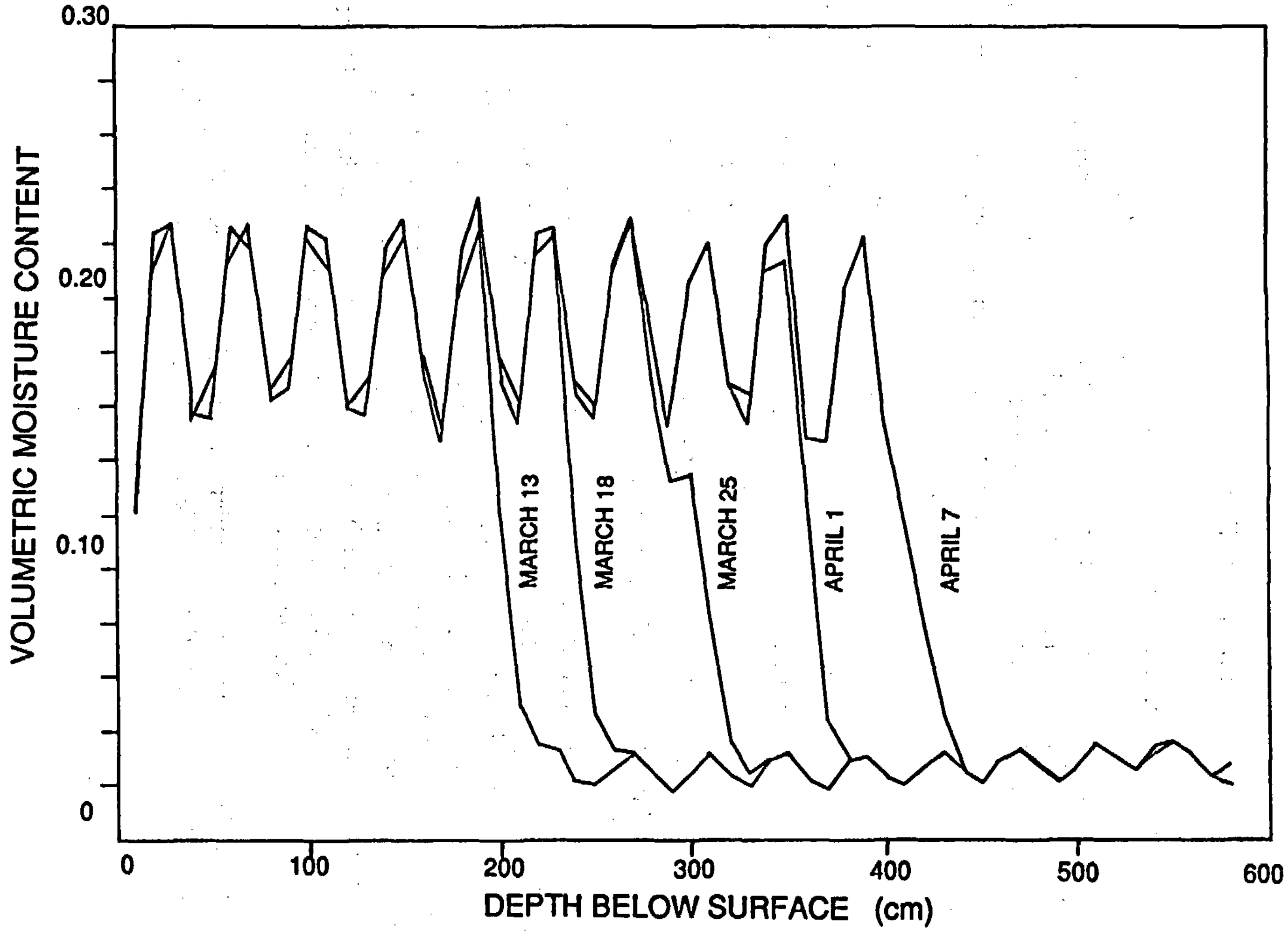

Figure 4-11. Field-measured moisture distribution during wetting cycle in the layered lysimeter [reproduced based on personal communication, P.J. Wierenga (1986), and Wierenga et al (1986a)]

The deterministic layered simulation presented here seems to simulate faster flow in the lysimeter than the experimental data would suggest. If the specific moisture capacity representation was refined to a more realistic functional form and possibly if a different local model for conductivity was used, the deterministic representation could probably be improved to better represent the experimental results of the physical system. Given the simplifications made and the limited amount of data available, results of the stochastic simulation, however, seem to compare quite well, at least on a qualitative basis. This demonstration is intended to illustrate that the stochasic method developed here can offer an alternative approach to simulating some problems, and that reasonable overall results can be obtained.

4.6 Two-Dimensional Application

4.6.1 Configuration and auxiliary conditions

The flow model to be analyzed numerically in the two-dimensional case is (4-4). Effective hydraulic conductivity in this case is a tensor with non-zero diagonal terms and zero off-diagonal terms; therefore, $\hat{K}_{11}$ and $\hat{K}_{22}$ must both be evaluated at each node point in the numerical grid and updated for each iteration and each time step. Boundary conditions for the 2D case are:

at $z = 0$,	$q_z = \text{constant}$	for $0 \le x \le 2$ m;
at $z = 0$,	$q_z = 0$	for $2\text{ m} < x \le LX$;
at $z = LZ$,	$H = \text{constant}$	for $0 \le x \le LX$;
at $x = 0$,	$\partial H/\partial x = 0$	for $0 \le z \le LZ$;
at $x = LX$,	$\partial H/\partial x = 0$	for $0 \le z \le LZ$.

Initial conditions for the 2D case are:

$H = \text{constant}$,	$0 \le z \le LZ$	for $0 \le x \le LX$.

A schematic diagram of the model system is shown in Figure 4-12 along with a representation of how the modelled configuration compares to the New Mexico field (trench) experiment (also, see Section 3.4). The values of XL and ZL in the numerical solution were chosen for each simulation to minimize computation time while adequately maintaining the desired boundary condition, meaning that the boundaries in the modelled system were set at the minimum sufficient distance from the propagating moisture front that would not affect the resulting tension solution for that problem. In the simulations described here, ZL ranged from 1.3 to 5.2 meters and XL ranged from 5 to 10 meters.

As in the 1D case, the selected boundary and initial conditions and the system configuration were designed to emulate the New Mexico field tests and were not intended to be general.

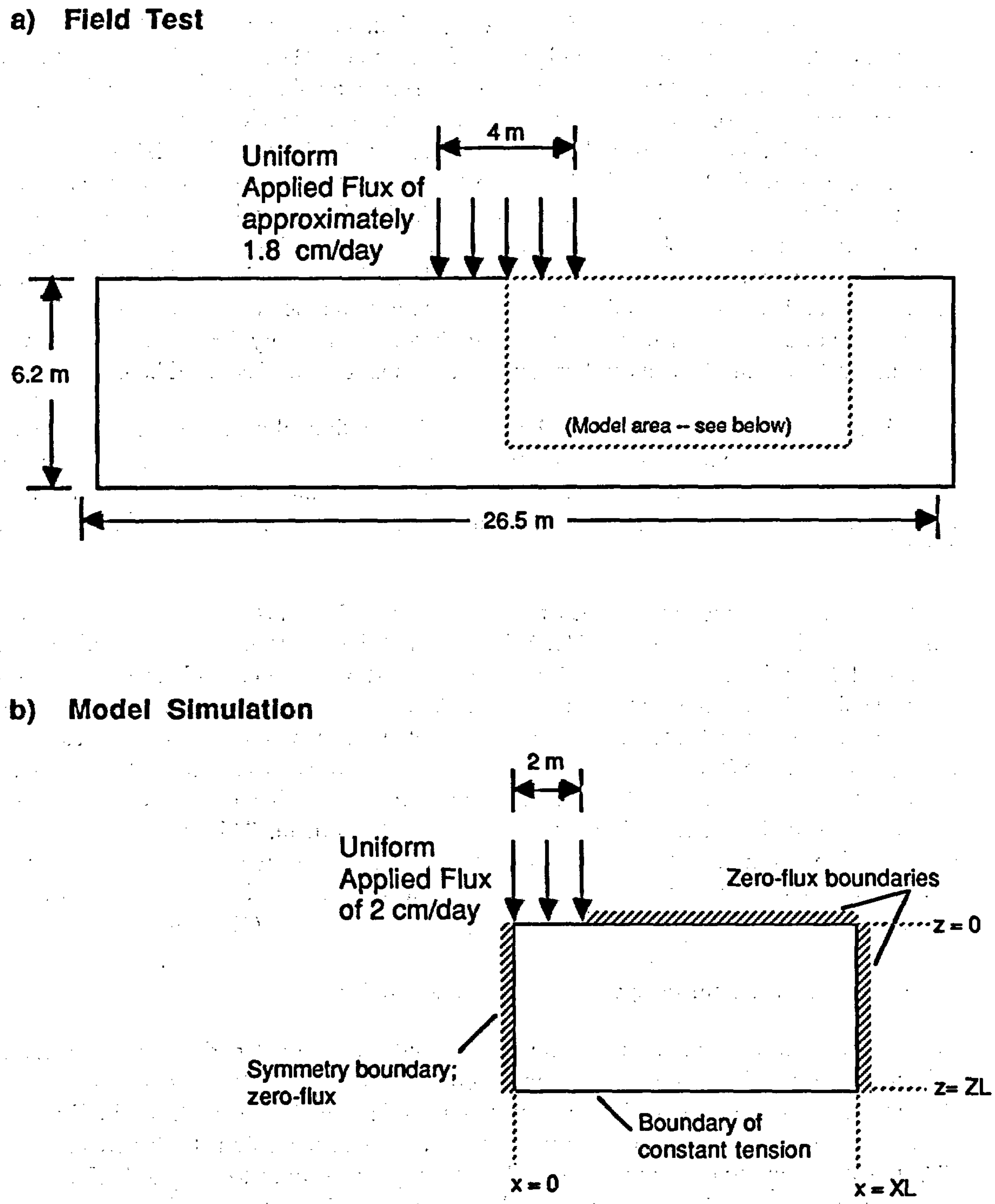

Figure 4-12. Configuration of the field experiment and its representation in the numerical model simulations for the two-dimensional case

4.6.2 Model input parameters

The 2D numerical model simulates flow in a vertical plane representing one-half of the symmetrical trench experiment (see Figure 4-12). As in the 1D case, application of the model requires values for the soil parameters: F, A, C(H) (mean values), σ_f^2, σ_a^2 (variances), and λ_1 (correlation length). Estimates for these parameters were developed as follows: all values except the correlation length were based on field data available at the time 2D simulation work began; these are limited to data for the topmost identified soil stratum at the trench site, as reported by Wierenga et al (1986b) (see Section 3.2.2). Means and variances were based on the laboratory analyses of the 50 soil cores collected along the 25-meter horizontal transect through the top stratum. As work progressed with the 2D simulations, additional laboratory soil parameter data became available for transects through other strata. However, for consistency of comparison among various simulation results, only the first-layer data were utilized for the required means and variances in the applications described here.

Selection of an appropriate correlation length requires additional data over the vertical extent of the system, and hence the single-layer information was inadequate. The vertical correlation length was estimated based on an early review of the field-saturated hydraulic conductivity data from Guelph permeameter measurements taken during excavation of the trench (see Section 3.2.2).

Based on these data and analyses described in Section 3.2, means, variances and a correlation length were selected for a "nominal" 2D simulation of the stochastic model. As discussed in sections 2.2.5 and 4.1, these nominal values were used with van Genuchten-type functions in a local re-linearization during the simulations. Parameters for the van Genuchten functions were based on mean values from fitted moisture-retention curves for the soil core samples of the topmost stratum (see discussion in Section 3.2.2). Parameter values for the nominal case are summarized in Table 4-2. The initial condition for the nominal case was assumed to be a uniform value of 1000 cm tension over the entire model domain. This represents a relatively dry condition within the fitted range of moisture-content versus tension curves, providing an initial moisture content of approximately 11 percent compared to the residual value of 10.2 percent and a saturated value of 36.8 percent [see Wierenga et al (1986b)].

4.6.3 Hysteresis and anisotropy of effective conductivity

For the chosen initial conditions, boundary flux, and soil parameters described above, and the effective conductivity functions including operational modifications described in Section 2.2.5, the range of hydraulic conductivities expected in the 2D simulations is shown in Figure 4-13, where the log of effective conductivity is plotted versus mean tension at selected values of $\partial H/\partial t$. Comparing to equations (4-3) and (4-4), K_{zz} corresponds to $\hat{K}_{11}$ and K_{xx} corresponds to $\hat{K}_{22}$. Recall Figure 4-4 which represents the one-dimensional case with linear forms underlying the effective functions, and compare the anisotropic character of the effective conductivity function in the two-dimensional case. Note that both the 1D and 2D cases reveal a hysteretic nature of the large-scale mean function, and that this hysteresis contributes significantly to the change in anisotropy observed in the 2D case as wetting or drying occurs. In particular, the anisotropy ratio of horizontal to vertical conductivity may be very large under

Table 4-2. Summary of Input Data for Selected 2D Flow Simulations

CASE	(units)	NOMINAL	DETERMINISTIC	LOWER INITIAL TENSION	LOWER VARIANCE ALPHA	LOWER CORRELATION LENGTH
TOTAL SIMULATION TIME	days	25	20	10	10	10
INITIAL TIME STEP SIZE	sec	60	60	60	60	60
TIME STEP MULTIPLIER	–	1.1	1.1	1.1	1.1	1.1
MAXIMUM TIME STEP SIZE	sec	3600	3600	3600	3600	3600
HORIZONTAL GRID SPACING	cm	20	20	20	20	20
VERTICAL GRID SPACING	cm	5	5	5	5	2.5
MODEL WET STRIP LENGTH (*)	m	2	2	2	2	2
SURFACE FLUX FACTOR, K	cm/day^2	3.73	3.73	3.73	3.73	3.73
FINAL SURFACE FLUX	cm/day	2.0	2.0	2.0	2.0	2.0
INITIAL TENSION	cm	1000	1000	500	1000	1000
RELATIVE ERROR TOLERANCE	–	0.001	0.001	0.001	0.001	0.001
MEAN SAT CONDUCTIVITY, K_G	cm/sec	9.23E-03	9.23E-03	9.23E-03	9.23E-03	9.23E-03
MEAN ALPHA (SLOPE PARAMETER)	cm^{-1}	0.117	0.117	0.117	0.117	0.117
σ_f^2 (VARIANCE OF $\ln K_s$)		0.36	0.0	0.36	0.36	0.36
σ_a^2 (VARIANCE OF α)	cm^{-2}	0.0007	0.0	0.0007	0.00035	0.0007
SAT MOISTURE CONTENT	vol/vol	0.368	0.368	0.368	0.368	0.368
RESIDUAL MOIST CONTENT	vol/vol	0.102	0.102	0.102	0.102	0.102
PARAMETER α_1		0.034	0.034	0.034	0.034	0.034
PARAMETER n		1.981	1.981	1.981	1.981	1.981
VERTICAL CORRELATION LENGTH, λ	cm	25	–	25	25	10

* based on simulation of one-half of the symmetric physical system.

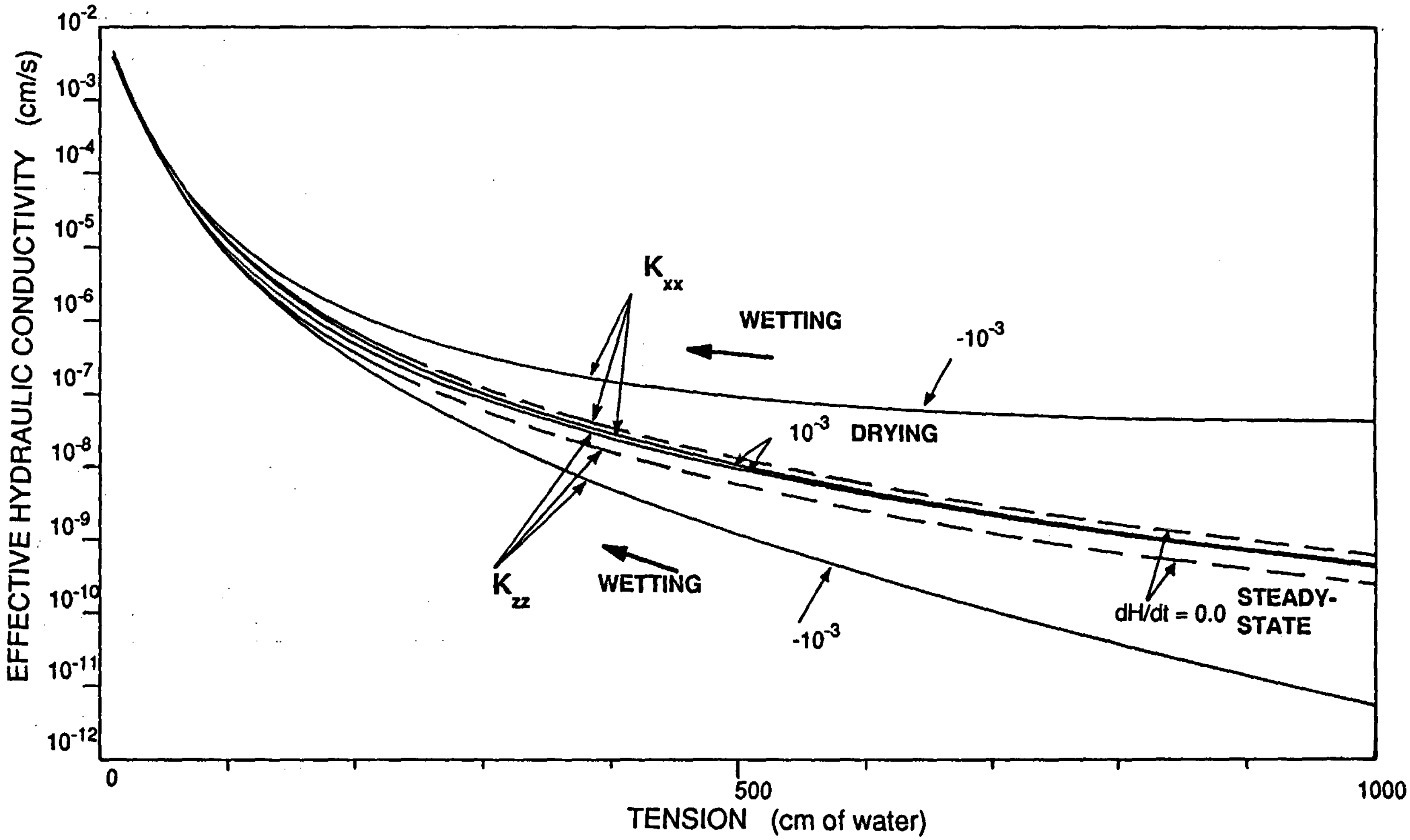

Figure 4-13. Effective hydraulic conductivity versus mean tension for selected values of $\partial H/\partial t$ during two-dimensional flow

high-tension (low moisture-content) conditions during a wetting cycle, but drops dramatically as tension falls (moisture content increases). Also, the anisotropy is evident but quite small as the system dries from an initially wet condition, approaching isotropy under drying conditions at higher tensions. For the stratified soil system assumed in these analyses, the anisotropy ratio under steady-state conditions is smaller than in the wetting case but larger than the drying case, and is sustained over a much wider range of tension compared to the drying case (see Figure 4–13). Although curves are presented in Figure 4-13 for only a few values of $\partial H/\partial t$, an infinite number of curves actually exist, bounded by the asymptotic values of effective conductivity for $\partial H/\partial t \rightarrow \pm \infty$. Also note that Figure 4-13 does not represent conditions encountered during a simulation; it is based on evaluation of the effective conductivity function over an arbitrary range of wetting/drying conditions, and is intended to illustrate the character of the function rather than the actual nature of flow.

Figure 4-13 illustrates a range of effective conductivities derived for the nominal set of input parameters. Of interest in these 2D analyses are the sensitivities of anisotropy and flow-field character to variations in the input parameters. Figure 4-14 shows the influence of selected parameters on anisotropy over a range of tensions. The ratio of horizontal to vertical effective hydraulic conductivity is plotted versus mean tension for selected values of σ_a^2, λ, and σ_f^2 while maintaining other parameters at constant values. The examples shown are for the wetting case with $\partial H/\partial t = -10^{-3}$ cm/s (compare with Figure 4-13). Figure 4–14a illustrates the significant influence of σ_a^2; the nominal value of σ_a^2 is 0.0007 cm^{-2}. This contribution to anisotropy is expeced based on equation (2-37) where σ_a^2 is seen to multiply the square of mean tension with opposite sign for $\hat{K}_{11}$ and $\hat{K}_{22}$ (recall, $\zeta^2 = \sigma_a^2/\sigma_f^2$). Figure 4-14b illustrates another significant term, the correlation length [λ]; the nominal value of λ is 25 cm. A greater degree of anisotropy is evident for more strongly layered systems (lower λ). Note the difference in ordinate scaling among Figures 4-14a, b, and c. The limited sensitivity of the anisotropy to σ_f^2 is illustrated by Figure 4-14c; the nominal value of σ_f^2 is 0.37. There is essentially no effect on anisotropy over the full range of simulated tension for as much as an order of magnitude change in this parameter. Other points regarding anisotropy of conductivity will be discussed later in comparing results of the nominal 2D case with the "sensitivity" simulations.

4.6.4 Model results for the nominal case

The nominal set of input data (see Table 4-2) were used to simulate wetting and drying cycles using the selected set of boundary and initial conditions (see Section 4.6.1 and Figure 4-12). Wetting from the ground surface at the nominal rate of 2 cm/day was simulated for a ten-day period. The boundary flux was then reduced to zero, and a drying cycle was simulated for an additional 15 days. Important features of the nominal 2D simulations include: bulk spatial character of the moisture plume and how this changes over time and within different regions of the plume; differences in the moisture plume between wetting and drying cycles; observations of the large-scale hysteretic and anisotropic components of the effective hydraulic conductivity; and, observations of the variance of mean tension and its spatial and temporal differences during the simulation.

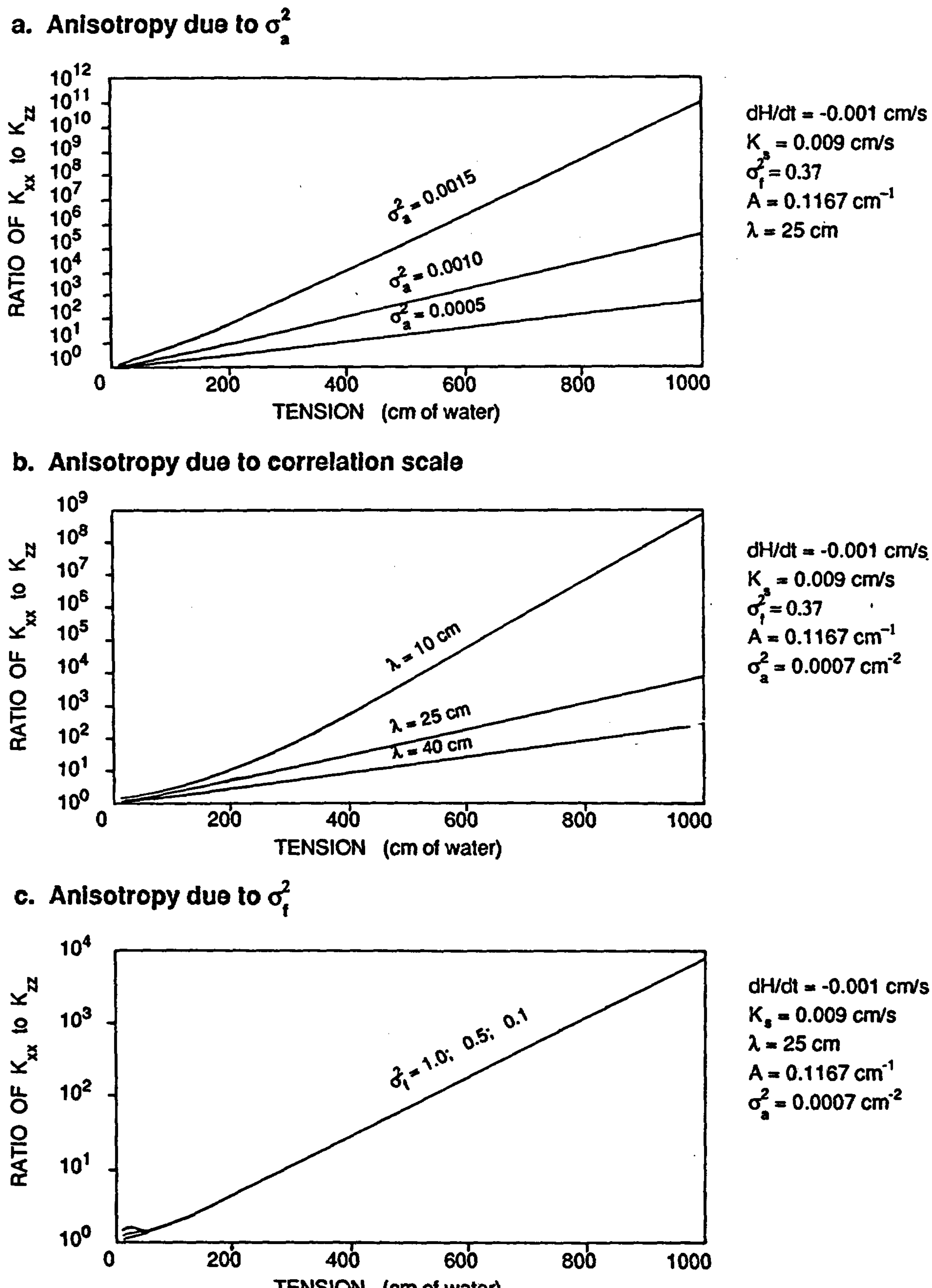

Figure 4-14. Contributions of selected input parameters to the anisotropy of effective hydraulic conductivity

The bulk characteristics of the propagating moisture plume are illustrated by drawing contour lines of equal mean tension over the two-dimensional space at selected times during the simulation. Recall that the initial tension of the system was 1000 cm of water. During the simulations, the wettest portion of the moisture plume reached a tension of approximately 75 cm of water. This tension value corresponds to an approximately steady-state condition of essentially vertical flow that was attained beneath the center of the wetted strip, with a conductivity equivalent to the applied flux rate of 2 cm/day. Based on this observation, consider the core region of the moisture plume to be represented by a mean tension of 100 cm (a 90 percent change from the initial condition). The fringe area of the moisture plume can be represented by a mean tension of 900 cm (a 10 percent change from the initial condition), and this is thought of as the "front" of the plume.

Based on results of the nominal 2D simulation, propagation of the moisture "front" and of the wetted core-area of the moisture plume is illustrated by constructing contours of equal tension at two-day intervals for the 10-day wetting cycle (see Figure 4–15). The core area of the plume shows relatively little horizontal spreading from the edge of the wetted strip, which is located at a distance of 2 meters from the centerline (see Figure 4–15a). Movement of this portion of the plume is largely in the vertical. This is in contrast to the drier fringe area of the plume, which propagates very strongly in the horizontal direction during the wetting cycle (see Figure 4–15b). Note that the "front" has moved only minimally further in the vertical direction, but has moved a considerable distance horizontally, as compared to the bulk wetted region of the plume. The gradient of mean tension is rather steep in the vertical direction and rather mild in the horizontal direction. This is further illustrated in Figure 4–16. Selected values of tension ranging from the wetted core area to the drier fringe area are plotted as contours for simulation times of 5 and 10 days in Figure 4–16a. The difference in vertical and horizontal gradients and the relative directional spreading of moisture can be clearly seen. This bulk character results not only from the additional gravitational component of flow in the vertical direction, but also more significantly from the anisotropic nature of the effective hydraulic conductivity. The tendency is to favor horizontal spreading in the stratified soil system modelled here, in which the horizontal conductivity, especially at high tension, can greatly exceed the vertical conductivity. Also, the gradient in the horizontal direction will tend to be less due to the higher conductivity, for a given flux, compared to the converse (steeper gradient and lower conductivity) in the vertical direction.

A redistribution of moisture occurs in the modelled system after the surface flux is reduced to zero at 10 days. The moisture propagation rates decrease, and the region near the ground surface begins to dry. Given sufficient time, a "bulb" of moisture would propagate through the system at decreasing rates, under diminishing gradients, eventually becoming non-distinct in the bulk system. The decrease in propagation rate and the diminished gradients are illustrated up to a time of 20 days by comparison of Figures 4-16a and b. Note that no "wet" region of tensions less than 100 cm remains in the system at the later times.

The hysteretic and anisotropic nature of the effective conductivity function is identified by examination of the temporal evolution of tension and conductivity at a selected spatial location during the wetting/drying cycle. During the 20-day period depicted in Figure 4-16, the tension and effective horizontal (K_{xx}) and vertical (K_{zz}) conductivities were recorded for a point

a. Propagation of core area of moisture plume

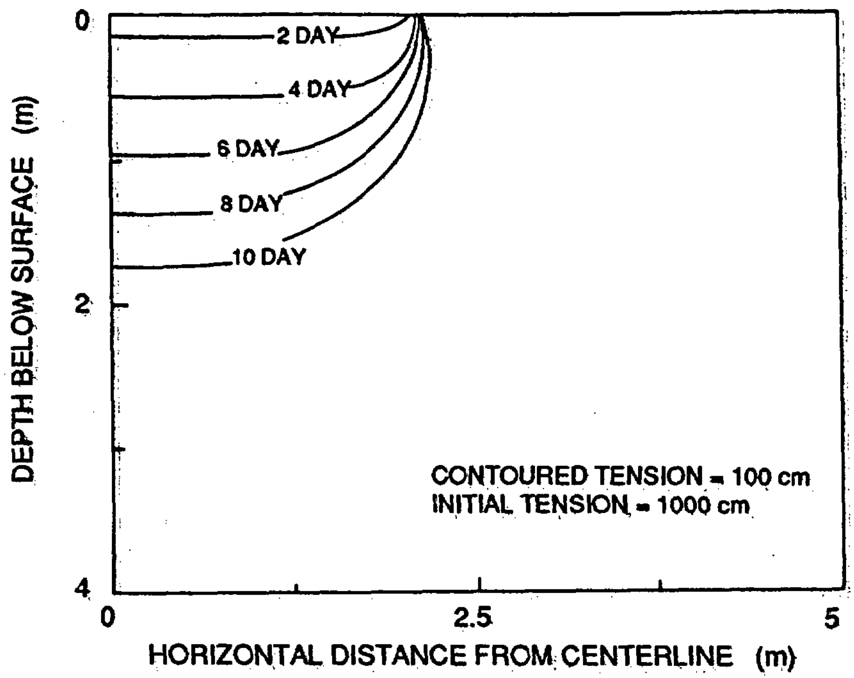

b. Propagation of fringe area of moisture plume

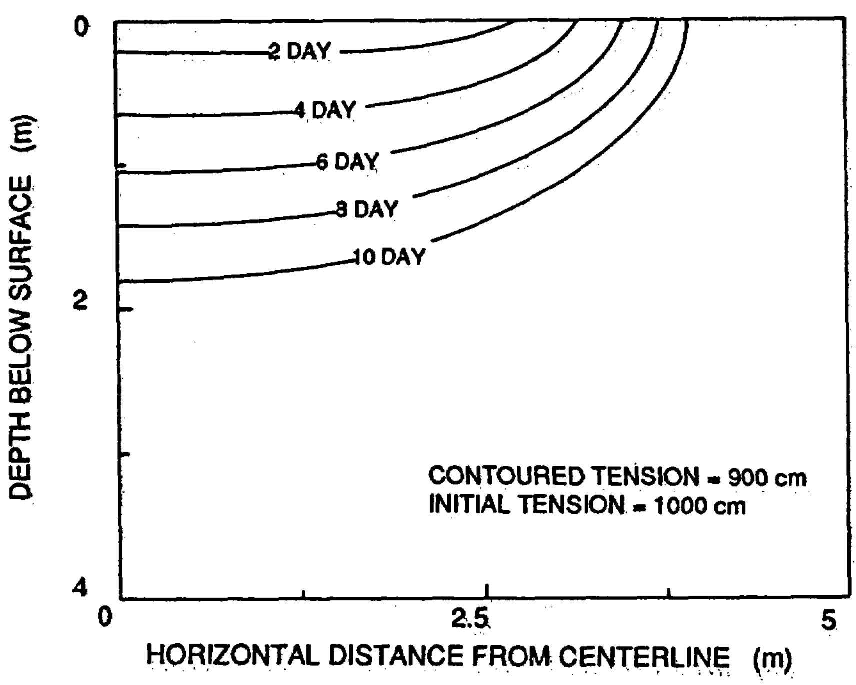

Figure 4-15. Tension distribution and the spreading of moisture during the wetting cycle; nominal simulation

a. Moisture distribution during wetting cycle

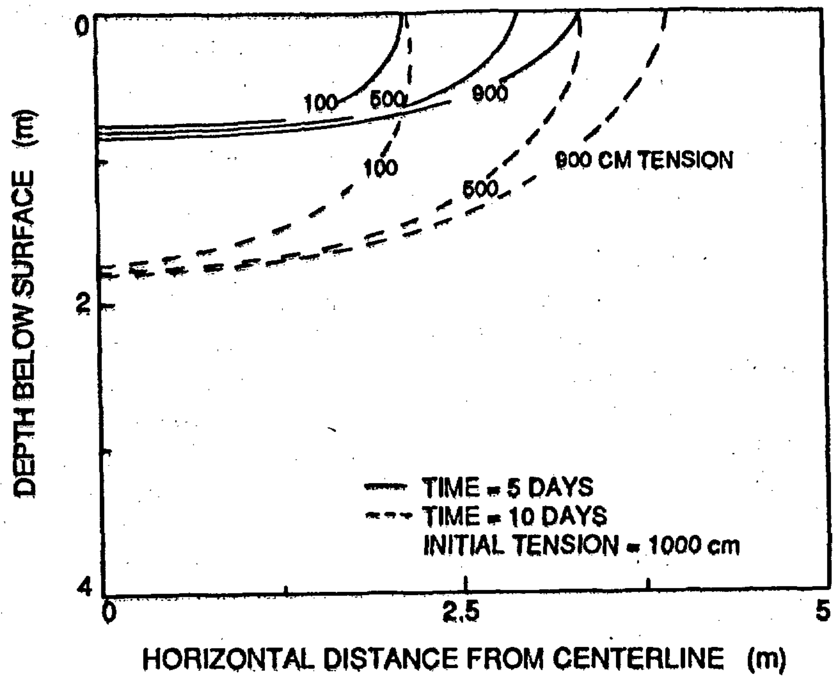

b. Moisture distribution during drying cycle

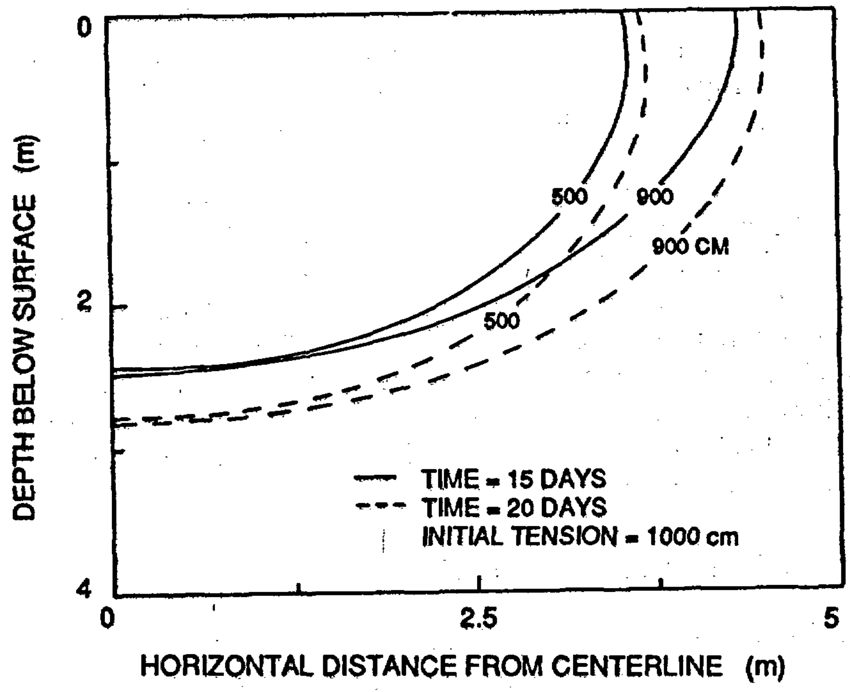

Figure 4-16. Spatial gradients of tension and the redistribution of moisture; nominal simulation

located 1 meter from the centerline at a depth of 0.5 meter. A plot of effective conductivity versus mean tension shows the anisotropy and hysteresis that is evident within the modelled system during the passage of the moisture front (see Figure 4–17). It is by coincidence that the two wetting curves shown in Figure 4-17 correspond almost exactly to those in Figure 4–13 for $\partial H/\partial t = -10^{-3}$ cm/sec. Also, the drying curves in Figure 4–17 clearly resemble those in Figure 4–13 for $\partial H/\partial t = 10^{-3}$ cm/sec. Based on the time scale shown in Figure 4–17, the wetting front passes more quickly and with a sharper gradient than the drying "front". Also, the anisotropy during wetting shows a difference in conductivities of as much as three orders of magnitude; it is less than one order of magnitude during drying.

Another more qualitative view of the bulk character of the propagating moisture plume is presented in Figure 4-18, which shows simulation results as spatial surfaces in a perspective view. Mean pressure head (the negative of tension) is illustrated for the wetting cycle (time = 5 days) and drying cycle (time = 15 days) in Figures 4-18a and d, respectively. In both cases, the distinction is between the smooth spatial gradients in the wetted core area of the plume and the steep gradients at the front. Also, compare the smoother gradients at the drier fringe area in the horizontal direction with the persistence of the steep gradient in the vertical direction. The variance of tension for these same simulation times is illustrated in Figures 4-18b and e. These figures are based on an evaluation of the variance expression derived in the theoretical development. As with the 1D simulations, the variance of mean tension is higher where the mean tension is higher (pressure is more negative) (see also Figure 4-9). The variance is lower and is essentially constant over space in the wetted region of the plume, where both the tension is lower and the gradients are flat. The variance increases in both the horizontal and vertical directions away from the wetted region, in areas where the gradients are steeper. Note the gradual increase in the horizontal direction as compared to the sharp peak in the vertical, in conjunction with the directional differences in the gradient of tension. As discussed above regarding the 1D simulations, these peaks in tension variance bring into question the assumption of stationarity of mean tension used in the theoretical development and raise doubt as to the validity of these results in the vicinity of steep gradients.

In the present simulations, mean moisture content is a function of mean tension and is evaluated within the model based on an expression similar to (3-1) using mean parameters and mean tension. This is illustrated in Figures 4-18c and f for the wetting and drying cycles, respectively. Similar to the tension profiles, note the spatial and temporal differences in gradients as the moisture plume evolves. Evident in the 15-day result is the "bulb" of moisture near the center of the wetted region, which can be seen from the contour lines of equal moisture content. Also shown is the drying that occurs near the ground surface as the plume propagates downward, and the much smoother gradients in the vertical direction behind the plume (the "drying front") as compared to the wetting front.

4.6.5 Model results for a deterministic analysis

Two-dimensional simulations were performed using a traditional deterministic analysis, for comparison to results of the nominal stochastic case. The deterministic case assumes that the modelled system is homogeneous and isotropic, with input parameters equal to the mean parameters of the nominal stochastic case. This deterministic analysis is equivalent to a special

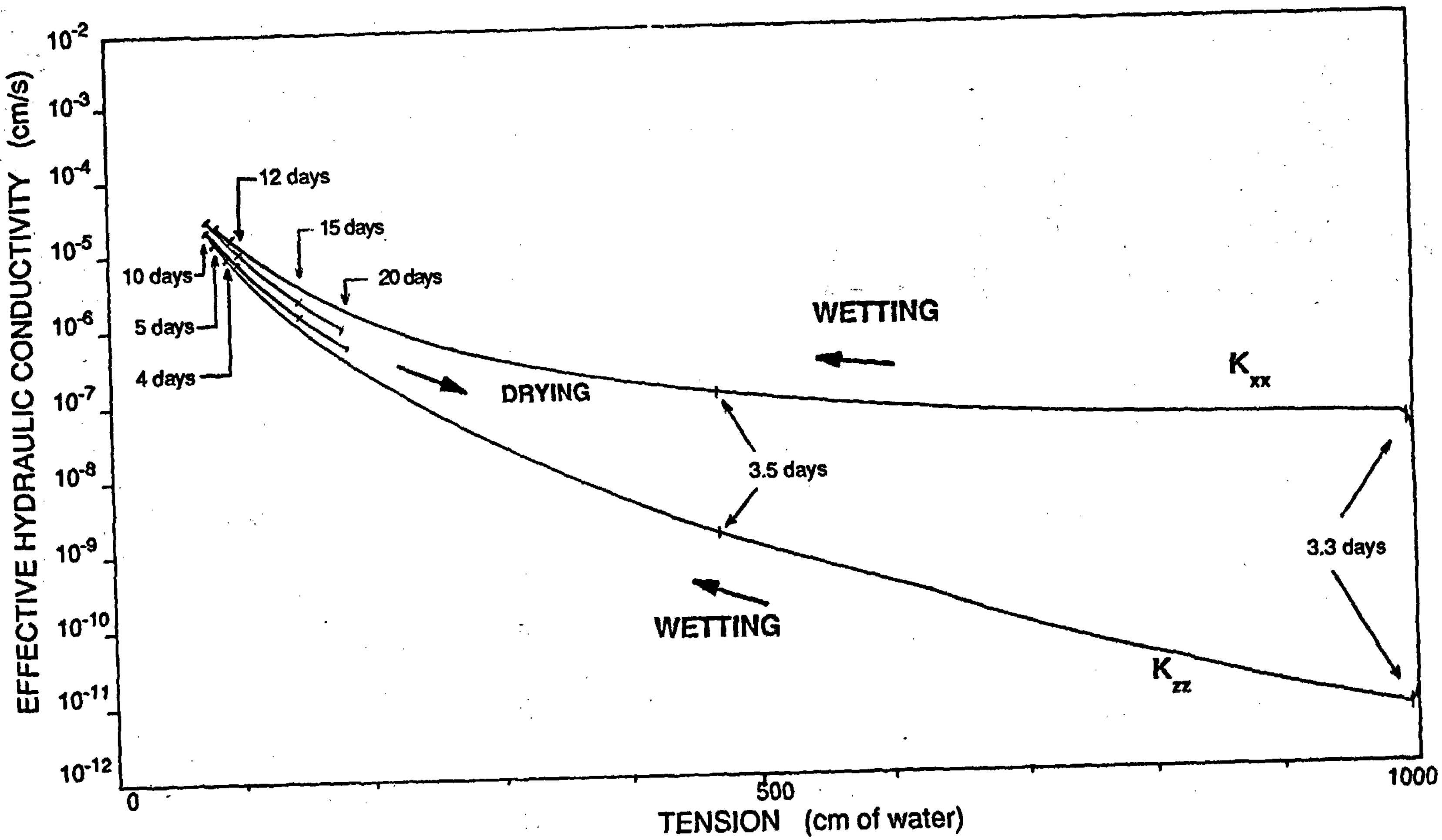

Figure 4-17. Hysteresis and anisotropy of effective hydraulic conductivity during the wetting/drying cycle at 0.5 meter depth under the wetted strip

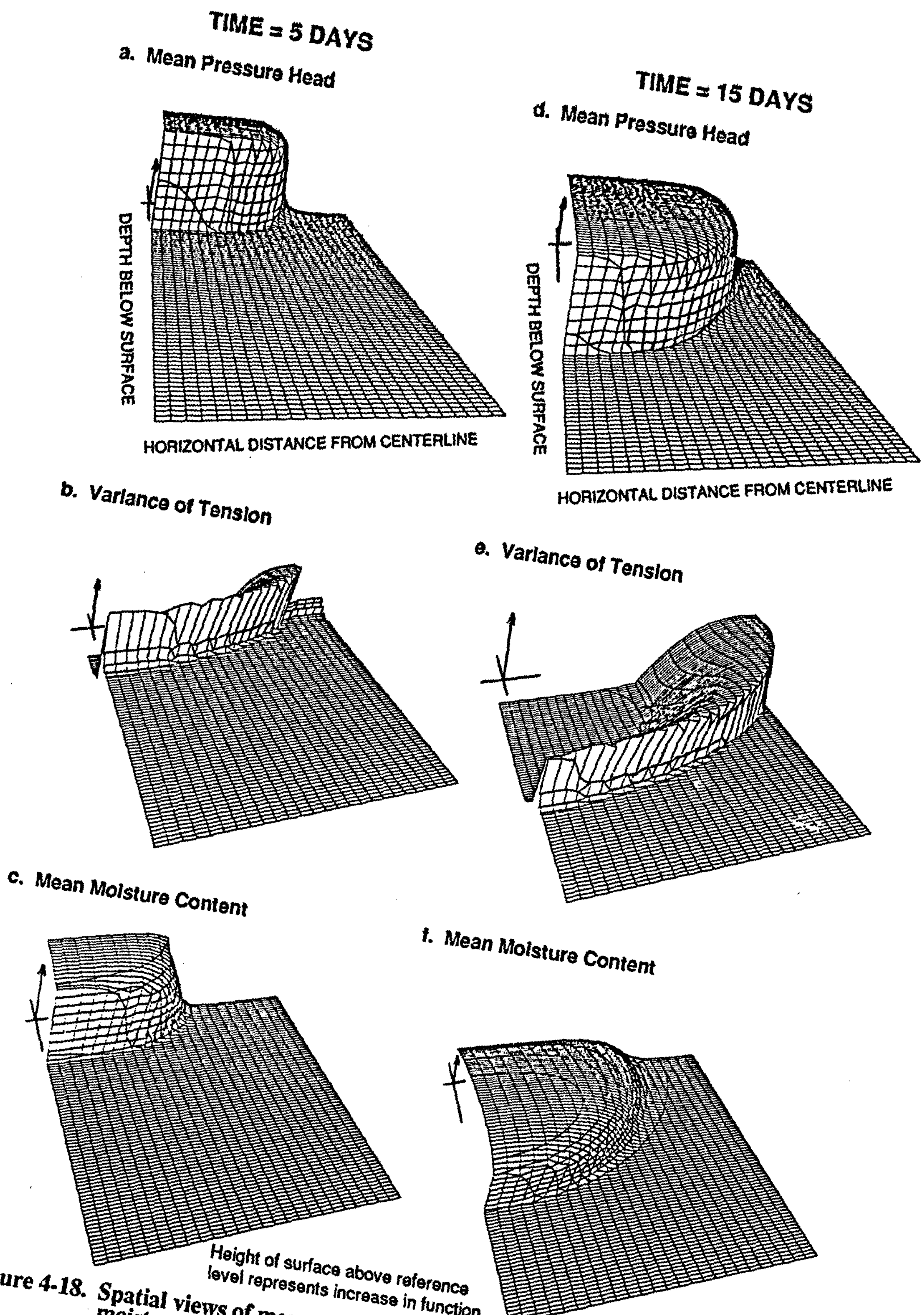

Figure 4-18. Spatial views of mean pressure, tension variance and mean moisture content during the wetting/drying cycle; nominal simulation

case of the stochastic analysis in which the variability of the input parameters is assumed negligible (i.e., the variance of the inputs is zero). During the simulation, hydraulic conductivity and specific moisture capacity are evaluated based on van Genuchten-type functions. Parameters are summarized in Table 4-2. Other aspects of the problem (initial and boundary conditions, system configuration, solution technique, and simulation period) are identical to the nominal stochastic case.

Based on results of the deterministic 2D simulation, propagation of the moisture front and of the wetted core-area of the plume is illustrated by contours of equal tension at two-day intervals for the 10-day wetting cycle (see Figure 4–19). Compared to the stochastic case (see Figure 4–15), the core-area of the plume shows less horizontal spreading and slightly faster vertical movement (see Figure 4–19a). Examination of the drier fringe area of the plume shows a much greater contrast between the deterministic and stochastic cases. The dry portions of the plume propagate in the horizontal direction more strongly in the stochastic case (see Figure 4–15b) than in the deterministic case (see Figure 4–19b). The difference in these directional rates of movement is much more pronounced in the stochastic analysis, due to the anisotropic character of the effective conductivity in that case. Again, note that this anisotropy is especially evident in the drier regions of the moisture plume.

The difference in vertical and horizontal gradients and the relative directional spreading of moisture in the deterministic case is illustrated in Figure 4–20. Compared to the stochastic case (see Figure 4–16) vertical gradients are milder and horizontal gradients are stronger. The wetted area of the plume (given by the 100-cm contour) is slightly larger, and the vertical extent of the plume as a whole is greater. The bulk character of the plume, and its distinction from the stochastic case, is more clearly evident in Figure 4-20b which shows the redistribution of moisture after the surface flux is set to zero at 10 days. The moisture plume continues to move at a noticeably faster vertical rate with much less horizontal spreading than the stochastic analysis predicts (see Figure 4-16b).

4.6.6 Model results for sensitivity analyses

Two-dimensional simulations were performed using the stochastic model with adjustments in values of selected input parameters to demonstrate the sensitivity of mean tension results to these inputs. The system configuration, boundary conditions, solution technique and wetting period are identical to the nominal stochastic case. Results are presented only for the 10-day wetting cycle.

The anisotropy of effective hydraulic conductivity is strongly sensitive to σ_a^2 and λ, and insensitive to σ_f^2 as shown in Figure 4-14. Greater anisotropic effects are also observed under drier conditions, as discussed above regarding the nominal simulation. Based on these considerations, 2D simulations for three cases were performed with a change in a single input parameter for each case, to investigate the sensitivity of the bulk character of the plume and the mean tension results. These cases include: a decrease in initial tension (resulting in a greater initial moisture content); a decrease in the variance of α (implying less spatial variability of the unsaturated conductivity function); and, a decrease in the vertical correlation length, λ

a. Propagation of core area of moisture plume

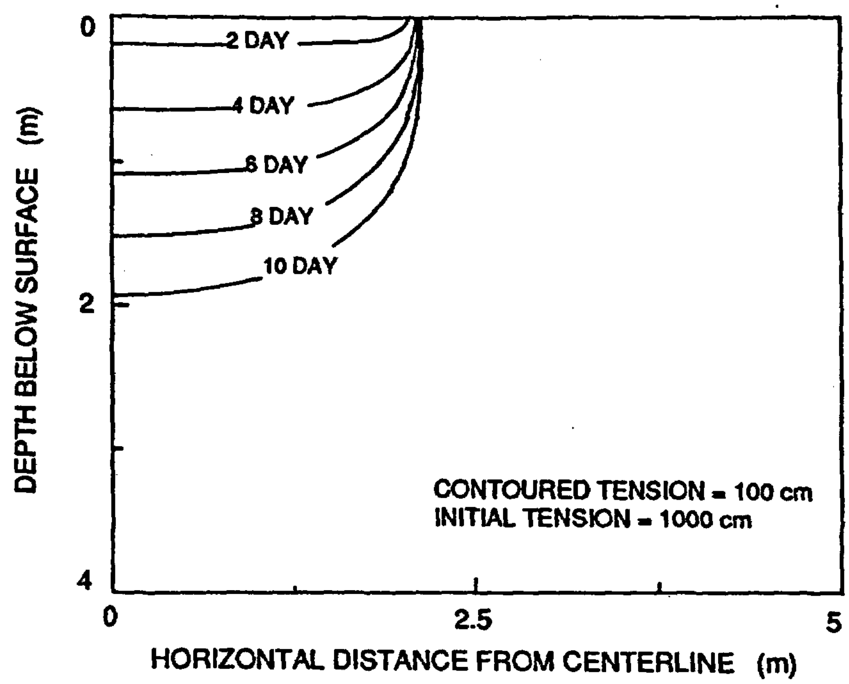

b. Propagation of fringe area of moisture plume

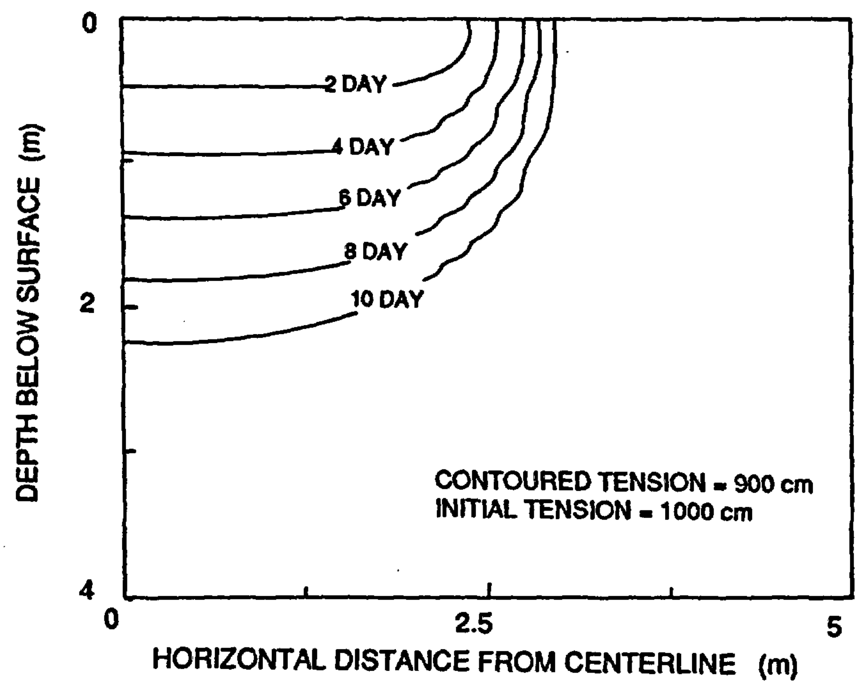

Figure 4-19. Tension distribution and the spreading of moisture during the wetting cycle; deterministic analysis

a. Moisture distribution during wetting cycle

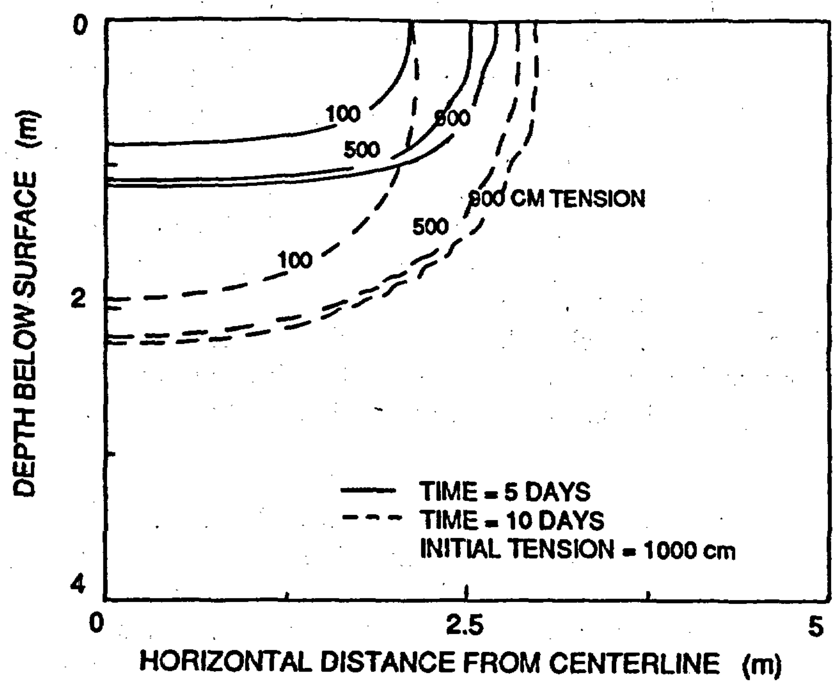

b. Moisture distribution during drying cycle

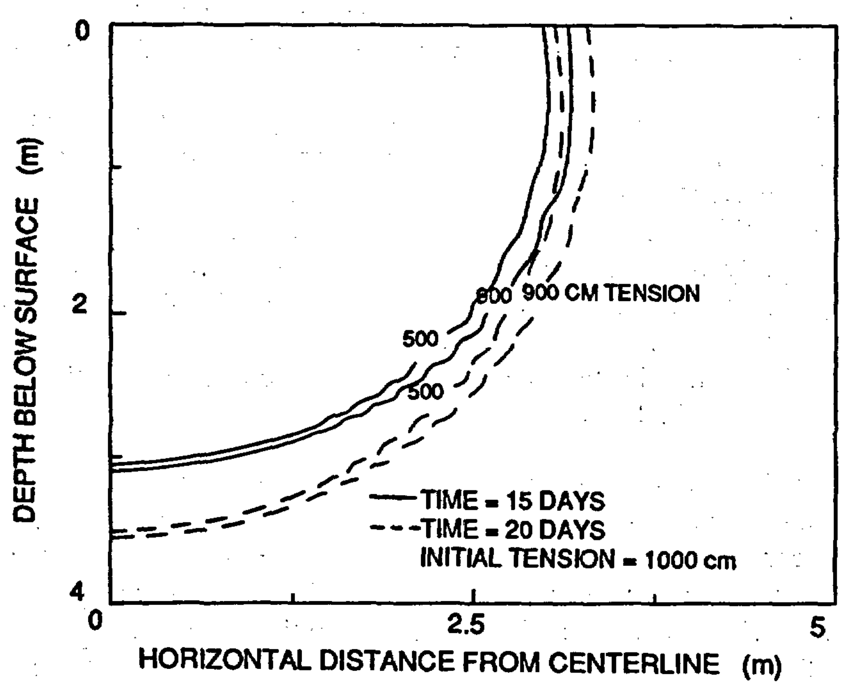

Figure 4-20. Spatial gradients of tension and the redistribution of moisture; deterministic analysis

(implying a greater degree of stratification and finer layering in the soil system). Input parameters for the sensitivity analyses are summarized in Table 4-2.

The initial tension of the modelled system was decreased from the nominal value of 1000 cm of water to a spatially uniform value of 500 cm. For this case, the initial conductivity is considerably greater than the nominal case (see, for example, Figure 4-13). However, the anisotropy is also significantly lessened since the vertical conductivity is more greatly affected by this change in tension than is the horizontal conductivity. Results of the 2D simulations illustrate these effects. The moisture plume propagates more rapidly in both the vertical and horizontal directions due to the higher hydraulic conductivities (as well as the initially higher moisture contents) as shown in Figure 4-21 which compares the nominal stochastic case to the wetter initial condition case. Also, the gradients of tension in the vertical direction appear to be more affected than the horizontal gradients; the vertical gradients are significantly milder whereas the horizontal gradients are not as noticeably different from the nominal case. This supports the concept that the anisotropy of conductivity is less pronounced in the wetter system.

The variance of α for the modelled system was decreased by a factor of 2 from the nominal value of 0.0007 cm^{-2} to a value of 0.00035 cm^{-2}. For this case, the anisotropy ratio of conductivity is decreased from the nominal value over the entire range of tension (see, for example, Figure 4-14a). Results of the 2D simulations illustrate this effect. The wetted core area of the moisture plume propagates slightly more rapidly in both the vertical and horizontal directions (see Figure 4-22). However, the drier fringe area propagates more rapidly in the vertical direction and less rapidly in the horizontal. These results appear "more deterministic" than the nominal case, due to the decreased variance of the input parameter. Also, tension gradients are milder in the vertical and stronger in the horizontal, compared to the nominal case. This also illustrates the lesser degree of anisotropy in the decreased σ_a^2 case.

The vertical correlation length, λ, was decreased by 20 percent from the nominal value of 25 cm to a value of 20 cm. For this case, the anisotropy ratio of conductivity is increased above the nominal value over the entire range of tension (see, for example, Figure 4-14b). Results of the 2D simulations illustrate this effect. The wetted core area of the moisture plume propagates slightly more rapidly in the vertical and horizontal directions, but the drier fringe area of the plume propagates much more rapidly in the horizontal direction than in the vertical (see Figure 4-23). Also, the tension gradients are significantly lessened in the horizontal direction. These results appear "less deterministic" due to the effect of stronger stratification and finer layering, as compared to the nominal case.

These analyses of the sensitivity of mean tension results and the bulk character of moisture propagation and spreading illustrate the importance of reliable input data, and demonstrate the relative significance of the selected parameters (see Table 4-3). Based on the present development of the stochastic theory, the soil properties that clearly play an important role are the degree of layering and structure in the soil system (incorporated in λ) and the spatial variability of the unsaturated hydraulic conductivity (incorporated in σ_a^2). The spatial variability of saturated conductivity (incorporated in σ_f^2), which is the parameter that is more

a. Mean result with nominal input parameters

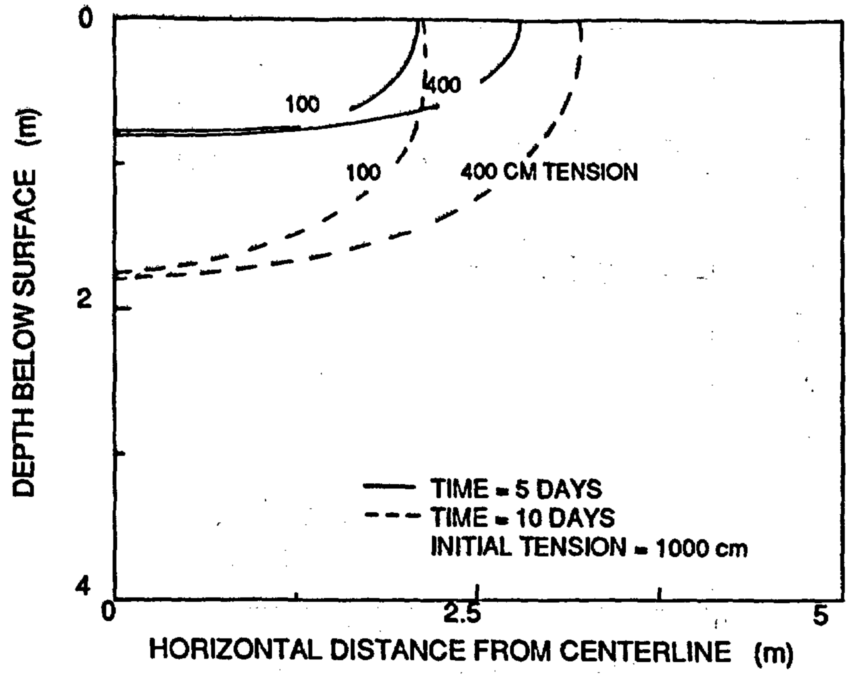

b. Mean result with wetter initial condition

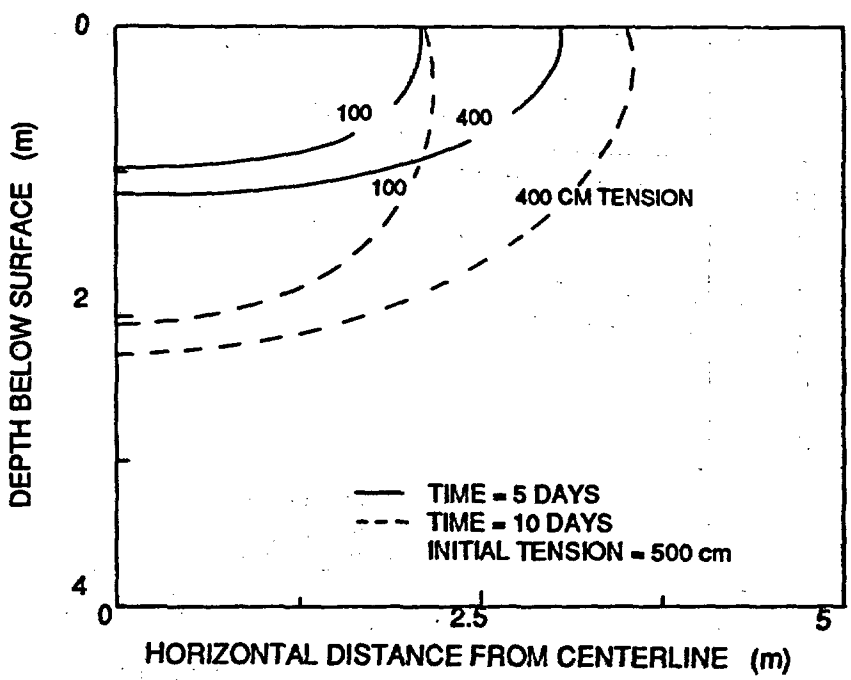

Figure 4-21. Tension distribution and the spreading of moisture during the wetting cycle; sensitivity to wetter initial conditions; stochastic analysis

a. Mean result with nominal input parameters

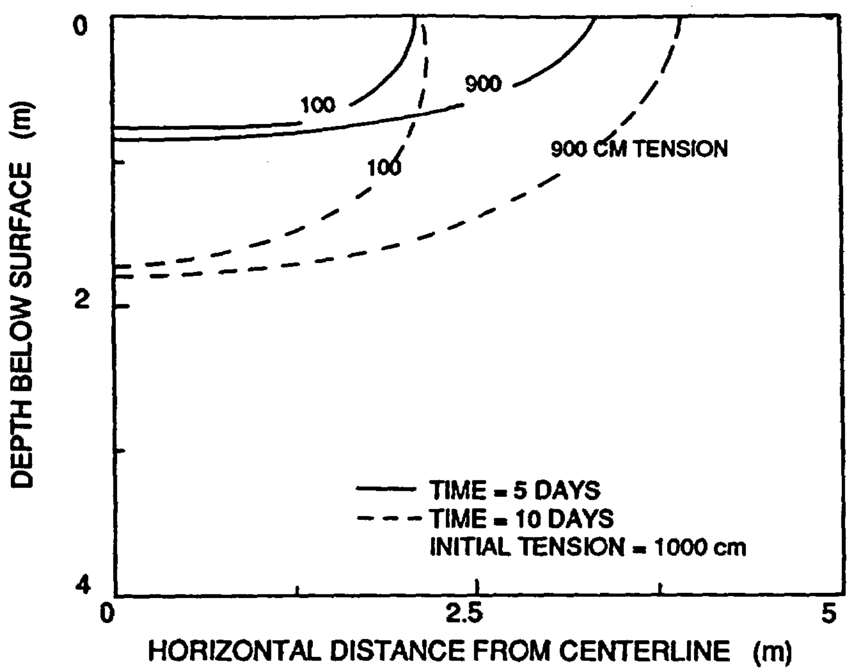

b. Mean result with decreased σ_a^2

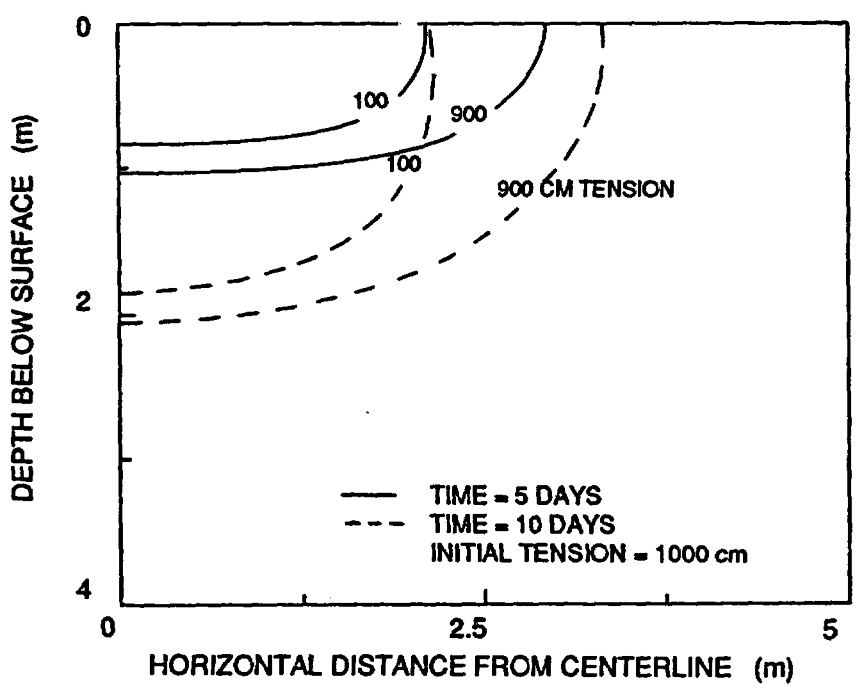

Figure 4-22. Tension distribution and the spreading of moisture during the wetting cycle; sensitivity to decreased σ_a^2; stochastic analysis

a. Mean result with nominal input parameters

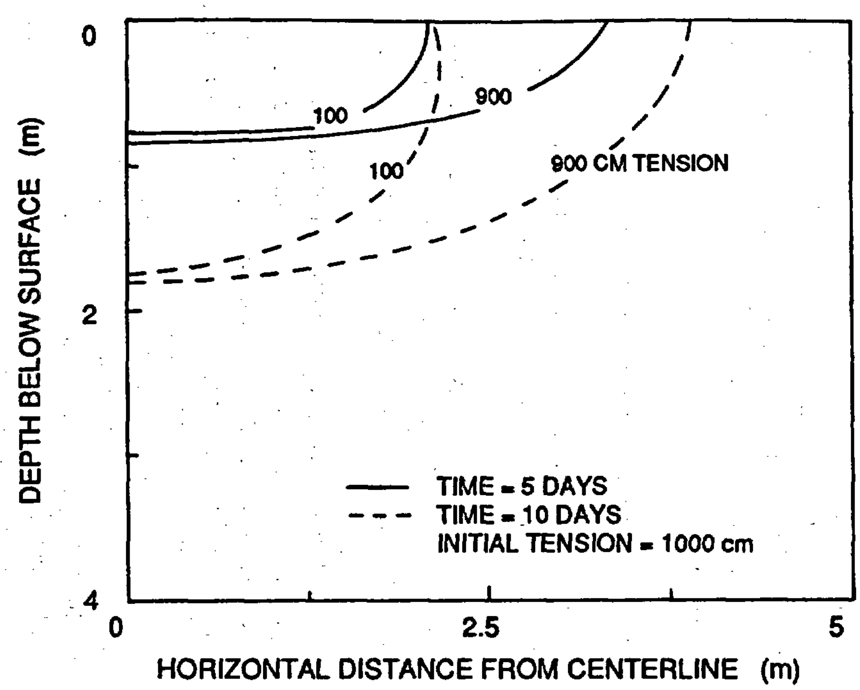

b. Mean result with decreased correlation length

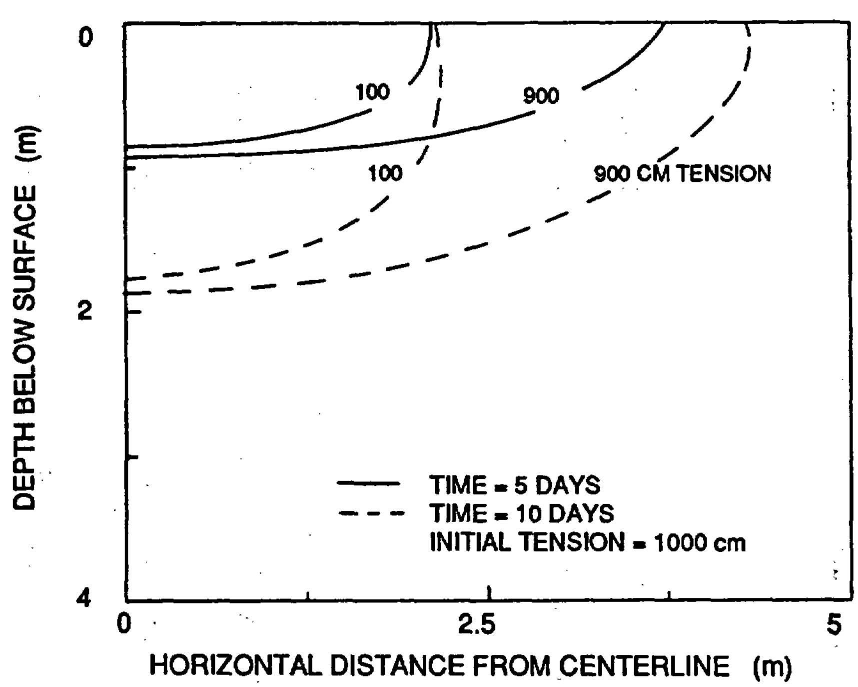

Figure 4-23. Tension distribution and the spreading of moisture during the wetting cycle; sensitivity to decreased correlation length; stochastic analysis

Table 4-3. Resulting Mean Flow Effects for Changes in Input Parameters

Simulation Parameter	Action Taken (*)	Resulting Effect
Vertical grid spacing	Decrease	Significant effect; improve accuracy of tension solution as measured by mass-balance errors; ability to solve low-conductivity, high-tension, steep-gradient problems; increase rate of iterative convergence; increase required computer storage and cpu time.
Horizontal grid spacing	Decrease	As above, with only moderate effect on each.
Vertical flux rate	Decrease	Decrease rate of vertical and horizontal moisture front propagation; increase ratio of horizontal to vertical moisture front spreading.
Initial tension	Decrease	Increase initial conductivity; lessen gradient of tension in region of the front, especially in vertical direction; increase rate of front propagation; moderately decrease ratio of horizontal to vertical spreading.
Log-conductivity slope parameter (alpha)	Decrease	Increase rate of vertical propagation of moisture front; significantly increase ratio of horizontal to vertical spreading.
Vertical correlation length	Decrease	Increase rate of horizontal moisture front propagation; decrease rate of vertical front propagation; significantly increase ratio of horizontal to vertical spreading.
Specific moisture capacity	Increase	Decrease rate of vertical and horizontal propagation of moisture front; slightly increase ratio of horizontal to vertical spreading; slightly steepen gradient of tension in region of the front.
Variance of log-conductivity	Increase	Minimal effect; increase rate of horizontal moisture front propagation; decrease rate of vertical front propagation; slightly increase ratio of horizontal to vertical spreading.

(*) with all other parameters held constant commonly estimated rather than σ_a^2 or λ, appears to play a relatively less important role, based on the present model analyses.

A review of available field data for early portions of the trench experiment provides a basis for preliminary comparisons with the simulated flow model results. The two-dimensional array of tensiometer readings from the trench wall was compared to the 5- and 10-day simulated tension values based on (i) the mean flow model of the stochastic theory using the nominal case inputs, and (ii) the deterministic flow model using the mean soils data as inputs. These comparisons suggest that the stochastic model is better able to simulate the lateral spreading of moisture observed in the field, as compared to the deterministic model. Also, the stochastic model appears to more accurately simulate the bulk propagation of moisture, based on the relative degree of horizontal and vertical spreading observed in the field.

4.7 Summary and Future Research Needs

Numerical simulation of the large-scale mean unsaturated transient flow model of Mantoglou and Gelhar (1985, 1987a, b, c) has been demonstrated for the case of stratified soils in one-dimensional and two-dimensional domains. As a simplification, the analysis neglects spatial variability of specific moisture capacity and emphasizes an examination of the large-scale flow effects due to heterogeneity of saturated and unsaturated hydraulic conductivity. Hysteresis and anisotropy of the effective conductivity, as developed in the stochastic theory, are demonstrated by the example simulations. The bulk character and the relative "smoothness" of the mean tension solution are shown and compared to a local-scale deterministic method. The variance of the mean tension solution is also calculated, for both 1D and 2D cases, showing the spatial variations in tension variance as moisture fronts propagate and also highlighting the uncertainty of theoretical assumptions of spatially-smooth tension gradients. An analysis of the sensitivity of the mean tension distribution and bulk moisture plume character to the input parameters has shown the importance of the correlation structure of the stratified system (parameter λ) and the variability of the unsaturated hydraulic conductivity function (parameter σ_a^2) in predicting the nature of large-scale unsaturated flow. A preliminary comparison of the stochastic and deterministic simulation models with 1D and 2D field-scale experiments at Las Cruces, New Mexico suggest that the stochastic method is better able to predict the bulk character of moisture propagating into layered soil systems and the anisotropic nature of flow in heterogeneous, stratified soils.

A brief review of literature describing field experiments has revealed the apparent sparcity of unsaturated soils data required for the determination of statistical inputs to stochastic models. Based on the literature reviewed, saturated hydraulic conductivity is most commonly reported. However, the sensitivity analyses presented here demonstrate the minor influence of σ_f^2 in defining the large-scale flow field. The parameters of greatest influence to the simulation results, σ_a^2 and λ, are usually lacking in the literature. Future stochastic modeling efforts will require suitably-determined values for these inputs. Research into reliable and efficient methods for field and laboratory measurements of these parameters should be encouraged. To emphasize, this implies actual experimental determinations of unsaturated hydraulic conductivity over a range of tension values, in order to provide a clear understanding of the parameter α (or its equivalent, if a different conductivity functional form is assumed in the stochastic theory development) with regard to its mean and variance. These measurements should circumvent the theoretical fitting of $K(\psi)$ based on soil moisture retention data, and the *ad hoc* determination of α based on arbitrarily selected relative water contents, as required for the examples presented here.

The computer simulations presented here required extremely long running times. Processing time on a DEC Microvax II approached actual simulation (field experiment) time for some examples of the 2D case. Efficient solution techniques for nonlinear systems of equations, in terms of both computer processing time and storage space, is a current research interest of many investigators. Continued research efforts should be strongly encouraged in light of the large-scale (and long-time) flow problems that are of interest in low-level-waste sitings and other studies involving expansive unsaturated soils. This need is especially acute for the stochastic modeling case due to the highly nonlinear and complicated nature of the functional forms involved.

Further studies involving the large-scale stochastic model should address several issues. The operational modifications, which were invoked here to simplify and expedite analyses for the example cases, should be carefully examined. In particular, improved numerical methods should be developed that provide inclusion of the spatial gradients within the iterative evaluation of the effective conductivity. These were assumed to be small and negligible, in accordance with the development of the stochastic theory. However, the example results show that the gradients of mean tension may be large (for example, near the propagating front). This has important implications with regard to anisotropic rates of spreading and bulk moisture propagation, as well as the determination of tension variance. The present results indicate that the mean solution may not be reliable in the vicinity of the moisture front, or that the stochastic theory may not apply in these regions. However, by neglecting spatial gradients, the present method negates a potentially important "feedback" mechanism within the iterative solution of the nonlinear functions. The inclusion of such terms may act to "smooth" the propagating front, affecting rates of spreading and propagation and the variance calculation. This has a potentially significant contribution to understanding the bulk character of the mean tension solution, and should be addressed in future studies.

The heterogeneity (spatial variability) of the specific moisture capacity function has been neglected in the examples presented here by assuming that the variance σ_γ^2 is zero. This is a simplification from the original theoretical development. Inclusion of this parameter changes the form of the unsteady mean flow equation by adding another time-derivative term; the equation is no longer analogous to the familiar Richards equation. This term may significantly affect large-scale storage properties, and its importance should be examined in future studies. The development of a new or special numerical technique may be required for an efficient solution.

The re-linearization of conductivity and moisture-capacity functions within the numerical solution is another topic for further research. This is coupled with the need for more-generalized functional forms of the local unsaturated soil properties within the theoretical development. The linear forms of the log-conductivity versus tension function and the moisture retention function, as in the theoretical development, were used in the numerical simulations for the 1D examples. These forms offered limited utility in the 2D case. The 1D examples involved a relatively limited range of simulated tension, moisture content, and conductivity; the 2D examples attempted to explore a wider range to provide a more realistic comparison to the field conditions at the trench site. Use of the linear forms in the 2D case caused insurmountable numerical difficulties and yielded physically meaningless results, based on the methods used here. Use of the van Genuchten functions and re-linearization to coincide with the stochastic theory provide reasonable results from the simulations, and a favorable comparison to field observations based on preliminary reviews. In this light, future research efforts should include further development of the stochastic theory to directly incorporate more-generalized functional forms into the analysis. This could be based on higher-order functions which would better approximate the local-scale unsaturated soil properties over a wider range of tension values. The importance of this improved representation of local-scale properties in understanding the large-scale character of unsteady unsaturated flow should be evaluated and compared to the present methods, with a consideration of data input and computational requirements.

CHAPTER 5

THE MEAN TRANSPORT MODEL

5.1 Introduction

The objective of this chapter is to demonstrate a solution procedure for the mean solute transport equation which incorporates the macrodispersivities predicted by the stochastic analysis summarized in Section 2-3. Section 5.2 contains a brief discussion of the random walk technique used to solve the large-scale transport equation (2-82) and Section 5.3 presents an application of the solution procedure to one of the two-dimensional flow cases discussed in Chapter 4. The results are intended to demonstrate a feasible solution approach incorporating the stochastic theory and are not a comparison with specific experimental data. The macrodispersivity values that enter in the mean transport equation are only approximate for the given test problem because (i) the theoretical development assumes that the flow field is steady; (ii) the derivation is based on the assumption of mild spatial gradients of tension (and, therefore, is not valid at the steep front); and, (iii) these values correspond to an asymptotic state which is reached only after the plume has travelled on the order of 10 correlation scales from the source location (and, therefore, over-estimate the actual values at early stages). In addition, comparison with field experiments requires sufficient knowledge of the properties (means, variances, correlation scales) of the parameters affecting the solution. Such information is not yet completely available. It is for these reasons that the results are only indicative of the potential of the stochastic theory and no comparison with field data is attempted.

5.2 Random Walk Model

The numerical methodology used to solve the mean equation is the random walk technique described in detail in Tompson et al (1988) and briefly presented in the following discussion. Although apparently not as well known as differential equation-based numerical approximations, random walk techniques have been applied extensively in subsurface hydrology to solve the transport equation [see, for example, Ahlstrom et al (1977); Schwartz (1978); Smith and Schwartz (1980); Schwartz and Donath (1980); Prickett et al (1981); Campbell et al (1981); Clerici and Baker (1983); Ackerer and Kinzelbach (1985); Uffink (1983, 1987)]. Additional background on applications in subsurface hydrology is available in deMarsily (1986), Chapter 12, where the method is described by the terms "discrete parcel random walk." Random walk techniques have also been applied in many areas of science [see Weiss (1983)], beginning with the original work of Einstein (1905) on Brownian motion.

Consider a system described by a state variable $\mathbf{x}(t)$ which changes, or more specifically, evolves probabilistically with time, t. For example, the state $\mathbf{x}(t)$ can be the location of a particle in a three-dimensional space. The particle moves due to deterministic forces (e.g., mean moisture flow in this application) as well as rapidly and irregularly fluctuating forces whose mean is zero. This kind of motion has generally been modeled by a simple equation of the form

$$\frac{dx}{dt} = A(x) + B(x) \cdot \xi(t) \tag{5–1}$$

which is commonly known as a nonlinear Langevin equation. The vector A(x) is a known function of the state and represents deterministic forces acting to change x. The tensor B(x) is also a known function of the state x and indicates directional characteristics of the random forces. Finally, the vector $\xi(t)$ is an idealized representation of the "rapidly" changing forces. It is chosen such that $\xi(t)$ and $\xi(t')$ are statistically independent for recognizably distinct times $t \neq t'$.

As a result of the random forces, such a system (or particle location) can be described at a later time only through a probabilistic expression, for example the probability density function f(x,t). Tompson et al (1988) describe the various steps that lead from (5–1) to the following equation that governs the evolution of f(x,t)

$$\frac{\partial}{\partial t} f + \frac{\partial}{\partial x_i}(Af) = \frac{\partial^2}{\partial x_i \partial x_j}\left(\frac{1}{2} B_{ik}B_{jk}f\right) \tag{5–2}$$

where A_i are the components of the vector A(x) and B_{ij} the entries of the tensor B(x) of (5–1). Equations of the above form are known as Fokker-Planck equations. Note that (5–2) is a partial differential equation relating the deterministic quantities f, A_i, and B_{ij}. It has a form quite similar to the mean transport equation (2-82) that is to be solved. More specifically, the unknown function f(x,t) is thought of as equivalent to $\theta\bar{c}(x,t)$, A_i relates to the velocity and B_{ij} to the macrodispersivities. Of course, in this form, (5-2) is as complicated to solve as (2-82). However, one can take advantage of (5-1), which is the equation generating (5-2), and rather than solve a partial differential equation solve a much simpler step equation like (5-1). Since (5-2) describes the probability density function (pdf) f(x,t) one would have to follow the movement of many particles that obey (5-1) and, therefore, create (or generate) the pdf f(x,t). Each particle is independent, with the common characteristic among the different particles being the deterministic forces A_i and the main difference among the different particles being the random movement. The solution of (5–1) is straightforward and far less computationally demanding than the solution of (5–2).

It should be emphasized that the only feature of the random walk model utilized in these analyses is that the solution of the Fokker-Planck equation (5-2) can be obtained by repetitively solving the much simpler Langevin equation (5-1). There is absolutely no connection between the "randomness" of the random walk technique and the "randomness" related to heterogeneity which forms the basis of the stochastic approach presented in Chapter 2. The objective here is to solve a deterministic equation, (2-82), that describes a deterministic quantity, namely the mean concentration. A finite-difference, finite-element or other technique could have been adopted instead of the random walk technique. The choice of the latter is based on the computational simplicity and feasibility compared to those traditional techniques.

The remaining task is to define the vector A and the tensor B in (5-1) so that they correspond to (2-82). Following Tompson et al (1988), the solute transport equation for unsaturated flow can be written

$$\frac{\partial(\bar{\theta}\,\bar{c})}{\partial t} + \frac{\partial}{\partial x_i}(q\bar{c}) = \frac{\partial}{\partial x_i}\left[\bar{\theta}\,D_{ij}\frac{\partial \bar{c}}{\partial x_j}\right] = \frac{\partial}{\partial x_i}\left[\frac{\partial}{\partial x_j}(D_{ij}\,\bar{\theta}\,\bar{c}) - \bar{c}\frac{\partial}{\partial x_j}\bar{\theta}\,D_{ij}\right] \tag{5-3a}$$

which can also be written

$$\frac{\partial(\bar{\theta}\,\bar{c})}{\partial t} + \frac{\partial}{\partial x_i}\left[\bar{\theta}\,\bar{c}\left(\bar{v}_i + \frac{1}{\bar{\theta}}\frac{\partial}{\partial x_j}\bar{\theta}\,D_{ij}\right)\right] = \frac{\partial^2}{\partial x_i \partial x_j}(D_{ij}\,\bar{\theta}\,\bar{c}) \tag{5-3b}$$

$$\text{where} \quad \bar{v}_i = \frac{q_i}{\bar{\theta}}\,,\quad D_{ij} = \frac{E_{ij} + \bar{q}\,A_{ij}}{\bar{\theta}} \tag{5-4}$$

With $f = \bar{\theta}\bar{c}$, (5-3) and (5-2) become equivalent when

$$\frac{1}{2}B_{ik}B_{jk} = D_{ij}$$

$$A_i = \bar{v}_i + \frac{1}{\bar{\theta}}D_{ij}\frac{\partial\bar{\theta}}{\partial x_j} + \frac{\partial}{\partial x_j}D_{ij} \tag{5-5}$$

and the step-equation used in the random walk is the discretized version of (5-1),

$$x_n = x_{n-1} + A(x_{n-1})\,\Delta t + B(x_{n-1})\,\Delta W(t_n) \tag{5-6}$$

where x_n refers to the location of the particle at time n, A and B are given from (5-5) and $\Delta W_j = z_j[\Delta t]^{1/2}$, z being a vector of independent random numbers at t_n. For the solution of (2-82), equation (5-6) must be solved repetitively for a large number of particles with appropriate coefficients A and B.

In the work presented here, the random walk algorithm is implemented based on a prismatic domain in three dimensions (and can easily be reduced to two or one only) where the velocity, moisture content and macrodispersivity fields are discretized over each cell (i.e., have a constant value in each grid cell but may vary from cell to cell). If the flow solution provides nodal values of tension and hydraulic conductivity, appropriate cell values must be calculated. These calculations are shown in Section 5.3 for the two-dimensional example application.

The random walk technique offers an attractive alternative for the solution of solute transport equations because it avoids the numerical dispersion and mass balance effects which are inherent with finite difference or finite element approximations when the dispersivity is much smaller than the spatial discretization. However, it has several limitations which will become evident from some results in Section 5.3. The random walk technique is absolutely mass conserving because the location of every particle (with an assigned mass) is determined at each time step in the calculation. The overall distribution of mass will therefore be correctly represented by the distribution of particles. However the computed concentration, evaluated as the mass in a specified volume, will be subject to errors depending on the number of particles and averaging volume used in the computation. Such errors will be especially noticeable when the number of particles in the averaging volume is small, as will be the case at the fringes of a plume or if a very small averaging volume is used. These errors appear as erratic fluctuations in the computed concentration. In the mathematical limit of an infinitely large number of particles and arbitrarily small averaging volume the error disappears; actual simulations, however, involve finite values. The calculated concentration distribution for a given simulation can be smoothed by using a large averaging volume but this may significantly distort the concentration profile, especially near steep fronts. In the solution of a particular problem, the selection of the number of particles and the averaging volume is usually accomplished through a series of trial simulations with increasing numbers of particles. Tompson et al (1988) discuss this issue further (see, for example, Section 5.5) give simulation examples which illustrate the convergence of the random walk solution to a known analytical solution.

5.3 Two-Dimensional Application

5.3.1 Methods and procedures

The problem solved in the two-dimensional application follows closely the mean unsaturated flow problem presented in Section 4.6. The mean transport equation is obtained from (2-82)

$$\frac{\partial}{\partial t}(\bar{\theta}\,\bar{c}) + \frac{\partial}{\partial x_i}(\bar{q}_i\bar{c}) = \frac{\partial}{\partial x_i}\left[(\bar{q}A_{ij} + E_{ij})\,\frac{\partial \bar{c}}{\partial x_j}\right] \tag{5–7}$$

which is solved in a domain that resembles the trench experiment at New Mexico (see Chapter 3). As in the mean flow analysis, the bottom and right side of the domain are placed far away from the source location so that they do not influence the solution. At the top it is assumed that no mass can escape (zero-flux boundary). The left side of the domain is also a zero-flux boundary due to symmetry. The initial condition sets a zero concentration over the entire domain. Mass is introduced into the system at the top boundary over the full width of the wet strip (2 meters in this symmetric problem). This is accomplished by releasing a uniform distribution of particles into the grid cells which represent this boundary at time=zero. For the stochastic analysis 20,000 particles are used; 2,000 particles are used in the deterministic case.

The results that are presented in the following correspond to the nominal case of a 10-day wetting cycle and 10-day drying cycle, shown in Section 4.6.4. The parameters needed for the solution of (5–7) are the mean moisture $[\bar{\theta}]$, the mean specific discharge $[\bar{q}_i]$, the local dispersivities [α_L and α_T; imbedded in E_{ij}] and the macrodispersivities [A_{ij}]. The first two, $\bar{\theta}$ and $\bar{q}_i$, are obtained as nodal values directly from the flow simulation of Section 4.6. The size and discretization of the simulation grid are identical for the flow and transport analyses. Since the transport and flow problems are uncoupled, input data for the transport analysis are provided by an independent simulation of the flow model. The time interval at which nodal values are updated from the flow simulation is a 24-hour cycle. The nodal values of tension and moisture from the flow results are converted to cell values for the transport analysis by a simple arithmetic average. To calculate cell values of specific discharge for the transport analysis, the following procedure was followed: along each side of the cell the specific discharge between the two nodes was computed by using the nodal values of tension and the geometric mean of the nodal effective hydraulic conductivities; a cell value of specific discharge was then determined by an arithmetic average of the values for each corresponding direction (the horizontal and vertical components yield a specific discharge vector for each cell). Tompson et al (1988) provide further discussion of the velocity vector input.

The flow and transport problems are solved independently and thus it is possible to consider different time intervals for updating the flow inputs for the random walk model. The trade-off is between the computer memory storage required for the computed values (over the 20 day duration) and the rate of change of the flow regime. In the example application, the choice of daily interval updating means that when the solute is introduced at time zero it encounters a flow and moisture field that corresponds to the 24-hour output from the flow simulation. These values are kept constant for a duration of 1 day and then a new update is read which corresponds to the output at day 2 from the flow simulation. Thus, there is a slight delay in the transfer of information from the flow to the transport simulation; however, such a feature is common in all unsteady flow and transport simulations. The effects caused by the delay of information transfer could be reduced with more frequent updating, with the corresponding computational tradeoff mentioned above.

The values of the local longitudinal and lateral dispersivities [α_L and α_T] were taken to be 1 cm and 0.1 cm, respectively, which are typical laboratory values. Of interest here is the evaluation of the macrodispersivities [A_{ij}]. The appropriate equations are presented in the Appendix, corresponding to the case of statistically anisotropic soil with arbitrary orientation of the mean flow. The macrodispersivity values depend directly on the flow conditions [through the flow factor γ^2 in (A-3)], the mean tension field and particularly the tension gradient [parameter L_2 in (A-4) and (2-21)]. Note that they change over time as the tension and flow conditions change over time. However, the dependence is only parametric [i.e., the tension and flow field were assumed constant when the evaluation of macrodispersivities was performed in Mantoglou and Gelhar (1985)]. Also, the macrodispersivities given in Section 2.3 assume that the spatial gradients of the mean tension field are mild; consequently, macrodispersivity values calculated near a steep moisture front, based on (A–3), would be approximate.

In light of the above discussion, a modeling compromise was adopted for the calculation of macrodispersivities. Since (A–3) is valid where tension gradients are mild, a macrodispersivity tensor evaluated at a region with mild gradients was calculated. This evaluation was then assumed to apply over the entire wetted plume. Note that such an operation is not always possible due to the tensorial (and consequently directional) characteristics of the macrodispersivity; in general, the principal axes of the macrodispersivity do not coincide with the flow direction. Since the flow direction changes in space in the example application (see Figures 4-15 and 4-16), special treatment would generally be required to preserve the directional characteristics. However, (A-3) shows that when lateral gradients are negligible, the predominant component of the macrodispersivity tensor is along the direction of the mean flow. Hence, it was assumed that the macrodispersivity tensor calculated for the example application has only one non-zero value [the longitudinal macrodispersivity A_{11}^{*}] which coincides with the direction of the mean flow. As noted above, this macrodispersion tensor was assumed to apply over the entire plume. However, the longitudinal macrodispersivity A_{11}^{*} for a given cell was oriented along the direction of the specific discharge vector within that cell. The local dispersivity values are then added to the macrodispersivity values [see (5-7)]; however, the effect is minimal in the example application due to the difference in magnitudes of these contributing components. At each time step this leads to a dispersivity tensor of the form

$$\begin{bmatrix} A_{11}^{*} + \alpha_L & 0 \\ 0 & \alpha_T \end{bmatrix} \tag{5-8}$$

which is oriented along the direction of the mean flow within each cell. Appropriate tensor transformations are then performed to rotate this tensor to the common vertical and horizontal system of axes.

Table 5-1 summarizes the values of A_{11}^{*} calculated for each day of the 20-day period (with wetting occurring during the first 10 days only). These macrodispersivities were calculated where gradients were mild; the region where tension values were under 100 cm was thought to be appropriate (see Figures 4-15 and 4-16). In particular, the region selected corresponds to the upper left block (5 cm by 20 cm in physical dimensions) of the flow domain.

5.3.2 Example results

In the following, the results from two simulations are presented. The flow field is the same in both and corresponds to the nominal case of the mean flow simulation discussed in Chapter 4. The first example, which will be referred to as the "deterministic" case, did not include macrodispersion as a transport mechanism. The only dispersive mechanisms modelled in this case were the local transverse and longitudinal dispersivities. The second example, which will be referred to as the "stochastic" case, included macrodispersivity effects [using (5-8) and macrodispersivity values from Table 5-1]. The particular characteristics associated with the stochastic analysis can thus be demonstrated.

The simulation results for the deterministic case, using 2000 particles which were injected at time = 0, are shown at 5-day intervals in Figure 5-1. The particles follow the general direction of the moisture propagation and disperse in the vertical direction slightly. Also, a very slow downward, gravity-driven movement can be observed after day 10 (recall that water input stopped at the end of day 10). These "snapshots" of the particle locations demonstrate another characteristic of unsaturated transport, namely the lag of the tracer pulse relative to the moisture front. While the tracer tends to move with the water into which it was injected, the moisture front moves more like a "pressure wave". From Fig. 4-16 we see that in 10 days the wetting

Table 5-1. Asymptotic Macrodispersivities for the 2-D Simulation (value in the principal axis)

Day	A^*_{11} (cm)
1	377
2	745
3	651
4	629
5	622
6	618
7	617
8	617
9	617
10	616
11	104 (drying started)
12	124
13	139
14	151
15	158
16	169
17	177
18	185
19	192
20	197

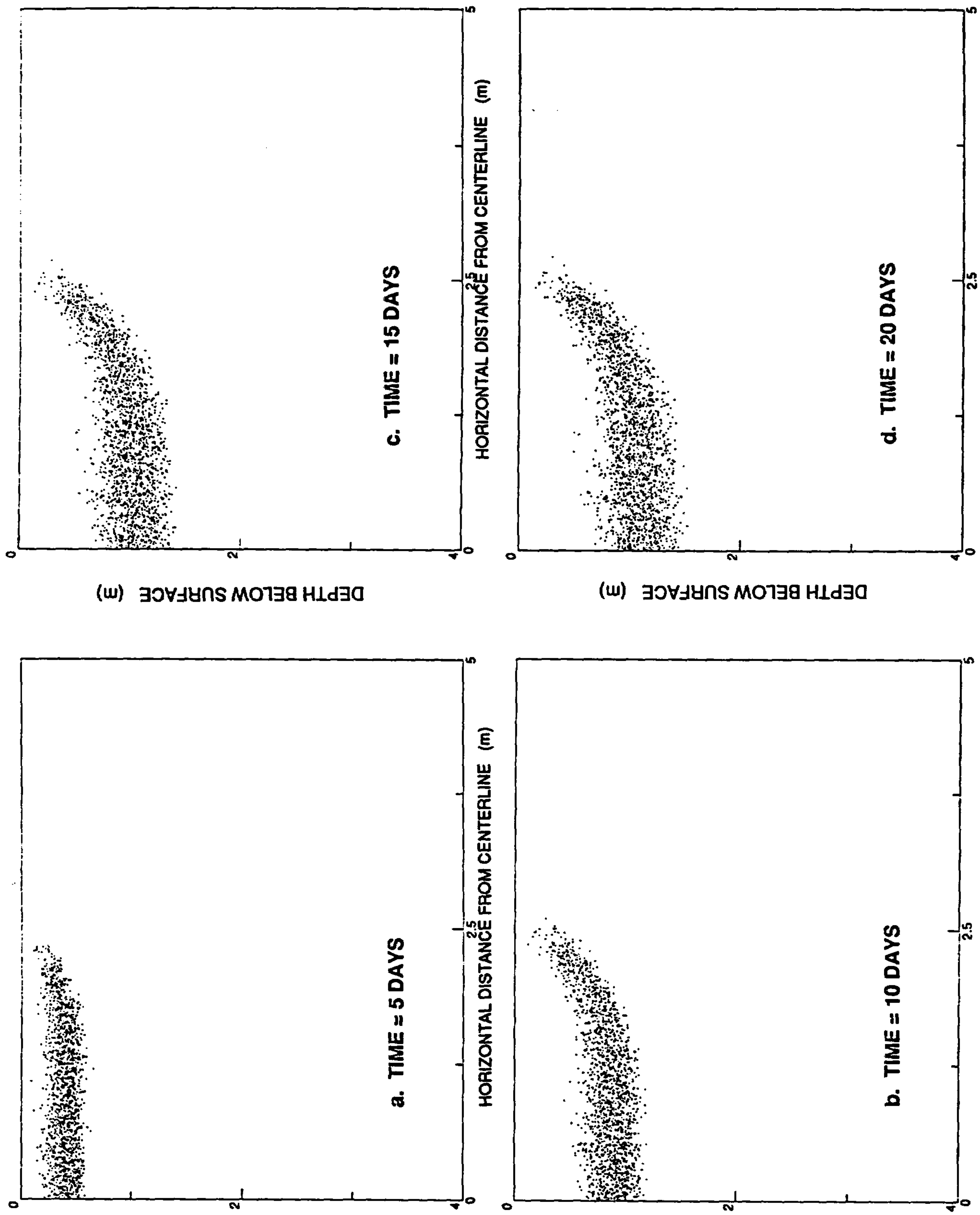

Figure 5-1. Spatial location of 2000 particles during wetting/drying cycle after impulse injection; deterministic case

front has penetrated downward at least 1.8 m whereas from Figure 5-1 the tracer pulse has moved down about 1.0 m.

Shown in Figure 5-2 are the comparable simulation results for the stochastic case using 20,000 particles and macrodispersivity effects in addition to the local components [see (5-8) and Table 5-1]. Under the influence of the higher macrodispersivity values, the particles disperse over most of the available wetted space, being bounded by the propagating moisture front. Compare Figure 5-2 to Figure 4-16, noting that the dry regions of the domain beyond the wetting front have a mean tension of 1,000 cm. A greater horizontal movement is also observed as compared to the deterministic case. This is caused by the moisture movement which is largely horizontal at the upper right part of the plume. To illustrate this point further, Figures 5-3 and 5-4 focus on a small portion of the particles to investigate their lateral spread. These figures compare the deterministic and stochastic simulation for only those particles injected between the 1.0 to 1.4 m and 1.4 to 2.0 m portions of the wetted strip. Figures 5-3a and 5-4a show the predominance of vertical movement for the particles released from 1.0 to 1.4 m. In contrast, when particles are released between 1.4 and 2.0 m (Figures 5-3b and 5–4b), there is a significant horizontal component to the particle movements, especially for the particles injected at the edge of the irrigated strip.

Bulk concentration is defined as the number of particles per grid cell, irrespective of moisture content. The particle locations presented in Figures 5-1 and 5-2 were converted to bulk concentrations and contours of equal concentration were drawn for the two-dimensional plane. The concentration distribution is presented as a surface in perspective view in Figure 5-5. The substantially different magnitude of the dispersion effects for the two cases can be clearly observed in these plots. Note also the "raggedness" of the bulk concentration surface; this is characteristic of the random walk technique used here. The larger the number of particles used to obtain the solution, the smoother the solution will become. The variability in the random walk solution around the actual smooth solution can be reduced; this depends on the square root of the number of particles used. For example, in the given case 80,000 particles would be required (compared to 20,000) in order to reduce the variability to half the present condition. This issue is further discussed by Tompson et al (1988).

Finally, the bulk concentration contours associated with Figure 5-5 are plotted in Figure 5-6. In the deterministic case the well defined pulse moves downward, while in the stochastic case the tracer spreads over the entire wetted space. Note the "rough" contour lines which depend on the number of particles used in the random walk solver.

5.4 Summary and Future Research Needs

As discussed in the introduction, the objective here was to demonstrate a solution procedure for the mean solute transport equation. The random walk algorithm adequately represents the unsteady mean flow and incorporates the varying magnitude of the macrodispersivities. Although the mean concentration exhibits some fluctuations, the bulk characteristics of the developing plume are quite clear. In the deterministic simulation the concentration distributions are quite smooth, even though only 2,000 particles were used. Quantitative analysis of the plume would be possible in this case.

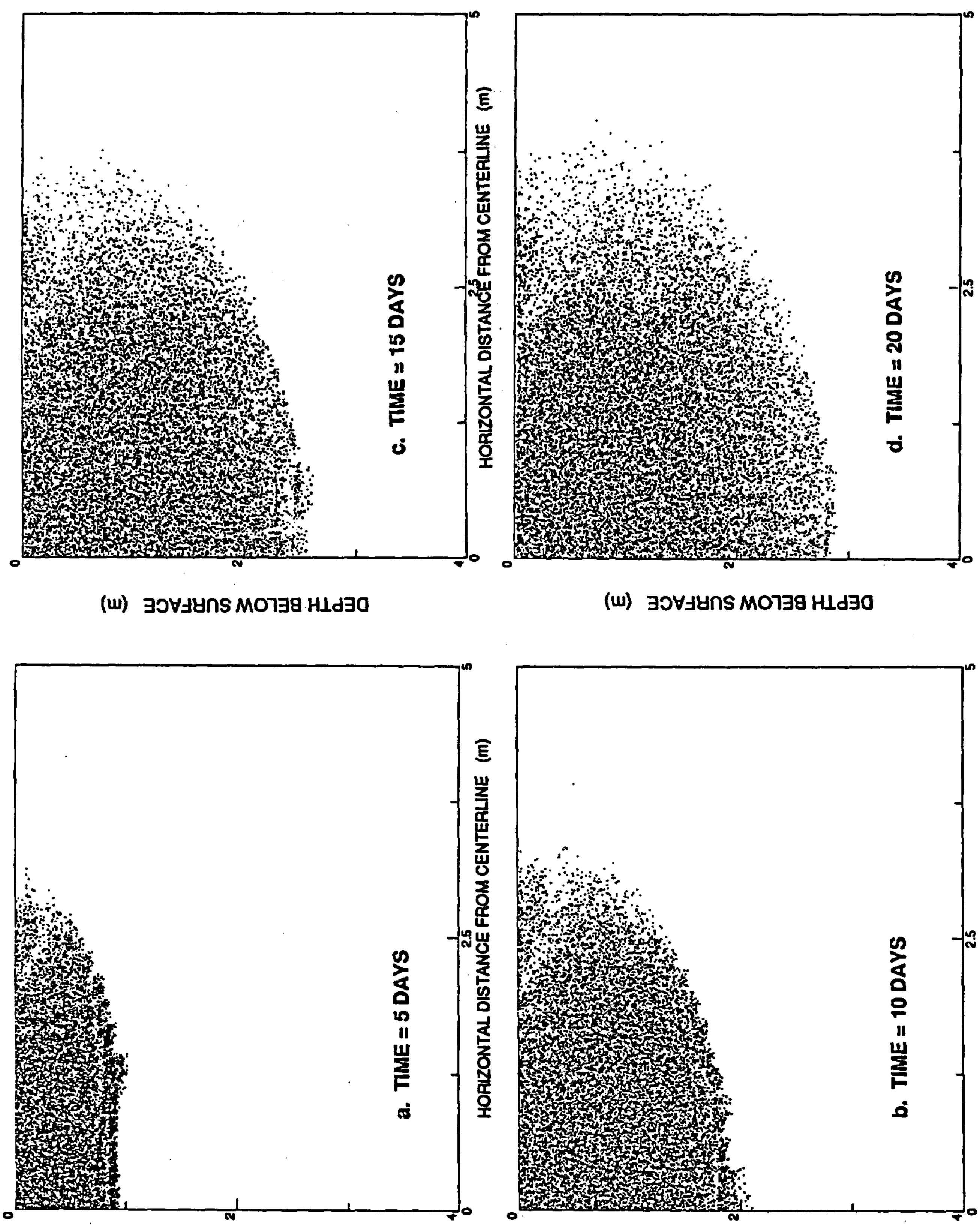

Figure 5-2. Spatial location of 20,000 particles during wetting/drying cycle after impulse injection; stochastic case

a. Particles released at surface between 1.0 and 1.4 meters

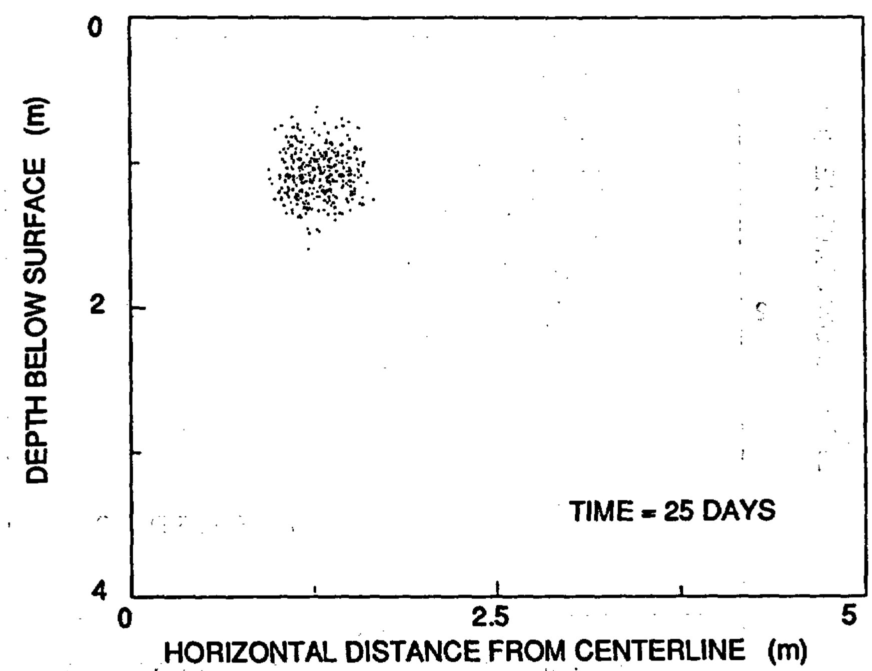

b. Particles released at surface between 1.4 and 2.0 meters

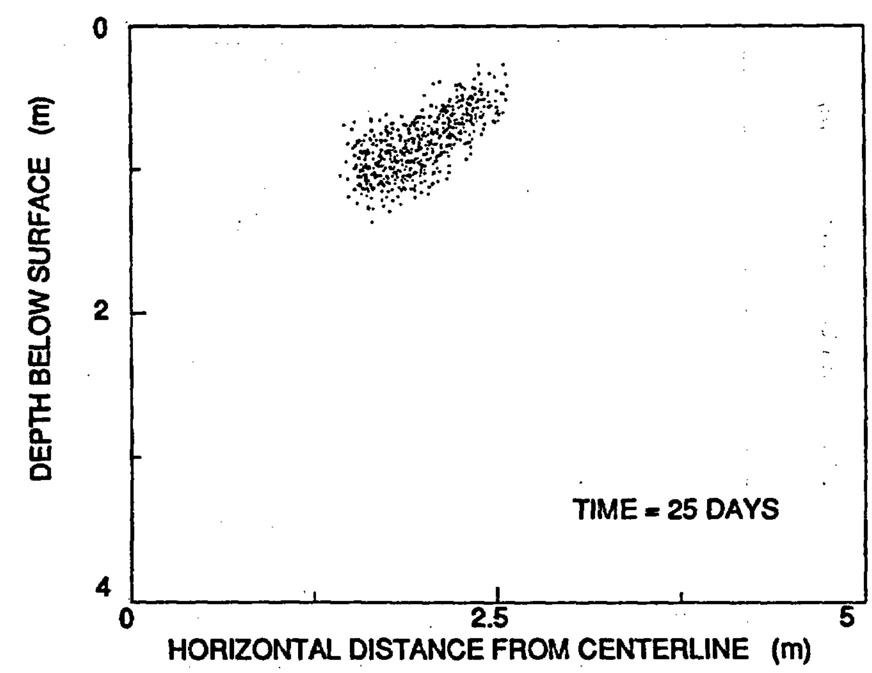

Figure 5-3. Longitudinal and lateral movement of selected particles; deterministic case

a. Particles released at surface between 1.0 and 1.4 meters

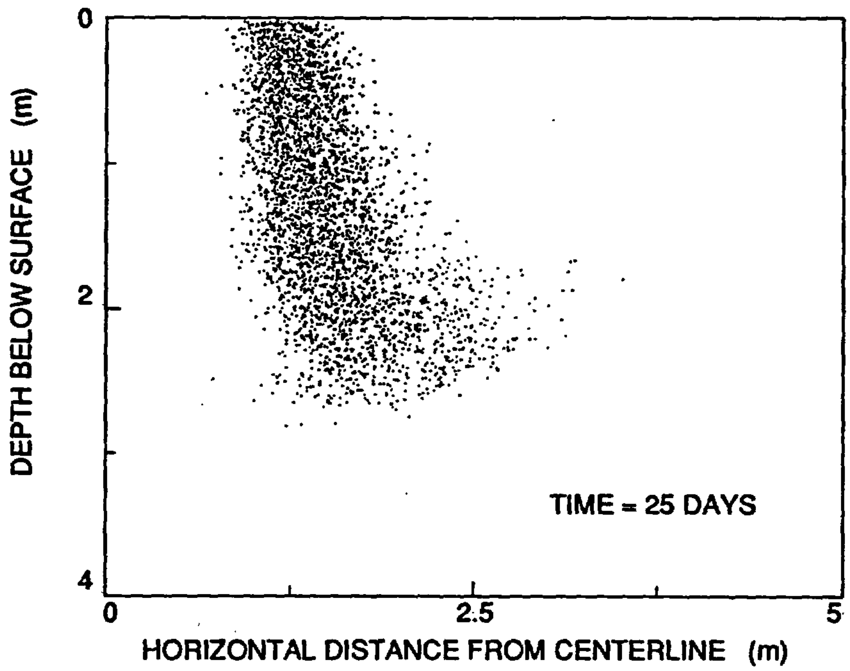

b. Particles released at surface between 1.4 and 2.0 meters

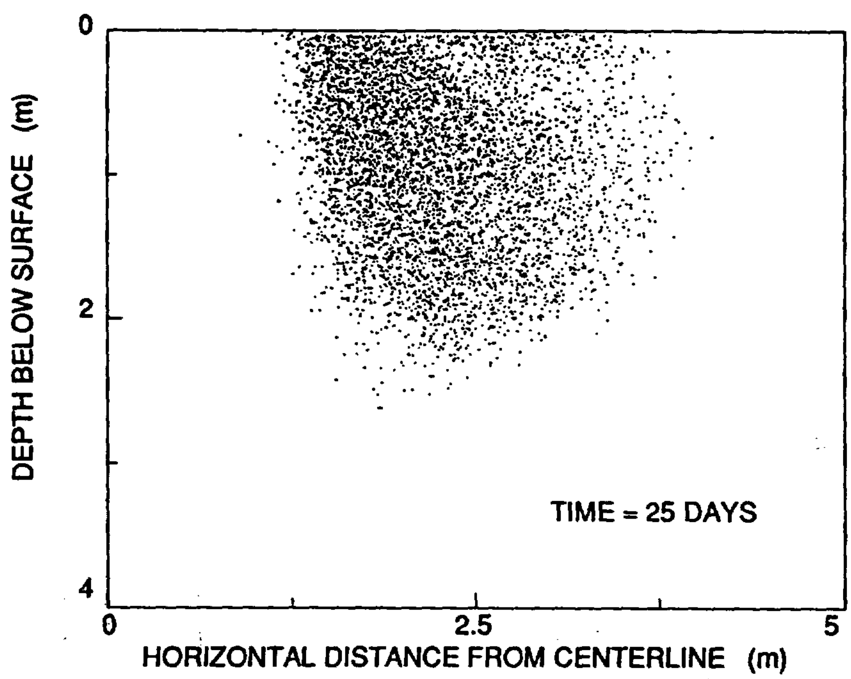

Figure 5-4. Longitudinal and lateral movement of selected particles; stochastic case

a. Local dispersivity only (deterministic case)

b. Macrodispersivity included (stochastic case)

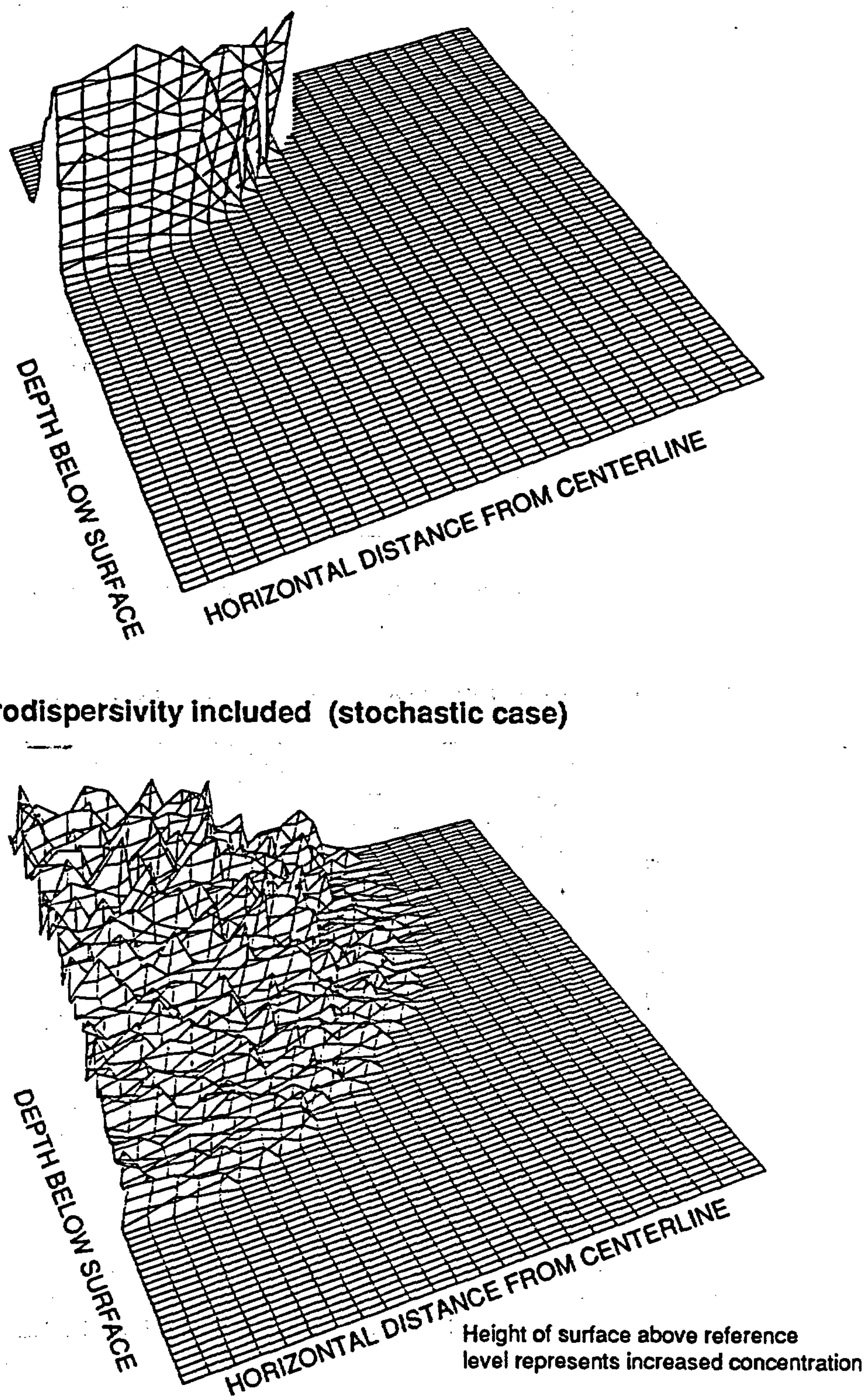

Figure 5-5. Perspective view of contoured data showing spatial variations of bulk concentration for time = 20 days

a. Local dispersivity only (deterministic case)

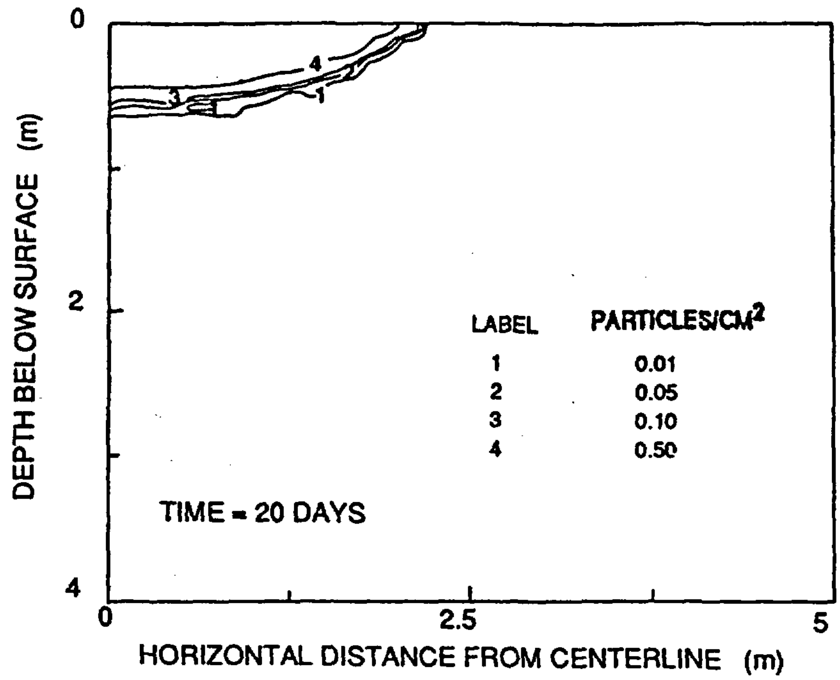

b. Macrodispersivity included (stochastic case)

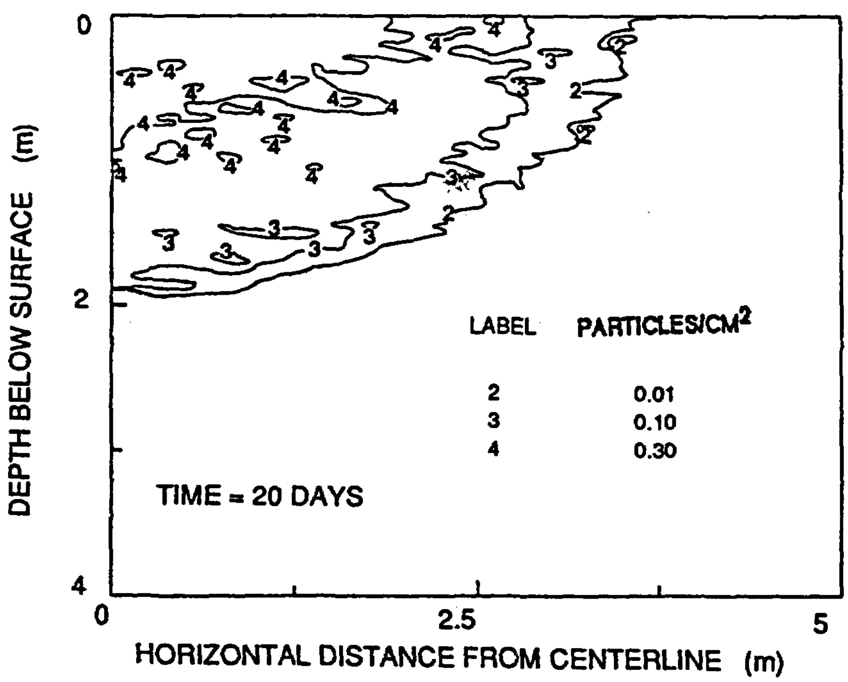

Figure 5-6. Contours of equal bulk concentration showing spatial variations within the plume for time = 20 days

For the stochastic simulation, a quantitative analysis cannot be recommended based on the present work due to the restricted nature of the theoretical development used as input to the simulation. Additional theoretical analyses are needed before a quantitative evaluation of the mean transport solution is attempted. The calculated values of macrodispersivity (Table 5–1) are considered to be unrealistically large for the two-dimensional application undertaken here. These unrealistic values most likely are related to the limitations of the theory: (i) the macrodispersivities were determined from theory based on an asymptotic evaluation valid only for relatively large displacement (on the order of 10 times the macrodispersivity); and, (ii) the macrodispersivities were determined from theory based on a steady-state assumption, in contrast to the clearly unsteady nature of flow and transport in the example application.

In conclusion, the example simulations show that the random walk algorithm provides an efficient method to solve the mean transport equation. Additional work is required with regard to definition of concentrations and the smoothness of the mean solution. Also, there is a need to extend stochastic theories to incorporate the influence of developing dispersion and unsteadiness.

CHAPTER 6

SUMMARY AND CONCLUSIONS

The major conclusions of the research described in this report can be summarized as follows:

1. MIT's stochastic theory of unsaturated flow and solute transport provides a practical way to incorporate small-scale variability into large-scale models. In particular, this theory may be used to derive multi-dimensional distributions of the mean capillary tension (or moisture content), contaminant concentration, and related quantities. In addition, the standard deviation of tension is provided as an aid to the analysis of predictive uncertainty. The mean equations are similar in form to those found in traditional deterministic models. The input parameters in the stochastic theory may, however, differ significantly from those of deterministic approaches. Models based on the stochastic approach appear to have computational requirements which are comparable to those of more traditional deterministic models.

2. The effective (large-scale) soil parameters derived in Chapter 2 depend on the statistical properties of the intercept ($\ln K_s$) and slope (α) of the local (small-scale) log hydraulic conductivity versus tension function. The properties of interest are the mean and variance of α [A and σ_a^2], the mean and variance of $\ln K_s$ [F and σ_f^2], and the vertical correlation scale [λ_1] (assumed the same for f and a). If a stochastic modeling approach is adopted, site investigations should be designed to provide accurate estimates of these parameters. The vertical and horizontal components of the effective conductivity tensor also depend on the mean tension and its time derivative, which generally vary throughout the domain of interest.

3. The stochastic theory predicts that the effective hydraulic conductivity of a stratified unsaturated soil will exhibit two properties which have important practical implications -- tension-dependent anisotropy and large-scale hysteresis. The anisotropy effect, which becomes very important in dry soils, may result in enhanced lateral spreading during wetting. The hysteresis effect essentially eliminates anisotropy during subsequent redistribution. Field experiments at Las Cruces, New Mexico are being designed to test these two predictions. Preliminary results confirm enhanced lateral spreading at high tensions during wetting.

4. Numerical simulations of the lysimeter and trench experiments at Las Cruces have been used to guide the experimental design. Some of the design variables considered include infiltration schedules, rates and areas, and the location of lysimeters, neutron probe access tubes, and solute samplers. The simulations compare reasonably well with measured one-dimensional lysimeter moisture and tension profiles. More information is needed on *in situ* soil properties, particularly unsaturated hydraulic conductivities, before a direct comparison can be made between simulation results and field observations taken at the trench.

5. Sensitivity analyses of the mean unsaturated flow model have identified the most important input parameters for the stratified soil case. The results are consistent with those anticipated from closed-form asymptotic expressions for the effective hydraulic conductivity. They indicate that the rate and shape of the moisture plume depend strongly on the mean and variance of α and the vertical correlation scale. The mean and variance of $\ln K_s$ are less important. Of particular interest is the wide variation of the vertical-to-horizontal anisotropy ratio (over several orders of magnitude) when the variance of α or the vertical correlation scale change by relatively modest amounts. The sensitivity results suggest that particular attention should be given to accurate estimation of these critical soil parameters.

6. Preliminary results indicate that the random walk approach for simulating mean solute transport is feasible. This Lagrangian approach is particularly attractive for unsaturated problems, where the tension-dependent macrodispersivity may vary over several orders of magnitude. This variation can lead to numerical dispersion problems when conventional Eulerian solution methods are used to solve the transport equation. Mean transport simulations for the trench experiment suggest that significant solute transport will be confined to wetted areas. The macrodispersivities used in these simulations are, however, based on a steady transport analysis which may not be adequate for the unsteady conditions which apply in the trench experiment. This leads to macrodispersivity values which are unrealistically high in some areas, particularly just behind the moisture front. Fortunately, the general theory can be extended to account for transient flow effects. When this is done, more thorough tests of the random walk transport model can be undertaken.

7. One of the primary limitations of existing techniques for simulating unsaturated flow and transport, either stochastic or deterministic, is the lack of detailed soils data, particularly the lack of direct measurements of unsaturated hydraulic conductivity. Further research is needed to develop and test accurate methods for determining the behavior of relatively dry field soils. These methods need to be sufficiently simple and efficient to permit field investigators to estimate the mean, variance, and correlation scales of important soil properties from samples or observations taken at a proposed disposal site.

8. The theoretical and simulation results presented in this report indicate that MIT's stochastic theory is a feasible alternative to more conventional deterministic approaches. There are several areas where improvements or extensions to this theory are needed. Topics which merit further investigation include the role of heterogeneity in the moisture retention curves, the effect of curvature in the local log hydraulic conductivity versus tension function (which is now assumed to be linear), unsteady transport theory, and the contribution of vapor transport. Theoretical results for statistically stratified soils and steady-state macrodispersivities need to be generalized and incorporated into the mean flow and transport models. Numerical algorithms need to be improved so that computational burdens can be reduced. Finally, the implications of the stochastic approach for model validation, site characterization, and performance assessment need to be investigated. Existing concepts in these areas tend to be based on deterministic

descriptions which do not account for heterogeneity and uncertainty. The stochastic viewpoint provides a rigorous way to introduce uncertainty into model-oriented evaluations of prospective low-level waste sites.

APPENDIX

Macrodispersivity evaluation for statistically anisotropic soil with arbitrary orientation of mean flow

Mantoglou and Gelhar (1985) evaluated A_{ij} in the particular case of a horizontally stratified soil and $\partial H/\partial x_j$ (j=2,3) being relatively small. In a statistically anisotropic formation, due to large lateral hydraulic conductivities, even small lateral gradients may produce significant lateral flow. In this case, the mean specific discharge vector **q** is not oriented towards the vertical direction x'_1 but it is inclined to the vertical direction with an angle ϕ (see Figure 2-7). Note that the mean flow model (2-18) predicts the components J'_1, J'_2, J'_3 of the mean gradient vector **J** in the principal axes of statistical anisotropy. In order to evaluate A_{ij} (from 2-80) and be able to use the mean transport model (2-60), the magnitude and direction of **q** was determined as a function of J'_1, J'_2, and J'_3. Under the assumption that $\partial H/\partial x_j$ is small, it holds that $L_j \approx J_j$ and $J_j \partial H/\partial x_j \approx 0$. The cross-spectral density function $S_{q_jq_i}$ was evaluated using

$$S_{q_jq_i}(k) = K_M^2 \frac{J_m J_n (\delta_{im}k^2 - k_i k_m)(\delta_{jn}k^2 - k_j k_n)}{k^4 + A^2 (L_j k_j)^2} \beta^2 S_{ff}(k) \qquad \text{(A–1)}$$

where $\beta^2 = (1 + \zeta^2 H^2)$ for f and a being uncorrelated and $\beta^2 = (1 - \zeta H)^2$ for f and a perfectly correlated.

Equation (A-1) is expressed in the system of axes x_1, x_2, x_3 which are not necessarily identical to the principal statistical anisotropy axes x'_1, x'_2, x'_3 (see Figure 2-7). Assuming an exponential covariance function for f and a, and using the transformation $k'_i = a_{ij}k_j$ where a_{ij} are the direction cosines $[a_{ij} = \cos(x'_j, x_i)]$, $S_{ff}(k)$ in (A-1) is given by

$$S_{ff}(k_1,k_2,k_3) = \frac{\sigma_f^2 \lambda_1 \lambda_2 \lambda_3}{\pi^2 [\,1 + \lambda_1^2 (a_{1j}k_j)^2 + \lambda_2^2 (a_{2j}k_j)^2 + \lambda_3^2 (a_{3j}k_j)^2]^2} \qquad \text{(A–2)}$$

Substituting (A-1) in (2-80) and using the fact that $\varepsilon = \alpha_L/\lambda_1 \ll 1$,

$$A_{11} = \frac{\sigma_f^2 \lambda_1 \lambda}{\pi \gamma^2 \Omega} (\,T_{22} + 2\xi^2 T_{23} + \xi^4 T_{33}) \qquad \text{(A–3a)}$$

$$A_{22} = \frac{\sigma_f^2 \lambda_1 \lambda}{\pi \gamma^2 \Omega} \frac{J_2^2}{J_1^2} \xi^4 T_{33} \qquad \text{(A–3b)}$$

$$A_{33} = \frac{\sigma_f^2 \lambda_1 \lambda}{\pi \gamma^2 \Omega} \frac{J_2^2}{J_1^2} \xi^4 T_{23} \qquad \text{(A–3c)}$$

$$A_{12} = \frac{\sigma_f^2 \lambda_1 \lambda}{\pi \gamma^2 \Omega} \frac{J_2}{J_1} \xi^2 (T_{23} + \xi^2 T_{33}) \quad \text{(A-3d)}$$

where the parameters

$$T_{22} = \iint_{-\infty}^{\infty} \frac{u_2^4}{(u_2^2 + \xi^2 u_3^2)^2 + A^2 L_2^2 \Omega^2 u_2^2} \frac{1}{(1 + u^2)^2} du_2 \, du_3 \quad \text{(A-4a)}$$

$$T_{23} = \iint_{-\infty}^{\infty} \frac{u_2^2 u_3^2}{(u_2^2 + \xi^2 u_3^2)^2 + A^2 L_2^2 \Omega^2 u_2^2} \frac{1}{(1 + u^2)^2} du_2 \, du_3 \quad \text{(A-4b)}$$

$$T_{33} = \iint_{-\infty}^{\infty} \frac{u_3^4}{(u_2^2 + \xi^2 u_3^2)^2 + A^2 L_2^2 \Omega^2 u_2^2} \frac{1}{(1 + u^2)^2} du_2 \, du_3 \quad \text{(A-4c)}$$

$$\xi^2 = \frac{\Omega^2}{\lambda^2} = \frac{\lambda_1^2}{\lambda^2} \sin^2\phi + \cos^2\phi \quad \text{(A-5)}$$

$$\Omega^2 = \lambda_1^2 \sin^2\phi + \lambda^2 \cos^2\phi \quad \text{(A-6)}$$

The integrals T_{22}, T_{23}, T_{33} can be reduced to one-dimensional integrals [see Appendix L of Mantoglou and Gelhar (1985)], which require further numerical integration. The angle ϕ is described in Figure 2-7. The parameters λ_1 and λ ($= \lambda_2 = \lambda_3$) are the correlation lengths in directions perpendicular and parallel to the direction of stratification, respectively. The parameter γ^2 is a flow factor and is given by

$$\gamma^2 = \frac{q^2}{K_M{}^2 J_1{}^2 \beta^2} \quad \text{(A-7)}$$

In the example application discussed in Chapter 5, γ^2 was evaluated using $\beta^2 = (1 + J^2H^2)$, $J_1=1$, and $q = \hat{K}_{11}$ [see (2-43)], assuming steady vertical flow for the selected grid cell. The value of K_M was estimated using exp [F(H)] · exp [-A(H)] where A(H) is given by (2-46) and F(H) is given by (2-48).

REFERENCES

Ababou, R., D. McLaughlin, L.W. Gelhar and A.F.B. Tompson. Numerical Simulations of Saturated/Unsaturated Flow Fields in Randomly Heterogeneous Porous Media. in: Proc. Int. Assoc. of Hydraulic Research Symposium on the Stochastic Approach to Subsurface Flow, Montvillargenne, France, June 1985.

Ababou, R., L.W. Gelhar and D. McLaughlin. Three-Dimensional Flow in Random Porous Media. Technical Report 318, R88-08, R.M. Parsons Lab, M.I.T, Cambridge, MA, 2 vols., 1988.

Ackerer, P. and W. Kinzelbach. Modelisation du transport de contaminant par la methode de marche au hasard: influence des variations du champ d'ecoulement au cours du temps sur la dispersion. Proc., International Symposium on the Stochastic Approach to Subsurface Flow, Montvillargenne, France, 1985.

Ahlstrom, S.W., H.P. Foote, R.C. Arnett, C.R. Cole and R.J. Serne. Multicomponent mass transport model: theory and numerical implementation. Report BNWL 2127, Battelle, Pacific Northwest Labs, Richland, WA, 1977.

Andersson, J. and A.M. Shapiro. Stochastic analysis of one-dimensional steady-state unsaturated flow: A comparison of Monte-Carlo and perturbation methods. Water Resources Research, 19(1), 121-133, 1983.

Baker, F.G. Variability of hydraulic conductivity within and between nine Wisconsin soil series. Water Resources Research, 14(1), 103-108, 1978.

Biggar, J.W. and D.R. Nielsen. Spatial variability of the leaching characteristics of a field soil. Water Resources Research, 12(1), 78-84, 1976.

Bouwer, H. Infiltration of water into non-uniform soil. J. Irrigation and Drainage Div. A.S.C.E., 4, 451-462, 1969.

Bras, R.L. and I. Rodriguez-Iturbe. Random Functions and Hydrology. Addison-Wesley, Reading, MA, 1985.

Bresler, E. and G. Dagan. Convective and pore scale dispersive solute transport in unsaturated heterogeneous fields. Water Resources Research, 17(6), 1683-1693, 1981.

Bresler, E. and G. Dagan. Unsaturated flow in spatially variable fields, 2, Applications of water flow models to various fields. Water Resources Research, 19(2), 429-435, 1983.

Byers, E. and D.B. Stephens. Statistical and stochastic analyses of hydraulic conductivity and particle-size in a fluvial sand. Soil Sci. Soc. of America Journal, 47, 1072-1081, 1983.

Campbell, J.A., D.E. Longsive and R.M. Cranwell. Risk methodology for geologic disposal of radioactive waste: the NWFT/DVM computer code users manual. Sandia National Labs Report SABD81-0886, 1981.

Carvallo, H.O., D.K. Cassel, J. Hammond, and A. Bauer. Spatial variability of in-situ unsaturated hydraulic conductivity of Maddock sandy loam. Soil Science, 121(1), 1-8, 1976.

Cassel, D.K. Spatial and temporal variability of soil physical properties following tillage of Norfolk loamy sand. Soil Sci. Soc. of America Journal, 47, 196-201, 1983.

Celia, M.A., L.R. Ahuja and G.F. Pinder. Orthogonal collocation and alternating direction procedures for unsaturated flow. accepted for publication, Advances in Water Resources, 1987.

Clerici, J.F. and J.E. Baker.Hydrogeologic models for siting of waste facilities. Proc., ASCE Irrigation and Drainage Div. Specialty Conf., Jackson, WY, 90-97, July 1983.

Dagan, G. Modeling of groundwater flow by unconditional and conditional probability. 1. Conditional simulations and the direct problem. Water Resources Research, 18, 813-833, 1982.

Dagan, G. Solute transport in heterogeneous porous formations. J. Fluid Mechanics, 145, 151-177, 1984.

Dagan, G. and E. Bresler. Unsaturated flow in spatially variable fields, 1, Derivation of models of infiltration and redistribution. Water Resources Research, 19(2), 413-420, 1983.

deMarsily, G. Quantitative Hydrogeology; Groundwater Hydrology for Engineers. Orlando: Academic Press, 1986.

Einstein, A. Uber die von der molekular-kinetischen theorie der warme gefordete bewegung von in ruhenden flussigkeiten suspendierten teilchen. Ann. der Physik, 17, 549-560, 1905.

El-Kadi, A. and W. Brutsaert. Applicability of effective parameters for unsteady flow in non-uniform aquifers. Water Resources Research, 21(2), 183-198, 1985.

Elrick, D.E., R.W. Sheard and N. Baumgartner. A simple procedure for determining the hydraulic conductivity and water retention of putting green soil mixtures. Proc., 4th International Turfgrass Research Conf., Guelph, Ontario, Canada, July 1980.

Elrick, D.E. et al. The "Guelph Permeameter" for measuring the field-saturated soil hydraulic conductivity above the water table. I. Theory, procedures and applications. Proc., Canadian Hyd. Symposium, Quebec City, Quebec, 1984.

Freeze, F.A. A stochastic conceptual analysis of one-dimensional groundwater flow in non-uniform homogeneous media. Water Resources Research, 11(5), 725-741, 1975.

Garabedian, S., L.W. Gelhar and M.A. Celia. Large-Scale Dispersive Transport in Aquifers: Field Experiments and Reactive Transport Theory. Technical Report 315, R88-01, R.M. Parsons Lab, M.I.T., Cambridge, MA, 1988.

Gardner, W.R. Some steady state solutions of the unsaturated moisture flow equation with application to evaporation from a water table. Soil Science, 85(4), 228-232, 1958.

Gatjem, Y.M., A.W. Warrick and D.E. Myers. Spatial dependence of physical properties of a typic torrifluvent soil. Soil Sci. Soc. of America Journal, 45, 709-715, 1981.

Gelhar, L.W. Stochastic Analysis of Solute Transport in Saturated and Unsaturated Porous Media. In: Advances in Transport Phenomena in Porous Media. Eds. J. Bear and M.Y. Corapcioglu, M. Nijhoff Pub., Dordrecht, NATO ASI Series, 657-700, 1987.

Gelhar, L.W. and C.L. Axness. Three-dimensional stochastic analysis of macrodispersion in aquifers. Water Resources Research, 19(1), 161-180, 1983.

Gelhar, L.W., A.L. Gutjahr and R.L. Naff. Stochastic analysis of macrodispersion in a stratified aquifer. Water Resources Research, 15(6), 1387-1397, 1979.

Gutjahr, A.L., L.W. Gelhar, A.A. Bakr and J.R. MacMillan. Stochastic analysis of spatial variability in subsurface flows, 2, Evaluation and application. Water Resources Research, 14(5), 953-959, 1978.

Hillel, D. Fundamentals of Soil Physics. Academic Press, New York, 1980.

Huyakorn, P.S. and G.F. Pinder. Computational methods in subsurface flow. Academic Press, New York, 1983.

Jury, W.J. Simulation of solute transport using a transfer function model. Water Resources Research, 18(2), 363-368, 1982.

Jury, W.J., L. Stolzy and P. Shouse. A field test of the function model for predicting solute transport. Water Resources Research, 18(2), 369-375, 1982.

Kies, B. Solute transport in unsaturated field soil and in groundwater. [Ph.D. Dissertation]. New Mexico State University, Las Cruces, NM, 1981.

Lumley, J.L. and H.A. Panofsky. The Structure of Atmospheric Turbulence. John Wiley, New York, 1964.

Mantoglou, A. and L.W. Gelhar. Capillary tension head variance, mean soil moisture content, and effective specific soil moisture capacity of transient unsaturated flow in stratified soils. Water Resources Research, 23(1), 47-56, 1987b.

Mantoglou, A. and L.W. Gelhar. Effective hydraulic conductivities of transient unsaturated flow in stratified soils. Water Resources Research, 23(1), 57-68, 1987c.

Mantoglou, A. and L.W. Gelhar. Large-scale Models and Effective Parameters of Transient Unsaturated Flow and Contaminant Transport Using Stochastic Methods, Tech. Report 299, R.M. Parsons Lab, M.I.T., Cambridge, MA, 1985.

Mantoglou, A. and L.W. Gelhar. Stochastic modeling of large-scale transient unsaturated flow systems. Water Resources Research, 23(1), 37-46, 1987a.

Mualem, Y. A new model for predicting the hydraulic conductivity of unsaturated porous media. Water Resources Research, 12(3), 513-522, 1976.

Mualem, Y. Anisotropy of unsaturated soils. Soil Sci. Soc. of America Journal, 48, 505-509, 1984.

Mulford, E.F. The Application of Stochastic Models to Numerical Simulations of Large Scale Unsaturated Flow [S.M. Thesis]. M.I.T., Cambridge, MA, 1986.

Naff, R.L. A Continuum Approach to the Study and Determination of Field Longitudinal Dispersion Coefficients [Ph.D. Dissertation]. N.M. Institute of Mining and Technology, Socorro, NM, 1978.

Nielsen, D.R., J.W. Biggar and K.T. Erh. Spatial variability of field measured soil-water properties. Hilgardia, 42(7), 215-260, 1973.

Office of the Federal Register, Code of Federal Regulations, Subparts C and D, 10, 672-678, 1987.

Philip, J.R. Field heterogeneity, some basic issues. Water Resources Research, 16(2), 443-448, 1980.

Philip, J.R. Theory of Infiltration. in: Advances in Hydroscience, 5, (V.T. Chow, ed.), 215-305. Academic Press, New York, 1969.

Prickett, T.A., T.C. Naymick, and C.G. Lonnquist, A "Random Walk" Solute Transport Model for Selected Groundwater Quality Evaluations, Illinois State Water Survey Bulletin 65, Champaign, 1981.

Reynolds, W.D. et al. The "Guelph Permeameter" for measuring the field-saturated soil hydraulic conductivity above the water table. II. The apparatus. Proc., Canadian Hyd. Symposium, Quebec City, Quebec, 1984.

Rubin, J. and R. Steinhardt. Soil water relations during rain infiltration, 1, Theory. Soil Sci. Soc. of America Journal., 26, 246-251, 1963.

Russo, D. A geostatistical approach to the trickle irrigation heterogeneous soil. 1. Theory. Water Resources Research, 19(3), 632-642, 1983.

Russo, D. and E. Bresler. Field determinations of soil hydraulic properties for statistical analyses. Soil Sci. Soc. of America Journal., 44, 697-702, 1980.

Russo, D. and E. Bresler. Effect of field variability in soil hydraulic properties on solutions of unsaturated water and salt flows. Soil Sci. Soc. of America Journal., 45, 675-81, 1981a.

Russo, D. and E. Bresler. Soil hydraulic properties as stochastic processes: I. An analysis of field spatial variability. Soil Sci. Soc. of America Journal., 45, 682-687, 1981b.

Schwartz, F.W. Applications of probabilistic-deterministic modeling to problems of mass transfer in groundwater systems. Proc., 3rd International Hydrology Symposium, Ft. Collins, 281-296, 1978.

Schwartz, F.W. and F.A. Donath. Scenario development and evaluation related to the risk assessment of high level radioactive waste depositories. U.S. Nuclear Regulatory Comm. Report NUREG/CR-1608, 1980.

Sharma, M., G. Gandu and C. Hunt. Spatial variability of infiltration in a watershed. Journal of Hydrology, 45, 101-122, 1980.

Sisson, J. and A. Lu. Field calibration of computer models for application to buried liquid discharges: a status report. Rockwell Hanford Operations Report RHO-ST-46, 1984.

Sisson, J.B. and P.J. Wierenga. Spatial variability of steady-state infiltration rates as a stochastic process. Soil Sci. Soc. of America Journal., 45, 699-704, 1981.

Smith, L. Spatial variability of flow parameters in a stratified sand. Mathematical Geology, 13(1), 1-21, 1981.

Smith, L. and R.A. Freeze. Stochastic analysis of steady-state groundwater flow in a bounded domain, 2, Two dimensional simulations. Water Resources Research, 15(6), 1543-1559, 1979.

Smith, L. and F.W. Schwartz. Mass transport, 1. a stochastic analysis of macroscopic dispersion. Water Resources Research, 16(2), 303, 1980.

Stephens, D.B. and K.R. Rehfeldt. Evaluation of closed-form analytical models to calculate conductivity in a fine sand. Soil Sci. Soc. America Journal, 49, 12-19, 1985.

Tompson, A.F.B., R. Ababou and L.W. Gelhar. Applications and Use of the Three-Dimensional Turning Bands Random Field Generator in Hydrology: Single Realization Problems, Tech. Report 313, R.M. Parsons Lab, M.I.T., Cambridge, MA, 1987.

Tompson, A.F.B., E.G. Vomvoris, L.W. Gelhar. Numerical Simulation of Solute Transport in Randomly Heterogeneous Porous Media: Motivation, Model Development and Application, Tech. Report 316, R.M. Parsons Lab, M.I.T., Cambridge, MA, 1988.

Uffink, G. A random walk model for the simulation of macrodispersion in a stratified aquifer. Proc., IAHS Symposia, IUGG 18th General Assembly, Hamburg, HS2, 1983.

Uffink, G. Modeling of solute transport with the random walk method. Proc., NATO Advanced Workshop on Advances in Analytical and Numerical Groundwater Flow and Quality Modeling, Lisbon, Portugal, HS2, June 1987.

U.S. Nuclear Regulatory Commission, Office of Nuclear Material Safety and Safeguards. Standard review plan for the review of a license application for a low-level radioactive waste disposal facility: safety analysis report. NUREG-1200, January 1987.

van Genuchten, M.Th. A closed-form equation for predicting the hydraulic conductivity of unsaturated soils. Soil Sci. Soc. America Journal, 44(5), 892-898, 1980.

Vanmarcke, E. Random Fields: Analysis and Synthesis. The MIT Press, Cambridge, MA, 1983.

Vieira, S., D. Nielsen and J. Biggar. Spatial variability of field measured infiltration rates. Soil Sci. Soc. of America Journal., 45, 1040-1048, 1981.

Vomvoris, E.G. Concentration Variability in Transport in Heterogeneous Aquifers: A Stochastic Analysis [Ph.D. Dissertation]. M.I.T., Cambridge, MA, 1986.

Warren, J.E. and H.S. Price. Flow in heterogeneous porous media. Trans. A.I.M.E., 222, 153-169, 1961.

Warrick, A.W. and A. Amoozegar-Fard. Areal prediction of water and solute flux in the unsaturated zone, Report EPA-60012-81-058, E.P.A., April 1981.

Warrick, A.W. and A. Amoozegar-Fard. Infiltration and drainage calculations using spatially scaled hydraulic properties. Water Resources Research, 15(5), 1116-1120, 1979.

Weiss, G.H. Random walks and their applications. American Scientist, 65-71, 1983.

Wierenga, P.J. et al. Validation of Stochastic Flow and Transport Models for Unsaturated Soils: A Comprehensive Field Study, Report No. NUREG/CR-4622; PNL-5875, August 1986a.

Wierenga, P.J. et al. Validation of Stochastic Flow and Transport Models for Unsaturated Soils. Research Report No.86-SS-01, Department of Agronomy and Horticulture, NMSU, Las Cruces, Annual Report, September 1986b.

Wierenga, P.J. et al. Validation of Stochastic Flow and Transport Models for Unsaturated Soils. Research Report. Department of Agronomy and Horticulture, NMSU, Las Cruces, 1988 in preparation.

Winter, C.L. et al. A perturbation expansion for diffusion in a random velocity field. S.I.A.M. J. App. Mathematics, 44, 411-424, 1984.

Yeh, T.-C., L.W. Gelhar and A.L. Gutjahr. Stochastic analysis of effects of spatial variability on unsaturated flow. Technical Report H-11, Hydrology Research Program, New Mexico Institute of Mining and Technology, Socorro, July 1982.

Yeh, T.-C., L.W. Gelhar and A.L. Gutjahr. Stochastic analysis of unsaturated flow in heterogeneous soils, 1, Statistically isotropic media. Water Resources Research, 21(4), 447-456, 1985a.

Yeh, T.-C., L.W. Gelhar and A.L. Gutjahr. Stochastic analysis of unsaturated flow in heterogeneous soils, 2, Statistically anisotropic media with variable α. Water Resources Research, 21(4), 457-464, 1985b.

Yeh, T.-C., L.W. Gelhar and A.L. Gutjahr. Stochastic analysis of unsaturated flow in heterogeneous soils, 3, Observations and applications. Water Resources Research, 21(4), 465-471, 1985c.

NRC FORM 335 (2-84) NRCM 1102, 3201, 3202

U.S. NUCLEAR REGULATORY COMMISSION

BIBLIOGRAPHIC DATA SHEET

SEE INSTRUCTIONS ON THE REVERSE

1. REPORT NUMBER (Assigned by TIDC, add Vol No., if any)
NUREG/CR-5094

2. TITLE AND SUBTITLE
Application of Stochastic Methods to the Simulation of Large-Scale Unsaturated Flow and Transport

3. LEAVE BLANK

4. DATE REPORT COMPLETED

MONTH	YEAR
April	1988

5. AUTHOR(S)
D.J. Polmann, E.G. Vomvoris, D. McLaughlin, E.M. Hammick, L.W. Gelhar

6. DATE REPORT ISSUED

MONTH	YEAR
September	1988

7. PERFORMING ORGANIZATION NAME AND MAILING ADDRESS (Include Zip Code)
Massachusetts Institute of Technology
Department of Civil Engineering
77 Massachusetts Avenue
Cambridge, MA 02139

8. PROJECT/TASK/WORK UNIT NUMBER

9. FIN OR GRANT NUMBER
FIN B8956

10. SPONSORING ORGANIZATION NAME AND MAILING ADDRESS (Include Zip Code)
Division of Engineering
Office of Nuclear Regulatory Research
U.S. Nuclear Regulatory Commission
Washington, D.C. 20555

11a. TYPE OF REPORT
Technical

b. PERIOD COVERED (Inclusive dates)
8/1/83 - 11/30/87

12. SUPPLEMENTARY NOTES

13. ABSTRACT (200 words or less)

Numerical simulations are used to demonstrate features of large-scale flow and transport in heterogeneous unsaturated soils using effective expressions derived from a stochastic theory developed at MIT. The case of stratified soil is examined for one- and two-dimensional (2D) flow and 2D transport. Finite-difference methods are used in the flow analysis and a random-walk algorithm is used for transport. Input parameters are derived from statistics of soil samples collected at the site of a large-scale tracer experiment conducted by New Mexico State University (NMSU). This study examines spatial variability of saturated and unsaturated hydraulic conductivity regarding effects on the bulk character of moisture flow and solute transport (directional rates of movement and spreading of the plume). The numerical simulations demonstrate tension-dependent anisotropy, hysteresis and macrodispersion derived in the stochastic theory based on this spatial variability. These features cannot be explained using conventional deterministic models. Preliminary results suggest that the stochastic theory is better able to simulate the bulk character of the NMSU flow experiments compared to a deterministic model. Sensitivity analyses identify major factors of soil variability which control moisture flow and spreading. Results of this study indicate the need for careful experimental design and soils data collection.

14. DOCUMENT ANALYSIS – a. KEYWORDS/DESCRIPTORS
unsaturated flow, unsaturated transport, numerical simulations, stochastic methods, large-scale modeling, hydraulic properties, spatial variability, field experiments, anisotropy, hysteresis, macrodispersion

b. IDENTIFIERS/OPEN-ENDED TERMS

15. AVAILABILITY STATEMENT
Unlimited

16. SECURITY CLASSIFICATION
(This page)
Unclassified
(This report)
Unclassified

17. NUMBER OF PAGES

18. PRICE

UNITED STATES
NUCLEAR REGULATORY COMMISSION
WASHINGTON, D.C. 20555

OFFICIAL BUSINESS
PENALTY FOR PRIVATE USE, $300

SPECIAL FOURTH-CLASS RATE
POSTAGE & FEES PAID
USNRC

PERMIT No. G-67

NUREG/CR-5094

APPLICATION OF STOCHASTIC METHODS TO THE SIMULATION OF LARGE-SCALE UNSATURATED FLOW AND TRANSPORT

SEPTEMBER 1988